

# **Numerical Modelling of Laterally Loaded Single Pile**

A.Lakshmi Rishitha

A Dissertation Submitted to  
Indian Institute of Technology Hyderabad  
In Partial Fulfillment of the Requirements for  
The Degree of Master of Technology/ Doctor of Philosophy



भारतीय प्रौद्योगिकी संस्थान हैदराबाद  
Indian Institute of Technology Hyderabad

Department of Civil Engineering

July, 2015

## Declaration

I declare that this written submission represents my ideas in my own words, and where others' ideas or words have been included, I have adequately cited and referenced the original sources. I also declare that I have adhered to all principles of academic honesty and integrity and have not misrepresented or fabricated or falsified any idea/data/fact/source in my submission. I understand that any violation of the above will be a cause for disciplinary action by the Institute and can also evoke penal action from the sources that have thus not been properly cited, or from whom proper permission has not been taken when needed.

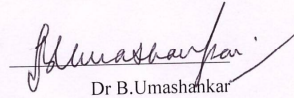
Rishitha  
(Signature)

A. Lakshmi Rishitha  
(A.Lakshmi Rishitha)

CE13M1010  
(CE13M1010)

## Approval Sheet

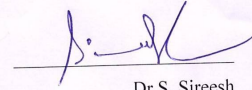
This thesis entitled '*Numerical Modelling of Laterally Loaded Single Pile*' by A.Lakshmi Rishitha is approved for the degree of Master of Technology from IIT Hyderabad.



Dr B.Umashankar

Assistant professor

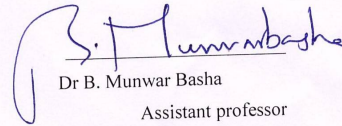
Department of Civil Engineering  
Indian Institute of Technology Hyderabad .



Dr S. Sireesh

Associate professor

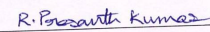
Department of Civil Engineering  
Indian Institute of Technology Hyderabad



Dr B. Munwar Basha

Assistant professor

Department of Civil Engineering  
Indian Institute of Technology Hyderabad



Dr R. Prashanth Kumar

Assistant professor

Department of Mechanical & Aerospace Engineering  
Indian Institute of Technology Hyderabad

## **Acknowledgements**

My sincere gratitude to my advisor Dr.B.Umashankar for his continuous support, help and motivation. I would also like to thank all the faculty members of Civil Engineering Department, IITH.

I am grateful to my family members for their invaluable support.

My heartfelt thanks to my seniors Hari Prasad, Sasanka Mouli, Vinay kumar and Raviteja and my classmates Ugesh, Thejesh, Anu George, Sahithi, Durga Prasad, Preethi sekar and Rajasekar.

I would also like to thank Sravani and Subhavana and my juniors Sushma, Sailaja and Jyothi for being supportive all through days.

Dedicated to

**My Family**

## **Abstract**

Design of piles under lateral loads requires not only estimation of ultimate load carrying capacity of the pile but also, the pile deflections need to be evaluated to determine the allowable loads. There are many approaches to estimate the lateral capacity of piles. Among them, IS code method is invariably used by engineers in our country. Numerical modelling using finite element (PLAXIS-3D) software is the advanced method to analyse piles in which all sorts of non-linearities could be modelled. The present work is done separately for sands and clays. First, a laterally loaded pile in homogenous sand is considered. Pile responses of single pile for various loadings obtained from the above three methods are compared and analysed. As there are large differences in maximum lateral deformations obtained from IS code method, subgrade reaction method when compared to numerical modelling there is a need to either modify them or propose a new method. The normalised load-deflection charts using numerical modelling which can be used easily are proposed. These charts are proposed considering various pile geometries like length, diameter, and eccentricity of pile and for different soil and pile properties. The charts are proposed both for linear elastic model and Mohr-Coulomb model and the results compared. The formation of plastic zones is also studied for a given pile with eccentricity ratios ( $e/B$  ratios equal to 0 and 6). Similarly for clays initially the lateral deformations at different loads for different soil consistencies obtained from IS code method and numerical modeling are compared. Then normalized charts are proposed for clays similar to that of sands for soft clay, medium stiff clay, and stiff clay. The normalized charts of different consistencies are compared. Finally the formation of plastic zones in clays for laterally loaded single pile is also studied.

# Nomenclature

$L$  – length of the pile

$B$  – diameter of a circular pile

$e$  – eccentricity of the pile

$E_p$  – stiffness of the pile material

$E_s$  – stiffness of the soil

$\Gamma_h$  – modulus of subgrade reaction

$T$  – stiffness factor

LE – linear elastic model

MC – Mohr Coulomb model

$\Phi$  – angle of shearing resistance of the soil

$S_u$  – undrained shear strength of soil

$z$  – depth of soil medium

$y$  – lateral deformation of the pile

# Contents

Declaration .....	<b>Error! Bookmark not defined.</b>
Approval Sheet .....	<b>Error! Bookmark not defined.</b>
Acknowledgements.....	iv
Abstract .....	vi
<b>Nomenclature.....</b>	<b>vii</b>
<b>1 Introduction.....</b>	<b>11</b>
1.1 Lateral Loads and Piles.....	11
1.1.1 Load Transfer Mechanisms(statics) of Piles.....	11
1.1.2 Kinematics and Failure Modes of Laterally Loaded Piles.....	13
1.2 Problem Definition.....	14
1.3 Limitations of Existing Methods.....	15
1.3.1 Subgrade Reaction Method.....	15
1.3.2 IS Code Method.....	15
1.4 Objectives.....	15
1.5 Layout of Report.....	16
<b>2 Literature Review.....</b>	<b>17</b>
2.1 Introduction.....	17
2.2 A Summary of Previous Research on Laterally Loaded Piles.....	17
2.2.1 Winkler Approach.....	17
2.2.2 p-y Method of Analysis.....	19
2.2.3 Elasticity Theory.....	21
2.2.4 Finite Element Method.....	22
2.3 IS Code Method.....	22



2.3.1	Background.....	22
2.3.2	Deformations and Moments.....	25
2.4	Subgrade Reaction Method.....	26
<b>3</b>	<b>Numerical Modelling.....</b>	<b>30</b>
3.1	General.....	30
3.2	Material Models.....	30
3.2.1	Linear Elastic Model.....	30
3.2.2	Mohr Coulomb Model.....	31
3.3	Limitations.....	31
3.3.1	Linear Elastic Model.....	31
3.3.2	Mohr Coulomb Model.....	31
3.4	Modelling and Soil Behaviour.....	32
3.5	Basic Model Parameters in Relation to Real Soil Behaviour.....	32
3.6	Model.....	32
3.7	Elements.....	33
3.8	Mesh Properties.....	33
3.9	Staged Construction.....	33
3.10	Mesh Convergence and Boundary Conditions Study.....	34
<b>4</b>	<b>Results and discussion - Part 1 Sands.....</b>	<b>39</b>
4.1	Comparison of Pile Responses of IS Code Method, Subgrade Reaction Method and Numerical Modelling for Sands.....	39
4.1.1	Maximum Lateral Deformation.....	40
4.1.2	Bending Moment.....	41
4.2	Normalised Load Deflection Charts.....	42
4.2.1	Using LE Model.....	43
4.2.2	Using MC Model.....	52

4.3	Comparison of Normalised Charts of LE and MC model.....	61
4.4	Study of Plastic Zone Formation.....	62
<b>5</b>	<b>Results and Discussion - Part 2 Clays.....</b>	<b>65</b>
5.1	Comparison of Pile Responses of IS Code Method and Numerical Modelling for Clays.....	65
5.2	Normalised Load Deflection Charts.....	70
5.2.1	Soft Clay.....	70
5.2.2	Medium Stiff Clay.....	78
5.2.3	Stiff Clay.....	86
5.3	Comparison of Normalised Charts of Soft Clay, Medium Stiff Clay and Stiff Clay..	94
5.4	Study of Plastic Zone Formation.....	97
<b>6</b>	<b>Conclusions.....</b>	<b>100</b>
<b>7</b>	<b>References.....</b>	<b>101</b>

# Chapter 1

## Introduction

### 1.1 Lateral Loads and Piles

Piles are commonly used to transfer vertical (axial) forces, arising primarily from gravity (e.g., the weight of a superstructure). Examples of structures where piles are commonly used as foundations are tall buildings, bridges, offshore platforms, defence structures, dams and lock structures, transmission towers, earth retaining structures, wharfs and jetties. However, in all these structures, it is not only the axial force that the piles carry; often the piles are subjected to lateral (horizontal) forces and moments. In fact, there are some structures (e.g., oil production platforms, earth retaining structures, wharfs and jetties) where the primary function of piles is to transfer lateral loads to the ground.

Wind gusts are the most common cause of lateral force (and/or moment) that a pile has to support. The other major cause of lateral force is seismic activity. The horizontal shaking of the ground during earthquakes generates lateral forces that the piles have to withstand. Certain buildings are also acted upon by lateral earth pressures, which transmit lateral forces to the foundations. That apart, depending on the type of structure a pile supports, there can be different causes of lateral forces. For tall buildings and transmission towers, wind action is the primary cause. For offshore oil production platforms, quays, harbours, wharfs and jetties, wave action gives rise to lateral forces. In the case of bridge abutments and piers, horizontal forces are caused due to traffic and wind movement. Dams and lock structures have to withstand water pressures which transfer as horizontal forces on the supporting piles. Defence structures often have to withstand blasts that cause lateral forces. In the case of earth retaining structures, the primary role of piles is to resist lateral forces caused due to the lateral pressures exerted by the soil mass behind the retaining wall. Sometimes, piles are installed into slopes where slow ground movements are taking place, in order to arrest the movement. In such cases, the piles are subjected only to lateral forces. Piles are used to support open excavations; here also, there is no axial force and the only role of the piles is to resist lateral forces.

#### 1.1.1 Load Transfer Mechanisms (statics) of Piles

A proper understanding of the load transfer mechanisms for piles is necessary for analysis and design. Piles transfer axial and lateral loads through different mechanisms. In the case of axial (vertical) loads, piles may be looked upon as axially loaded columns; they transfer loads to the ground by shaft friction and base resistance (Fig 1.1). As a pile is loaded axially, it slightly settles and the surrounding soil mass offers resistance to the downward movement. Because soil is a frictional material, frictional forces develop at the interface of the pile shaft and the surrounding soil that oppose the downward pile movement. The frictional forces acting all along the pile shaft partly resist the applied axial load and are referred to as shaft resistance, shaft friction, or skin friction. A part of the axial load is transferred

to the ground through the bottom of the pile (commonly referred to as the pile base). As a pile tries to move down, the soil mass below the pile base offers compressive resistance to the movement. This mechanism is called base resistance or end-bearing resistance. The total resistance (shaft friction plus end-bearing resistance) keeps a pile in equilibrium with the applied load. Piles that transfer most of the axial load through the base are called *end-bearing* piles, while those that transfer most of the load through shaft friction are called *friction* piles. For end-bearing piles, it is necessary to have the pile base inserted into a strong layer of soil (e.g., dense sand, stiff clay, or rock). Typically, engineers would prefer to design end-bearing piles because the base resistance is more reliable than shaft friction. However, if no such strong layer is available at a site, then engineers have to rely only on shaft friction; in such a case the pile is called a *floating pile*.

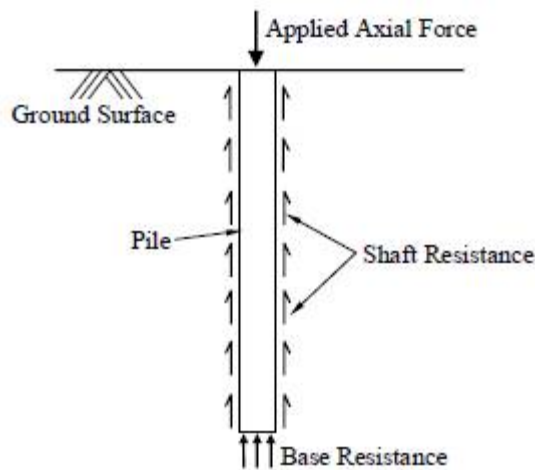


**Figure 1.1: Load transfer mechanism of axially loaded piles**

In the case of lateral loads, piles behave as transversely loaded beams. They transfer lateral load to the surrounding soil mass by using the lateral resistance of soil (Fig 1.2). When a pile is loaded laterally, a part or whole of the pile tries to shift horizontally in the direction of the applied load, causing bending, rotation, or translation of the pile (Fleming et. al 1992, Salgado 2008). The pile presses against the soil in front of it (i.e., the soil mass lying in the direction of the applied load), generating compressive and shear stresses and strains in the soil that offers resistance to the pile movement. This is the primary mechanism of load transfer for lateral loads. The total soil resistance acting over the entire pile shaft balances the external horizontal forces. The soil resistance also allows satisfaction of moment equilibrium of the pile.

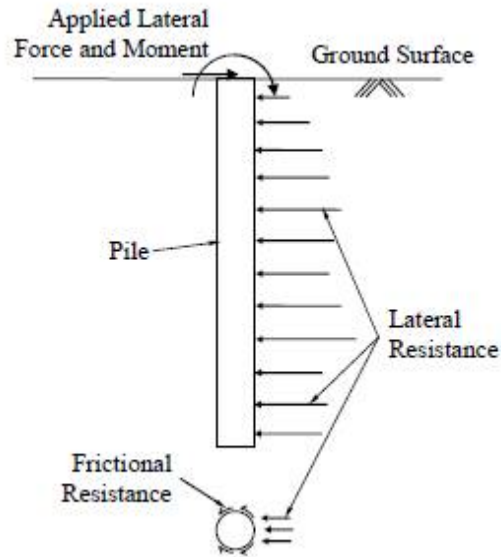


**Figure 1.2: Load transfer mechanism of laterally loaded single pile**

### **1.1.2 Kinematics and Failure Modes of Laterally Loaded Piles**

The kinematics of axially loaded piles is simple, the pile moves vertically downward under the acting load and, if the resistive forces (i.e., shaft and base resistances) exceed the limit values, then the pile suffers excessive vertical deflection (plunging) leading to collapse. The kinematics and failure mechanisms of laterally loaded piles are more complex and vary depending on the type of pile. Since laterally loaded piles are transversely loaded, the pile may rotate, bend, or translate (Fleming et al. 1992, Salgado 2008). As the pile moves in the direction of the applied force, a gap may also open up between the back of the pile and the soil over the top few meters. If the pile is short and stubby, it will not bend much but will rotate or even translate (Fig 1.3). Such piles are called rigid piles. If the pile is long and slender, then it bends because of the applied load (Fig 1.4). These piles are called flexible piles. In most practical situations, piles are long enough to behave as flexible piles. For flexible piles, the laterally loaded pile problem is one of soil-structure interaction, i.e., the lateral deflection of the pile depends on the soil resistance and the resistance of the soil in turn depends on the pile deflection.

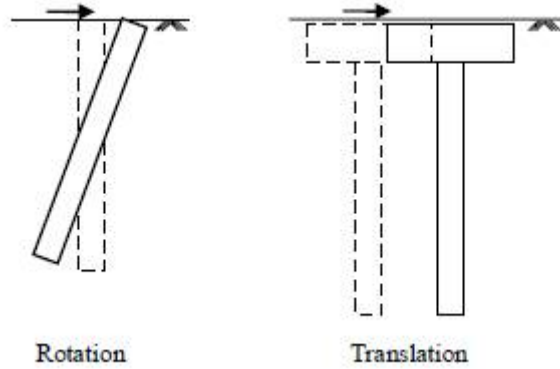


**Figure 1.3: Failure modes of short piles**

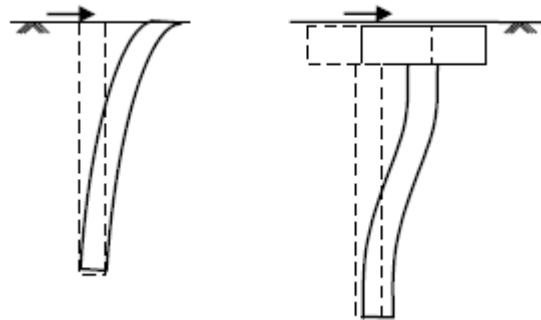


**Figure 1.4: Failure modes of long piles**

## 1.2 Problem Definition

Several methods are available in the literature for the analysis of laterally loaded piles. However in this thesis the pile responses using three methods are compared. One of the methods being subgrade reaction method which is based on Winkler's soil model the other one is the simplified method prescribed in the Indian Standard IS 2911-2002 for estimating the pile response, which is used invariably by the structural engineers and the third one is advanced numerical method using finite elements.

The main purpose of this research is to compare the pile responses like lateral deformation and bending moment for different loads obtained from these methods for sands and clays. As there are certain limitations with IS code method and subgrade reaction method, the normalised load deflection charts are proposed using numerical modelling which can be used for piles of different geometries and different properties of soil and pile.

### **1.3 Limitations of Existing Methods**

#### **1.3.1 Subgrade Reaction Method**

This approach is relatively crude and is obviously not as sophisticated as analyses based on elastic continuum theories.

1. The modulus of subgrade reaction is not a unique property of the soil, but depends intrinsically on pile characteristics and the magnitude of deflection,
2. The method is semi-empirical in nature,
3. Axial load effects are ignored, and
4. The soil model used in the technique is discontinuous, i.e., the linearly elastic Winkler springs behave independently and thus displacements at a point are not influenced by displacements or stresses at other points along the pile.

In spite of these drawbacks, the subgrade reaction approach has been widely employed in foundation practise because it provides simple means of analysis.

#### **1.3.2 IS Code Method**

The following are the features of IS code based method

1. It is applicable for flexible piles where the maximum depth coefficient  $L/T$  is equal to or exceeds 4.0.
2. IS 2911-2002 underestimates the pile head deflections for  $L/T < 3.0$  for both free headed and fixed head piles
3. IS: 2911 may predict the load very close to the actual values (especially for long term loading based on the expressions specified in IS: 2911). However, it will under predict the displacement which may cause serviceability problem.

### **1.4 Objectives**

1. To review IS codal provisions for laterally loaded piles (IS 2911 (Part 1/Sec 1): 2010)
2. To compare pile responses like maximum deflection and maximum bending moment obtained from IS code and subgrade reaction method with advanced numerical model using finite element method (PLAXIS- 3D)
3. To propose normalised load deflection charts for various pile geometries, soil and pile properties using advanced numerical modelling through linear elastic model and Mohr-Coulomb model for sands.
4. To propose normalised load deflection charts for various pile geometries, soil and pile properties for clays.

## 1.5 Layout of Report

The report is structured into following main parts:

Chapter 1 briefly describes the real life situations where laterally loaded piles are employed, the load transfer mechanism, failure modes, and kinematics of the laterally loaded piles. Then it defines the present research, remarks the limitations of the few of the existing methods of laterally loaded pile analysis like IS code method, subgrade reaction method, determines the objectives of the research, and draws the outlines.

Chapter 2 reviews the literature relating to the main research. This is aimed to provide the basic knowledge, which is required for the analysis of the research as well as for the interpretation of the results. With this purpose, three main points are described as follows

The first one summarizes different methods on situations of the piles loaded laterally by soil movements in order to provide an overview of the laterally loaded pile behaviour. In addition, by these methods the helpful information will be selected to support the analysis of the present research.

The second one elaborates the IS code method prescribed in IS 2911(part1/ sec1): 2010 for laterally loaded piles. It provides a clear overview of the background and step by step procedure to be followed to determine pile responses like deflections and moments.

The third one explains subgrade reaction method, the model behind this method is Winkler's model and it is also described. The equations to determine pile deflections and rotations both for free-head pile and fixed-head pile are derived from the basic equation

Chapter 3 gives an overview about the finite element software - PLAXIS 3D- used for numerical modelling. The material models used in modelling are explained with their limitations. The parameters in relation to real soil behaviour are understood. Details about model, type of elements, mesh properties, and staged construction are given. Finally mesh convergence and boundary conditions study is carried out to fix the boundary dimensions and mesh size for the actual model.

Chapter 4 provides the results obtained for sands. Initially the pile responses like lateral deformations, and bending moments obtained from IS code method, subgrade reaction method, and numerical modelling are compared to study the trend. Then normalised charts are proposed using numerical modelling for different geometries and properties of piles and different soil properties using two material models Linear elastic model and Mohr-Coulomb model. The plastic points for minimum and maximum eccentricities are obtained and they are understood.

Chapter 5 gives the results for clays. The lateral pile deformations for different loads and different clay consistencies obtained from IS code method and numerical modelling are compared. Normalised charts are proposed for clays of different consistencies like soft clay, medium stiff clay, and stiff clay. Then the formation of plastic zones for clays are studied.

Chapter 6 presents the conclusions drawn from the study.



# Chapter 2

## Literature Review

### 2.1 Introduction

Many different methods of analysis have been proposed to solve the problem of a laterally loaded pile, where the problem can be generally defined as computing pile deflection and bending moment as a function of depth below the ground surface. Methods which are based on the theory of elasticity are not generally applicable for design due to the inadmissibility of assigning single values to the required soil parameters. Some methods are based on the theory of subgrade reaction and on simplifying assumptions, such as assuming a variation of the sub grade modulus with depth and that the soil is linearly elastic (Winkler, 1887; Hetenyi, 1946; Terzaghi, 1955; Broms, 1964; Broms, 1964). These simplifying assumptions reduce the difficulty in obtaining a solution to the problem, but errors of an unknown magnitude are introduced into the solution.

Three criteria must be satisfied in the design of pile foundations subjected to lateral forces and moments: 1) the soil should not be stressed beyond its ultimate capacity, 2) deflections should be within acceptable limits, and 3) the structural integrity of the foundation system must be assured. The first criteria can be addressed during design using ultimate resistance theories such as those by Broms (1964a, 1964b) or Brinch Hansen (1961). The second and third criteria apply to deflections and stresses that occur at working loads.

### 2.2 A Summary of Previous Research on Laterally Loaded Piles

A brief review of the most widely recognized analytical techniques is provided in this section. Many of these techniques can be modified to predict the behaviour of closely spaced piles, or pile groups. Analytical methods for predicting lateral deflections, rotations and stresses in single piles can be grouped under the following four headings:

- Winkler approach,
- p-y method,
- Elasticity theory, and
- Finite element methods.

#### 2.2.1 Winkler Approach

The Winkler approach, also called the subgrade reaction theory, is the oldest method for predicting pile deflections and bending moments. The approach uses Winkler's modulus of subgrade reaction concept to model the soil as a series of unconnected linear springs with a stiffness,  $E_s$ , expressed in

units of force per length squared ( $FL^{-2}$ ).  $E_s$  is the modulus of soil reaction (or soil modulus) defined as:

$$E_s = \frac{-p}{y} \quad (2.1)$$

where  $p$  is the lateral soil reaction per unit length of the pile, and  $y$  is the lateral deflection of the pile (Matlock and Reese, 1960). The negative sign indicates the direction of soil reaction is opposite to the direction of the pile deflection. Another term that is sometimes used in place of  $E_s$  is the coefficient (or modulus) of horizontal subgrade reaction,  $k_h$ , expressed in units of force per unit volume (Terzaghi 1955). The relationship between  $E_s$  and  $k_h$  can be expressed as:

$$E_s = k_h B \quad (2.2)$$

where  $B$  is the diameter or width of the pile.  $E_s$  is a more fundamental soil property because it is not dependent on the pile size. The behaviour of a single pile can be analysed using the equation of an elastic beam supported on an elastic foundation (Hetenyi 1946), which is represented by the 4th order differential beam bending equation:

$$E_p I_p \frac{d^4 y}{dx^4} + Q \frac{d^2 y}{dx^2} + E_p y = 0 \quad (2.3)$$

where  $E_p$  is the modulus of elasticity of the pile,  $I_p$  is the moment of inertia of the pile section,  $Q$  is the axial load on the pile,  $z$  is the vertical depth, and  $y$  is the lateral deflection of the pile at point  $z$  along the length of the pile. The governing equation for the deflection of a laterally loaded pile, obtained by applying variational techniques (minimization of potential energy) to the beam bending equation (Reddy 1993), and ignoring the axial component, is:

$$\frac{d^4 y}{dx^4} + \frac{E_s}{E_p I_p} y = 0 \quad (2.4)$$

Solutions to the above equation have been obtained by making simplifying assumptions regarding the variation of  $E_s$  (or  $k_h$ ) with depth. The most common assumption is that  $E_s$  is constant with depth for clays and  $E_s$  varies linearly with depth for sands. Poulos and Davis (1980) and Prakash and Sharma (1990) provide tables and charts that can be used to determine pile deflections, slopes, and moments as a function of depth and non-dimensional coefficients for a constant value of  $E_s$  with depth. The soil modulus for sand and normally consolidated clay is often assumed to vary linearly with depth, as follows:

$$E_s = k z \quad (2.5)$$

where  $k$  is the constant of horizontal subgrade reaction, in units force per volume. For this linear variation of  $E_s$  with depth, Matlock and Reese (1960) and Poulos and Davis (1980) present non-dimensional coefficients that can be used to calculate pile deflections, rotations, and bending moments for various pile-head boundary conditions. Gill and Demars (1970) present other formulations for the variation of  $E_s$  with depth, such as step functions, hyperbolic functions, and exponential functions.

The subgrade reaction method is widely employed in practice because it has a long history of use, and because it is relatively straight forward to apply using available chart and tabulated solutions, particularly for a constant or linear variation of  $E_s$  with depth. Despite its frequent use, the method is often criticized because of its theoretical shortcomings and limitations. The primary shortcomings are:

1. The modulus of subgrade reaction is not a unique property of the soil, but depends intrinsically on pile characteristics and the magnitude of deflection,
2. The method is semi-empirical in nature,
3. Axial load effects are ignored, and
4. The soil model used in the technique is discontinuous, i.e., the linearly elastic Winkler springs behave independently and thus displacements at a point are not influenced by displacements or stresses at other points along the pile (Jamiołkowski and Garassino 1977).

Modifications to the original subgrade reaction approach have been proposed to account for some of these shortcomings. One of these modifications attempts to convert the Winkler model to a continuous model by coupling the springs using an inter-spring shear layer component (Georgiadis and Butterfield 1982). This model also accounts for the contribution of edge shear along the pile boundaries. The model has not gained widespread acceptance because of difficulties associated with obtaining soil parameters necessary to develop coefficients for use in the model (Horvath 1984). McClelland and Focht (1956) augmented the subgrade reaction approach using finite difference techniques to solve the beam bending equation with nonlinear load versus deflection curves to model the soil. Their approach is known as the p-y method of analysis. This method has gained popularity in recent years with the availability of powerful personal computers and commercial software such as COM624 (1993) and LPILE Plus3.0 (1997). A brief summary of the p-y method of analysis is presented in the following section.

### **2.2.2 p-y Method of Analysis**

The p-y approach for analysing the response of laterally loaded piles is essentially a modification or “evolutionary refinement” (Horvath 1984) of the basic Winkler model, where  $p$  is the soil pressure per unit length of pile and  $y$  is the pile deflection. The soil is represented by a series of nonlinear p-y curves that vary with depth and soil type.

The method is semi-empirical in nature because the shape of the p-y curves is determined from field load tests. Reese (1977) has developed a number of empirical or “default” curves for typical soil types

based on the results of field measurements on fully instrumented piles. The most widely used analytical expression for p-y curves is the cubic parabola, represented by the following equation:

$$\frac{P}{P_{ult}} = 0.5 \left( \frac{y}{y_{50}} \right)^{1/3} \quad (2.6)$$

where  $p_{ult}$  is the ultimate soil resistance per unit length of pile and  $y_{50}$  is the deflection at one-half the ultimate soil resistance.

The deflections, rotations, and bending moments in the pile are calculated by solving the beam bending equation using finite difference or finite element numerical techniques. The pile is divided into a number of small increments and analysed using p-y curves to represent the soil resistance.

In this representation, the axial load in the pile,  $Q$ , is implicitly assumed constant with depth, to simplify computations. This assumption does not adversely affect the analysis because  $Q$  has very little effect on the deflection and bending moment. Furthermore, the maximum bending moment is generally only a relatively short distance below the ground line, or pile cap, where the value of  $Q$  is undiminished (Reese, 1977).

Four additional equations are necessary to balance the number of equations and the number of unknowns in the finite difference formulation. These four equations are represented by boundary conditions, two at the pile top and two at the bottom of the pile. At the bottom of the pile, one boundary condition is obtained by assuming a value of zero moment, or:

$$EI \left( \frac{d^2 y}{dx^2} \right) = 0 \quad (2.7)$$

The second boundary condition at the pile bottom involves specifying the shear of the pile using the following expression at  $z = L$ :

$$EI \left( \frac{d^3 y}{dx^3} \right) + Q \left( \frac{dy}{dx} \right) = V \quad (2.8)$$

where  $V$  is the shear force, which is usually set equal to zero for long piles.

The two boundary conditions at the top of the pile depend on the shear, moment, rotation, and displacement circumstances at the pile top. These are generalized into the following four categories:

1. Pile not restrained against rotation. This is divided into two subcategories: (a) “flagpole” and (b) free-head conditions.
2. Vertical load applied eccentrically at the ground surface (moment loading condition).
3. Pile head extends into a superstructure or is partially restrained against rotation (partially restrained condition).
4. Pile head rotation is known, usually assumed = 0 (fixed-head condition).

The p-y method is readily adapted to computer implementation and is available commercially in the computer programs LPILEPlus 3.0 (1997) and COM624 (1993). The method is an improvement over the subgrade reaction approach because it accounts for the nonlinear behaviour of most soils without the numerical limitations inherent in the subgrade reaction approach. However, the method has some limitations, as described below:

1. The p-y curves are independent of one another. Therefore, the continuous nature of soil along the length of the pile is not explicitly modelled.
2. Suitable p-y curves are required. Obtaining the appropriate p-y curve is analogous to obtaining the appropriate value of  $E_s$ ; one must either perform full scale instrumented lateral load tests or adapt the existing available standard curves (default curves) for use in untested conditions. These default curves are limited to the soil types in which they were developed; they are not universal.
3. A computer is required to perform the analysis.

Other representations of p-y curves have been proposed such as the hyperbolic shape by (Kondner 1963). Evans (1982) and Mokwa et al. (1997) present a means of adjusting the shape of the p-y curve to model the behaviour of soils that have both cohesion and friction using Brinch Hansen's (1961) f-c ultimate theory. In situ tests such as the dilatometer (Gabr 1994), cone penetrometer (Robertson et al. 1985), and pressuremeter (Ruesta and Townsend 1997) have also been used to develop p-y curves.

### **2.2.3 Elasticity Theory**

Poulos (1971a, 1971b) presented the first systematic approach for analysing the behaviour of laterally loaded piles and pile groups using the theory of elasticity. Because the soil is represented as an elastic continuum, the approach is applicable for analysing battered piles, pile groups of any shape and dimension, layered systems, and systems in which the soil modulus varies with depth. The method can be adapted to account for the nonlinear behaviour of soil and provides a means of determining both immediate and final total movements of the pile (Poulos 1980).

Poulos's method (1971a, 1971b) assumes the soil is an ideal, elastic, homogeneous, isotropic semi-infinite mass, having elastic parameters soil stiffness  $E_s$  and Poisson's ratio  $\mu_s$ . The pile is idealized as a thin beam, with horizontal pile deflections evaluated from integration of the classic Mindlin equation for horizontal subsurface loading. The Mindlin equation is used to solve for horizontal displacements caused by a horizontal point load within the interior of a semi-infinite elastic-isotropic homogeneous mass. Solutions are obtained by integrating the equation over a rectangular area within the mass. The principle of superposition is used to obtain displacement of any points within the rectangular area.

The pile is assumed to be a vertical strip of length  $L$ , width  $D$  (or diameter,  $D$ , for a circular pile), and flexural stiffness  $E_p I_p$ . It is divided into  $n+1$  elements and each element is acted upon by a uniform

horizontal stress  $p$ . The horizontal displacements of the pile are equal to the horizontal displacements of the soil. The soil displacements are expressed as:

$$\{y_s\} = \frac{d}{E_s} [I_s] \{p\} \quad (2.9)$$

where  $\{y_s\}$  is the column vector of soil displacements,  $\{p\}$  is the column vector of horizontal loading between soil and pile, and  $[I_s]$  is the  $n+1$  by  $n+1$  matrix of soil displacement influence factors determined by integrating Mindlin's equation, using boundary element analyses (Poulos 1971a). The finite difference form of the beam bending equation is used to determine the pile displacements. The form of the equation varies depending on the pile-head boundary conditions. Poulos and Davis (1980) present expressions for free-head and fixed-head piles for a number of different soil and loading conditions. One of the biggest limitations of the method (in addition to computational complexities) is the difficulty in determining an appropriate soil modulus,  $E_s$ .

## 2.2.4 Finite Element Method

The numerical modeling techniques based on the FE provide versatile tools that are capable of modeling soil continuity, soil nonlinearity, soil–pile interface behavior, and 3D boundary conditions. In particular, FE analysis is a continuum approach, so it can consider coupled soil–pile interaction automatically, which the traditional load transfer method cannot. Finite element techniques have been used to analyse complicated loading conditions on important projects and for research purposes. Salient features of this powerful method include the ability to apply any combination of axial, torsion, and lateral loads; the capability of considering the nonlinear behaviour of structure and soil; and the potential to model pile-soil-pile-structure interactions. Time dependent results can be obtained and more intricate conditions such as battered piles, slopes, excavations, tie-backs, and construction sequencing can be modelled.

## 2.3 IS Code Method

### 2.3.1 Background

According to IS code method the pile is replaced by a cantilever, fixed at some depth and ignoring the soil support above that depth. The length of which is a function of subgrade reaction of the surrounding soil and the pile geometry. The equivalent cantilever length  $L_e = L_1 + L_f$  as shown in Fig 2.1, where  $L_1$  is the length of the pile above ground level and  $L_f$  is defined as a function of ( $L_1/T$  or  $L_1/R$ ). However, the method described is applicable only for flexible piles, where the maximum depth coefficient  $L/T$  is equal to or exceeds 4.0.

The first step is to determine if the pile will behave as a short rigid unit or as an infinitely long flexible member. This is done by calculating the stiffness factor  $R$  or  $T$  for the particular combination of pile

and soil. Having calculated the stiffness factor, the criteria for behaviour as a short rigid pile or as a long elastic pile are related to the embedded length  $L$  of the pile. The depth from the ground surface to the point of virtual fixity is then calculated and used in the conventional elastic analysis for estimating the lateral deflection and bending moment.

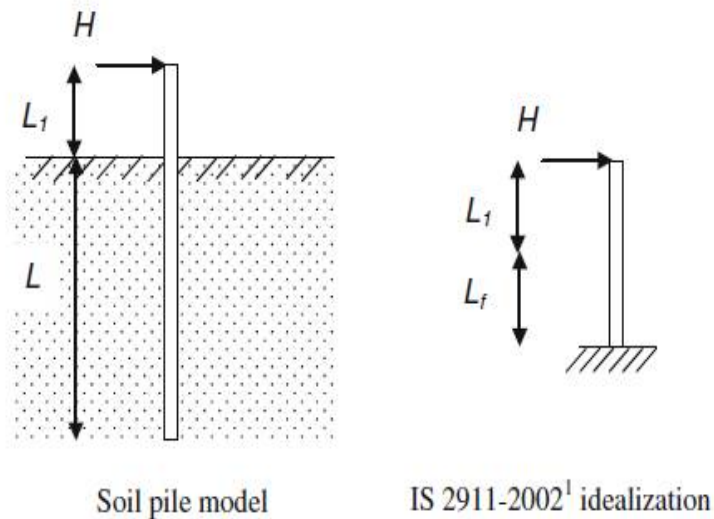


Figure 2.1: Cantilever modelling of laterally loaded pile (IS 2911.1.1.2010)

For Piles in Sand and Normally Loaded Clays

Stiffness factor  $T$ , in m

$$T = \sqrt[3]{\frac{EI}{\eta_h}} \quad (2.10)$$

where  $E$  = Young's modulus of pile material in  $\text{MN/m}^2$

$I$  = M.I of the pile cross-section in  $\text{m}^4$

$\eta_h$  = modulus of subgrade reaction in  $\text{MN/m}^3$ . The range of  $\eta_h$  for various types of sands which are classified based on SPT number for dry and submerged conditions of sands are given in Table 2.1

Table 2.1: Modulus of Subgrade Reaction for Granular Soils,  $\eta_h$  ( $\text{MN/m}^3$ )

Sl.no	Soil type	N (blows/30cm)	Range of $\eta_h$ ( $\text{MN/m}^3$ )	
			Dry	Submerged
1.	Very Loose sand	0-4	<0.4	<0.2
2.	Loose sand	4-10	0.4-2.5	0.2-1.4
3.	Medium sand	10-35	2.5-7.5	1.4-5.0
4.	Dense sand	>35	7.5-20.0	5.0-12.0

For piles in preloaded clays:

$$\text{Stiffness factor } R, \text{ in m} = \sqrt[4]{\frac{EI}{KB}} \quad (2.11)$$

E = Young's modulus of pile material in MN/m<sup>2</sup>

I = M.I of the pile cross-section in m<sup>4</sup>

K = (k<sub>1</sub>\*0.3)/ (1.5\*B)

B = width or diameter of pile in m

For different kinds of clays which are classified based on unconfined compressive strength the range of modulus of subgrade reaction is given in Table 2.2.

Table 2.2: Modulus of Subgrade Reaction for Cohesive Soil, k<sub>1</sub>, in MN/m<sup>3</sup>

Sl.no	Soil Consistency	Unconfined Compressive Strength (kN/m <sup>2</sup> )	Range of k <sub>1</sub> (MN/m <sup>3</sup> )
1.	Soft	25-50	4.5-9.0
2.	Medium stiff	50-100	9.0-18.0
3.	Stiff	100-200	18.0-36.0
4.	Very stiff	200-400	36.0-72.0
5.	Hard	>400	>72

Fig 2.2 shows the depth of fixity obtained as a function of stiffness factor.

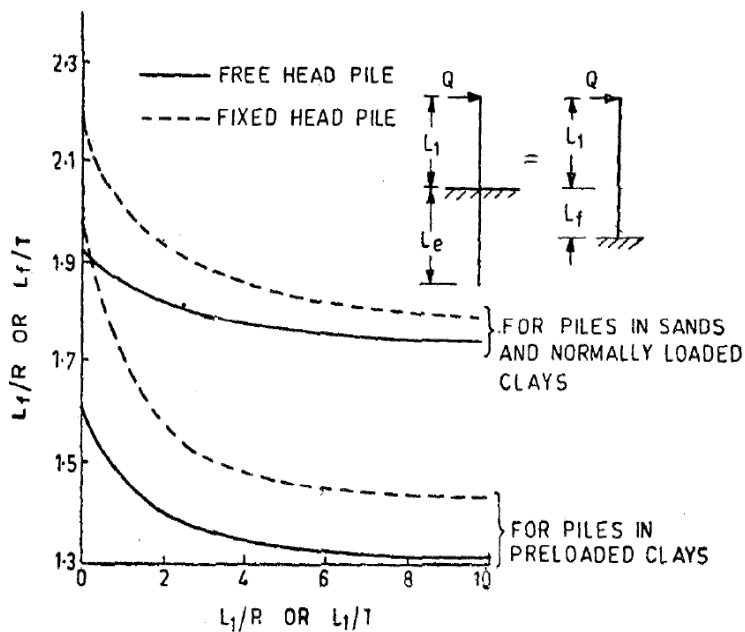


Figure 2.2: Depth of Fixity (IS 2911.1.1.2010)



### 2.3.2 Deflections and Moments

Equivalent cantilever approach gives a simple procedure for obtaining the deflections and moments due to relatively small lateral loads. This requires the determination of depth of virtual fixity  $z_f$ . The depth to the point of fixity may be read from the plots given in Fig. 2.3.  $e$  is the effective eccentricity of the point of load application obtained either by converting the moment to an equivalent horizontal load or by actual position of the horizontal load application.  $R$  and  $T$  are the stiffness factors described earlier.

For a free head pile deflection,  $y = \frac{H(e+z_f)^3}{3EI} * 10^3$  (2.12)

and for a fixed head pile deflection,  $y = \frac{H(e+z_f)^3}{12EI} * 10^3$  (2.13)

The fixed end moment of the equivalent cantilever is higher than the actual maximum moment ( $M$ ) of the pile. The actual maximum moment is obtained by multiplying the fixed end moment of the equivalent cantilever by a reduction factor,  $m$ . The fixed end moment of the equivalent cantilever is given by:

$$M_f = H(e + z_f) \text{ (free head pile)} \quad (2.14)$$

$$= \frac{H(e+z_f)}{2} \text{ (fixed head pile)} \quad (2.15)$$

The actual maximum moment ( $M$ ) =  $m(M_f)$

where 'm' is reduction factor which can be obtained from Fig 2.3 for a free head pile and from Fig 2.4 for a fixed head pile.

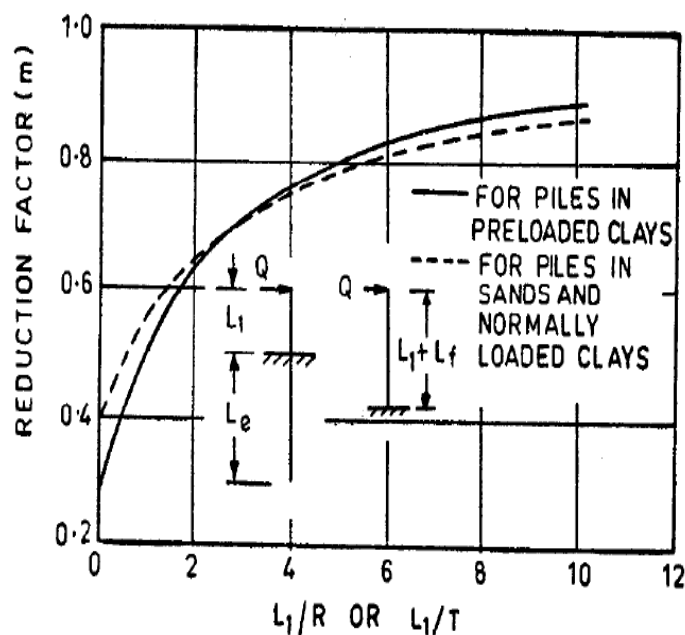


Figure 2.3: Reduction factors for free head pile (IS 2911.1.1.2010)

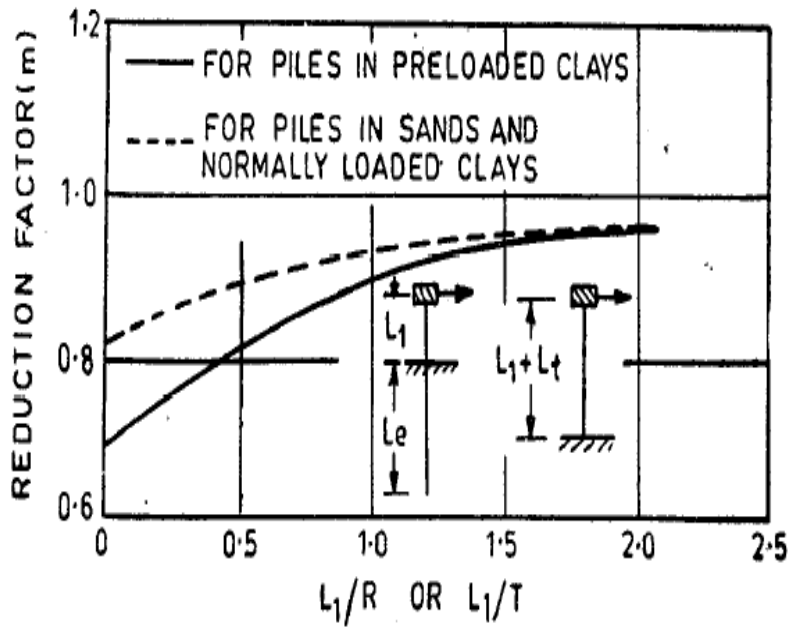


Figure 2.4: Reduction factors for fixed head pile (IS 2911.1.1.2010)

## 2.4 Subgrade Reaction Method

The complete background of this method is given in section 2.2.1. Winkler's model characterizes the soil as a series of unconnected linearly-elastic springs so that deformation occurs only where loading exists as shown in Figure 2.5.

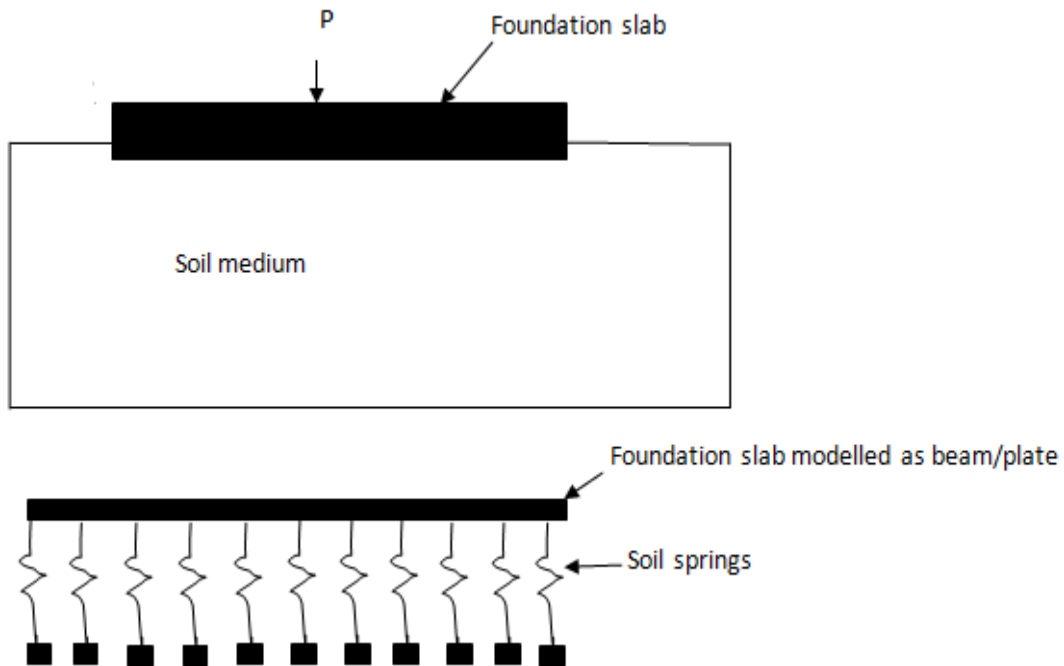


Figure 2.5: Equivalent foundation resting on Winkler spring bed

The obvious disadvantage of this soil model is the lack of continuity; real soil is at least to some extent continuous, since the displacements at a point are influenced by stresses and forces at other points within the soil. This method provides a relatively simple means of analysis and enables factors such as nonlinearity, variation of soil stiffness with depth, and layering of the soil profile to be taken into account readily, if only approximately. In addition, despite the many difficulties in determining the modulus of subgrade reaction of real soil, a considerable amount of experience has been gained in applying the theory to practical problems, and a number of empirical correlations are available for determining the modulus.

Winkler's model (1867) stated that the reaction force of a laterally loaded pile is proportional to the displacement. Pressure (P) and deflection (y) are related through the coefficient of horizontal subgrade reaction ( $k_h$ ),

$$P = k_h y \quad (2.16)$$

The pile is considered as a thin rod which satisfies the following equation:

$$E_p I_p \frac{d^4 y}{dz^4} = -P.B \quad (2.17)$$

Where:

$E_p$  = Modulus of elasticity of pile

$I_p$  = Moment of inertia of pile

z = Depth

B = Diameter of pile

Combining equation (2.16) and (2.17),

$$E_p I_p \frac{d^4 y}{dz^4} + k_h .B .y = 0 \quad (2.18)$$

Equation (2.18) is written in the form of finite difference as follows:

$$E_p I_p \left( \frac{y_{i-2} - 4y_{i-1} + 6y_i - 4y_{i+1} + y_{i+2}}{\delta^4} \right) + (k_h .B .y_i) = 0 \quad (2.19)$$

Equation (2.19) leads to:

$$y_{i-2} - 4y_{i-1} + \alpha_i y_i - 4y_{i+1} + y_{i+2} = 0 \quad (2.20)$$

$$\alpha_i = 6 + \frac{k_{hi} L^4 B}{E_p I_p n^4} \quad (2.21)$$

where,

n = number of intervals throughout the length of pile

$k_{hi}$  = coefficient of horizontal subgrade reaction at point i.

Equation (2.20) is applied at all the nodes of the elements of the pile as shown in Fig 2.6

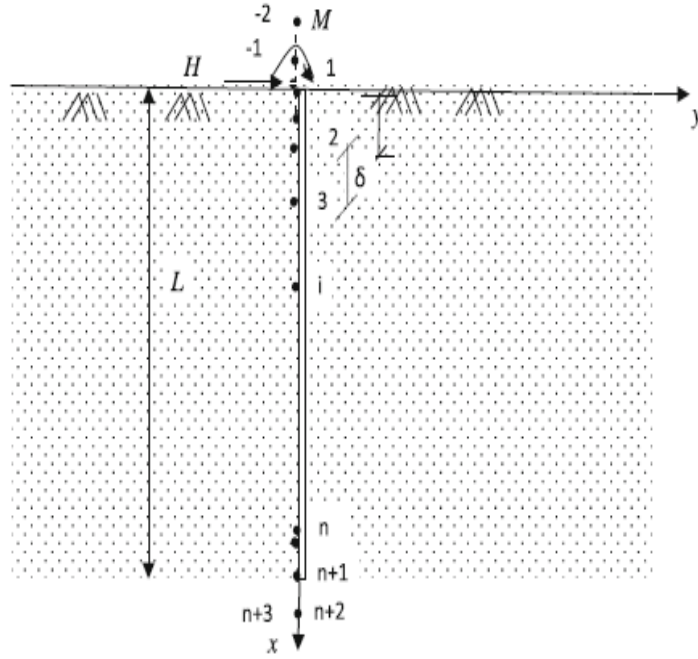


Figure 2.6: Distribution of nodes and elements along the length of the pile (Poulos & Davis, 1980)

Free head pile:

$$\text{Shear force, } E_p I_p \frac{d^3 y}{dx^3} = Q_E \quad (2.22)$$

Thus,

$$-y_{-2} + 2y_{-1} - 2y_2 + y_3 = \frac{Q_E L^3}{E_p I_p n^3} \quad (2.23)$$

$$\text{Moment: } E_p I_p \frac{d^2 y}{dx^2} = M_E \quad (2.24)$$

$$\text{Hence, } y_2 - 2y_1 + y_{-1} = \frac{M_E L^2}{E_p I_p n^2} \quad (2.25)$$

Fixed head pile:

$$\text{Shear force, } E_p I_p \frac{d^3 y}{dx^3} = Q_E \quad (2.26)$$

$$-y_{-2} + 2y_{-1} - 2y_2 + y_3 = \frac{Q_E L^3}{E_p I_p n^3} \quad (2.27)$$

Rotation:

$$E_p I_p \frac{dy}{dx} = 0 \quad (2.28)$$

$$\text{Hence } y_2 - y_{-1} = 0 \quad (2.29)$$

For floating piles shear force and moment at pile tip is zero

$$-y_{n-1} + 2y_n - 2y_{n+2} + y_{n+3} = 0 \quad (2.30)$$

$$y_n - 2y_{n+1} + y_{n+2} = 0 \quad (2.31)$$

Thus the equations are framed for every node of the pile and then when these are solved using Matlab, the deflections at the respective nodes of the pile are obtained. Of all these nodes, the maximum deflection is obtained at the free end of the free headed pile which is of primary interest.

# Chapter 3

## Numerical Modelling

### 3.1 General

PLAXIS 3D is a finite element package intended for three-dimensional analysis of deformation and stability in geotechnical engineering. It is equipped with features to deal with various aspects of complex geotechnical structures and construction processes using robust and theoretically sound computational procedures.

With PLAXIS 3D, complex geometry of soil and structures can be defined in two different modes. These modes are specifically defined for soil or structural modeling. Independent solid models can automatically be intersected and meshed. The staged constructions mode enables a realistic simulation of construction and excavation processes by activating and deactivating soil volume clusters and structural objects, application of loads, changing of water tables, etc. PLAXIS 3D is a user friendly 3d geotechnical program offering flexible and interoperable geometry, realistic simulation of construction stages, a robust and reliable calculation kernel, and comprehensive and detailed post-processing, making it a complete solution for daily geotechnical design and analysis.

### 3.2 Material Models

The mechanical behaviour of soils may be modelled at various degrees of accuracy. Hooke's law of linear, isotropic elasticity, for example may be thought of as the simplest available stress-strain relationship. As it involves only two parameters, i.e., Young's modulus  $E$  and Poisson's ratio, it is generally too crude to capture essential features of soil and rock behaviour. For modelling massive structural elements and bedrock layers, however, linear elasticity tends to be appropriate. Out of several models only linear elastic and Mohr-coulomb models are used in this work. So the overview of these models is:

#### 3.2.1 Linear Elastic model (LE)

The linear elastic model is based on Hooke's law of isotropic elasticity. It involves two basic elastic parameters, i.e., Young's modulus  $E$  and Poisson's ratio  $\mu$ . The Linear Elastic (LE) soil model is the most basic and straight forward soil model. The LE soil model is perfectly elastic and does not account for plastic deformations, therefore soil failure is not accounted for. A LE model should be applied where users are confident that elastic soil conditions are present or where there is sufficiently high factor of safety against failure. LE model should be used only for small strain response. When applied to pile foundations, a LE soil model considerably over-estimates pile-to-pile interaction and thus can provide an overly-conservative estimate of pile group settlement.

### **3.2.2 Mohr-Coulomb model (MC)**

The Mohr-Coulomb (MC) soil model is an advancement on the LE soil model in that soil failure is accounted for according to the Mohr-Coulomb failure criterion i.e.,  $\tau = c + \sigma \tan(\phi)$ . The linear elastic perfectly-plastic Mohr-Coulomb model involves five input parameters, i.e.,  $E$  and  $\mu$  for soil elasticity;  $\phi$  and  $c$  for plasticity and  $\phi$  as the angle of dilatancy. This Mohr-coulomb model represents a 'first-order' approximation of soil rock behaviour. It is recommended to use this model for a first analysis of the problem considered. For each layer one estimates a constant average stiffness or a stiffness that increases linearly with depth. Due to this stiffness, computations tend to be relatively fast and one obtains a first estimate of deformations.

### **3.3 Limitations**

Although much care has been taken for the development of PLAXIS code and its soil models, the simulation of reality remains an approximation, which implicitly involves some inevitable numerical and modelling errors. Moreover, the accuracy at which reality is approximated depends highly on the expertise of the user regarding the modelling of the problem, the understanding of the soil models and their limitations, the selection of model parameters, and the ability to judge the reliability of the computational results.

Some of the limitations of the currently using models are listed below:

#### **3.3.1 Linear Elastic Model**

Soil behaviour is highly non-linear and irreversible. The linear elastic model is insufficient to capture the essential features of soil. The use of the linear elastic model may, however be considered to model strong massive structures in the soil or bedrock layers. Stress states in the linear elastic model are not limited in any way, which means that the model shows infinite strength. Be careful using this model for materials that are loaded up to their material strength.

#### **3.3.2 Mohr-Coulomb Model**

The linear elastic perfectly-plastic Mohr-Coulomb model is a first order model that includes only a limited number of features that soil behaviour shows in reality. Although the increase of stiffness with depth can be taken into account, the Mohr-Coulomb model does neither include stress-dependency nor stress-path dependency nor strain dependency of stiffness or anisotropic stiffness. In general, effective stress states at failure are quite well described using the Mohr-Coulomb failure criterion with effective strength parameters. For undrained materials, the Mohr-Coulomb model may be used with the friction angle set to zero degrees and the cohesion set to  $c_u$ , to enable a direct control of undrained shear strength. In this case note that the model does not automatically include the increase of shear strength with consolidation

### **3.4 Modelling of Soil Behaviour**

Soil and rock tend to behave in a highly non-linear way under load. This non-linear stress-strain behaviour can be modelled at several levels of sophistication. Clearly, the number of model parameters increases with the level of sophistication. The well-known Mohr-Coulomb model can be considered as a first order approximation of real soil behaviour. This elastic perfectly-plastic model requires five basic input parameters, namely Young's modulus,  $E$ , Poisson's ratio,  $\mu$ , cohesion,  $c$ , friction angle,  $\phi$ , and dilatancy angle,  $\psi$ . As geotechnical engineers tend to be familiar with the above five parameters and rarely have any data on other soil parameters, attention will be focused here on this basic soil model. PLAXIS also supports some advanced soil models.

### **3.5 Basic Model Parameters in Relation to Real Soil Behaviour**

To understand the five basic model parameters, typical stress-strain curves as obtained from standard drained triaxial tests are considered (Figure 3.1). The material has been compressed isotropically up to some confining stress  $\sigma_3$ . After this, the axial pressure  $\sigma_1$  is increased whilst the radial stress is kept constant. In this second stage of loading geomaterials tend to produce curves as shown in Figure 3.1a. The increase in the volume (or volumetric strain) is typical for sands and is also frequently observed for rocks. Figure 3.1b shows the test results put into an idealised form using the Mohr-Coulomb model. The figure gives an indication of the meaning and influence of the five basic model parameters. Note that the dilatancy angle  $\psi$  is needed to model the irreversible increase in volume.

### **3.6 Model**

In PLAXIS 3D Foundation, the generation of a 3D finite element model begins with the creation of a geometry model. A geometry model is a composition of bore holes and horizontal work planes. The work planes are used to define geometry lines and structures contour lines along the elevation level. The bore holes are used to define the local soil stratigraphy, ground surface level and pore pressure distribution. From the geometry model, a 2D mesh is generated first, after which an extension into the third dimension (the y-direction) can be made. PLAXIS 3D Foundation automatically generates this 3D mesh, taking into account the information from the work planes and the bore holes. Thus the full 3D geometry model including all objects appearing in any work plane at any construction stage has been defined. PLAXIS 3D Foundation has various special elements to model all kinds of structures, such as beam, floor, and wall elements. However, no special type of element is applied to model the pile. Representing the pile with 3D solid element limits a number of piles can be modelled due to the memory capacity of the PC.



### 3.7 Elements

In PLAXIS 3D Foundation, the basic soil elements of a 3D finite element mesh are the 15-node wedge elements. These elements are generated from the 6-node triangular elements as generated in the 2D mesh. Due to the presence of non-horizontal soil layers, some 15-node wedge elements may degenerate to 13-node pyramid elements or even to 10-node tetrahedral elements. The 15-node wedge element is composed of 6- node triangles in horizontal direction and 8-node quadrilaterals in vertical direction. The accuracy of the 15-node wedge element and the compatible structural elements are comparable with the 6-node triangular elements in a 2D PLAXIS analysis. Higher order element types, for example comparable with the 15-node triangle in a 2D analysis, are not considered for a 3D foundation analysis because this will lead to large memory consumption and unacceptable calculation times.

### 3.8 Mesh Properties

PLAXIS allows for a fully automatic generation of finite element mesh. The generation of the mesh is based on a robust triangulation procedure, which results in “unstructured” meshes. These meshes may look disorderly, but the numerical performance of such meshes may yield better results than for regular structured meshes. The mesh generator requires a general meshing parameter which represents the average element size,  $l_e$ , computed based on the outer geometry dimensions ( $x_{min}$ ,  $x_{max}$ ,  $y_{min}$ ,  $y_{max}$ ) using the following relationship:

$$l_e = \sqrt{\frac{(x_{max} - x_{min})(y_{max} - y_{min})}{n_c}} \quad (3.1)$$

where  $n_c = 25$  (very coarse mesh)

= 50 (coarse mesh)

= 100 (medium mesh)

= 200 (fine mesh)

= 400 (very fine mesh)

### 3.9 Staged Construction

PLAXIS allows for the option to change the geometrical configurations by activating and deactivating clusters or structural objects, which is convenient to simulate the installation of the pile as a material wish-in-place, for the purpose of the study in the following. Also the program allows an accurate and realistic simulation of the actual construction stages such as the loading changes of the reaction system during the process of pile loading. The material properties and pore pressure distribution can also be changed at each stage.

### 3.10 Mesh Convergence and Boundary Conditions Study

This study is to fix the size of mesh and the boundary dimensions of the soil model. The study is carried out using the field data of Incheon site in South Korea performed by Youngho Kim, Sangseom Jeong in 2010 on laterally loaded piles.

A 3D FE model to simulate the response of a single pile under lateral loads in clay using PLAXIS 3D Foundation is presented here. The details of the soil stratigraphy are shown in the following PLAXIS model Fig 3.2

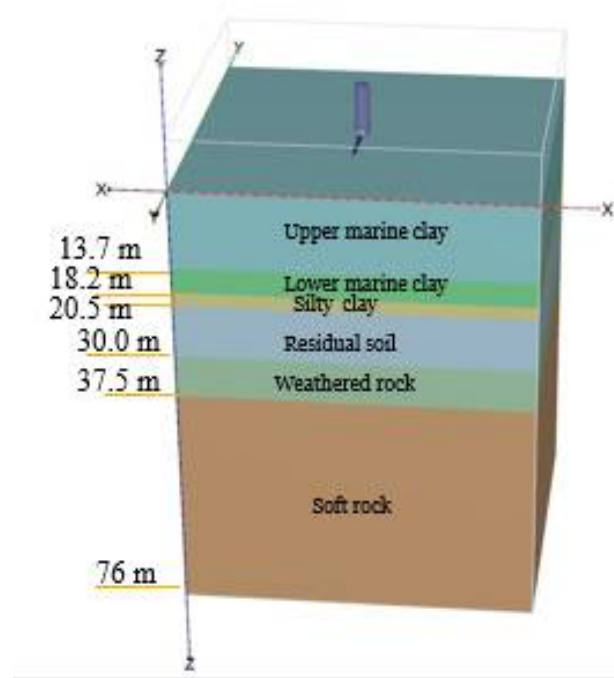


Figure 3.1: PLAXIS 3D model showing soil stratification of Incheon site

A pile of diameter 2.4m and embedded length 45m is driven into the soil with an eccentricity of 9m above the surface of the ground. The overall dimensions of the model boundaries comprise a width of 11 times the pile diameter ( $D$ ) from the pile centre and a height equal to the pile length ( $L$ ) plus a further  $0.7 L$  below the pile-toe level. These dimensions were considered adequate to eliminate the influence of boundary effects on the pile performance. The mesh consists of 15-node wedge elements, with a total of 17,500 nodes.

The material properties of the soil layers and drilled shaft are shown in Table 3.1

Table 3.1: Material properties

Material	Model	$\gamma_{sat}$ (k N/m <sup>3</sup> )	$\phi$	$C_u$ (k Pa)	$\nu$	E (M Pa)	$R_{inter}$
Drilled shaft	Elastic	25	-	-	0.2	36400	-
Upper clay	M.C	17.5	-	15-30	0.49	3-15	0.50
Lower clay	M.C.	17.5	-	30-50	0.49	15-25	0.50
Silty clay	M.C.	17.8	-	70	0.49	27	
Residual soil	M.C.	18	34	-	0.49	35	0.70
Weathered rock	Elastic	20.2	-	-	0.25	110	-
Soft rock	elastic	20.5	-	-	0.25	200	-

The deformation profile along the depth for loads 425kN and 765kN are obtained from PLAXIS for various mesh sizes and are compared with field values. It was observed that the model with medium sized mesh gave converging results. Fig 3.3 shows the medium sized mesh with finer mesh around the pile

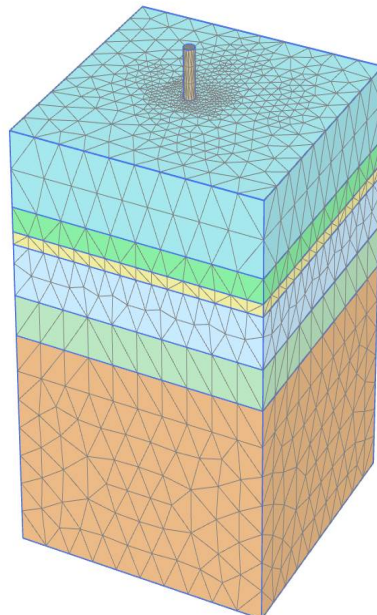
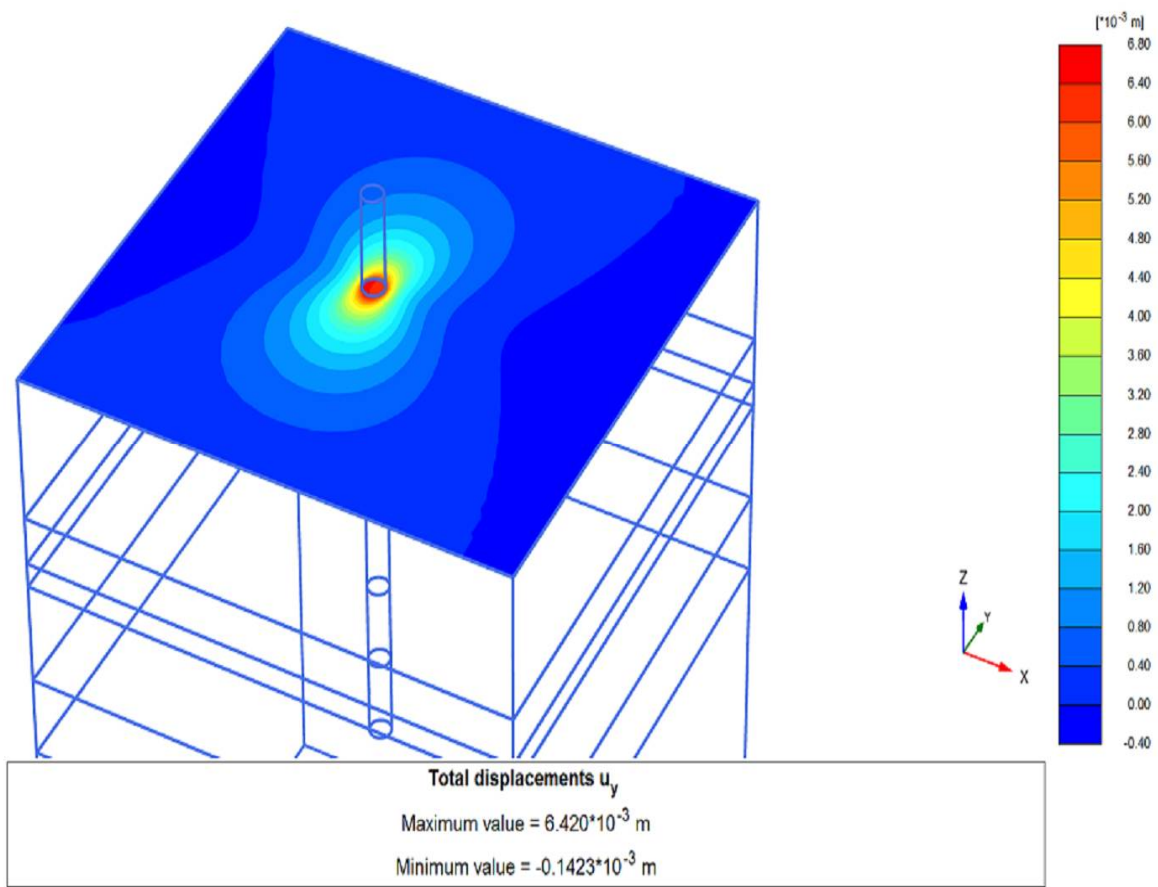
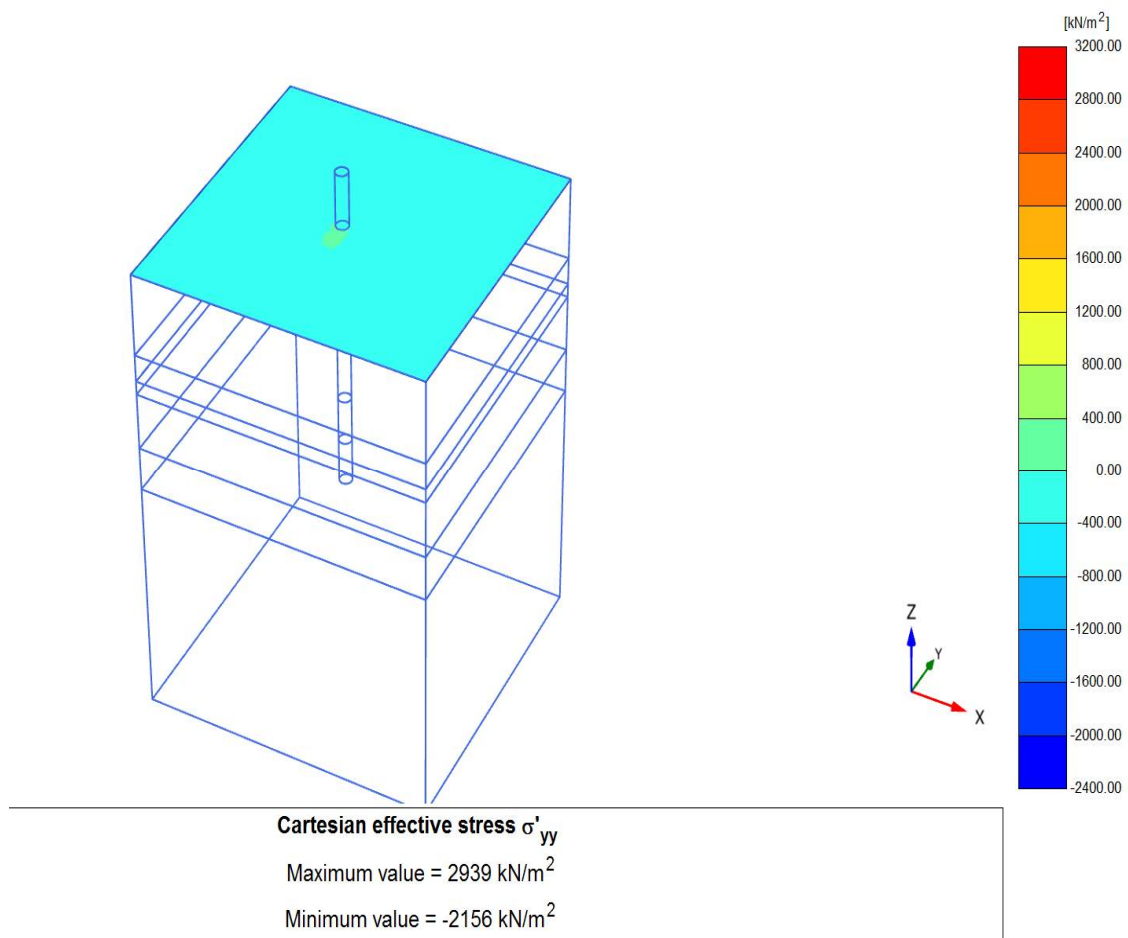


Figure 3.2: Medium sized mesh for Incheon site model



**Figure 3.3: Deformation Contours**

From the above deformation contours it can be observed that the max deformation contour in red colour is around the pile, while the deformation contour near the boundaries have zero deformation.



**Figure 3.4: Stress Contours**

From Fig 3.4 it is observed that the stress contour near the boundaries is having a value of 0 kPa. It can be inferred that the deformations and stresses are well within the boundaries. So the given boundary conditions can be adopted for further modelling.

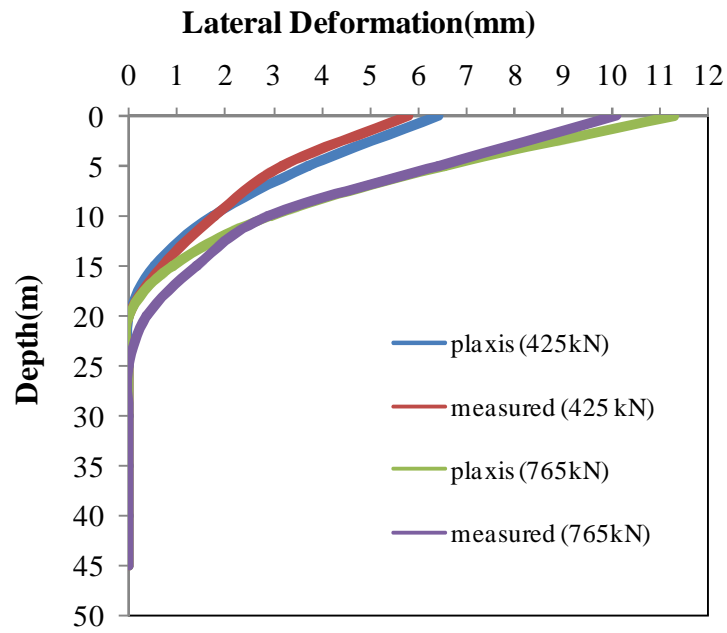


**Figure 3.5: Comparison of lateral deformations along the depth**

From the above Fig 3.5 it can be observed that the lateral deformation at depths greater than 20m is almost zero. PLAXIS results and measured field results are coinciding except for the free head deformation. PLAXIS results are overestimating the maximum lateral deformation which occurs at the top for a free head pile. Also this deviation is very small and it can be neglected. Therefore PLAXIS could be used for further research to get approximately closer values compared to field results.

# Chapter 4

## Results and Discussion - Part 1 Sands

### 4.1 Comparison of Pile Responses of IS Code Method, Subgrade Reaction Method and Numerical Modeling for Sands

To know the trend of deformations obtained from IS code method and subgrade reaction method, they are compared with the deformations obtained from PLAXIS 3D. This comparison is done for modulus of subgrade reaction of soil ranging from 2600kN/m<sup>3</sup> to 12500kN/m<sup>3</sup> with total of six cases where three are for dry soil type and the other three for submerged soil type. For IS code method and subgrade reaction method the key parameter for determining deformations is modulus of subgrade reaction of the soil, whereas in PLAXIS modeling the key parameter is stiffness of the soil.

Relation between modulus of subgrade reaction and soil stiffness:

A more widely accepted relation between modulus of subgrade reaction and material properties of elastic soils, suggested by Vesic (1961) is:

$$k_s = \frac{(0.65 E_p)}{B(1-\mu_s^2)} \left[ \frac{E_s B^4}{E_p I_p} \right]^{1/12} \quad (4.1)$$

FE method solution proposed by Zhou et al.(2011)

$$k_s = \frac{1.098 E_s}{D} \left( \frac{D}{D_{ref}} \right)^{0.3} \left[ \frac{E_s D^4}{E_p I_p} \right]^{1/12} \quad (4.2)$$

The dimensions of the soil model are shown in Fig 4.1. A pile of length 5m circular in cross section with 0.5m diameter is used. The moment of inertia of the pile is 0.003068 m<sup>4</sup>. The stiffness of the pile is 27.4E6 kN/m<sup>2</sup>. A point load of 100kN is applied at the top of the pile.

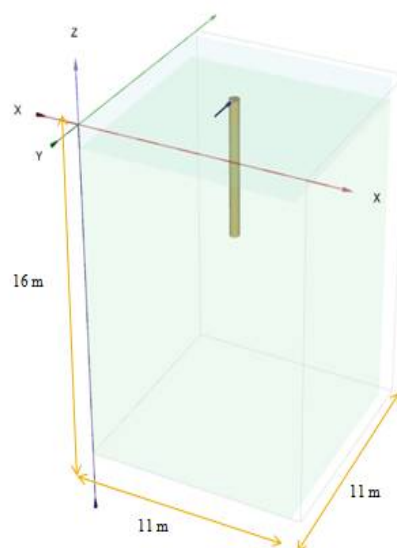


Figure 4.1: Soil-pile model

#### 4.1.1 Maximum Lateral Deformations

The soil stiffness values for the respective modulus of subgrade reactions are shown below. The deformations obtained for different soil stiffness values from IS code method, subgrade reaction method and numerical modeling when a load of 100kN is applied are shown in Table 4.1:

Table 4.1: Deformations obtained from various methods

Soil type	Modulus of subgrade reaction (kN/m <sup>3</sup> )	Soil Stiffness E <sub>s</sub> (kN/m <sup>2</sup> )		Poisson's ratio	Max Deformation (mm)			
		Vesic (1961)	Zhou et al. (2011)		IS Code	S.R method	Plaxis – 3D	
							Vesic (1961)	Zhou et al. (2011)
Dry	2600	3109	2466	0.25	42	57	31	38
	7700	8241	6717	0.30	25	21	15	17
	20000	19234	16212	0.35	16	9.5	8.7	9.5
Submerged	1500	1872	1484	0.25	55	74	59	73
	5200	5736	4675	0.30	30	30	22	26
	12500	12464	10506	0.35	20	14	12	13.6



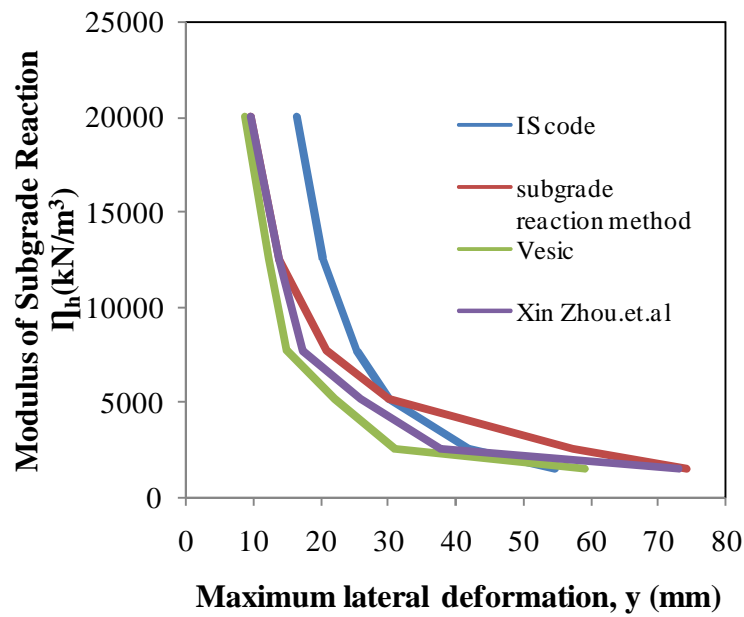


**Figure 4.2: Maximum lateral deformation obtained from different methods**

The graphical representation of Table 4.1 is shown in Fig 4.2. The deformations obtained from IS code are over estimating for higher values of  $\Gamma_h$  when compared to numerical modeling, whereas for lower values of  $\Gamma_h$  the difference is less. Overall the deviation of the deformations from IS code when compared to numerical modeling is about 35% for lower values of  $\Gamma_h$  and about 50% for higher values of  $\Gamma_h$ . In subgrade reaction method the trend is reverse. For lower values of  $\Gamma_h$  the deviation is 50% whereas for higher values of  $\Gamma_h$  it is 15%.

#### 4.1.2 Bending Moment

The bending moment profile along the depth of the pile from the three methods is shown in Fig 4.3. It can be observed that the bending moment profile obtained from subgrade reaction method and numerical modeling are almost coinciding whereas for IS code method it is increasing linearly with maximum bending moment at the fixed end of the cantilever.

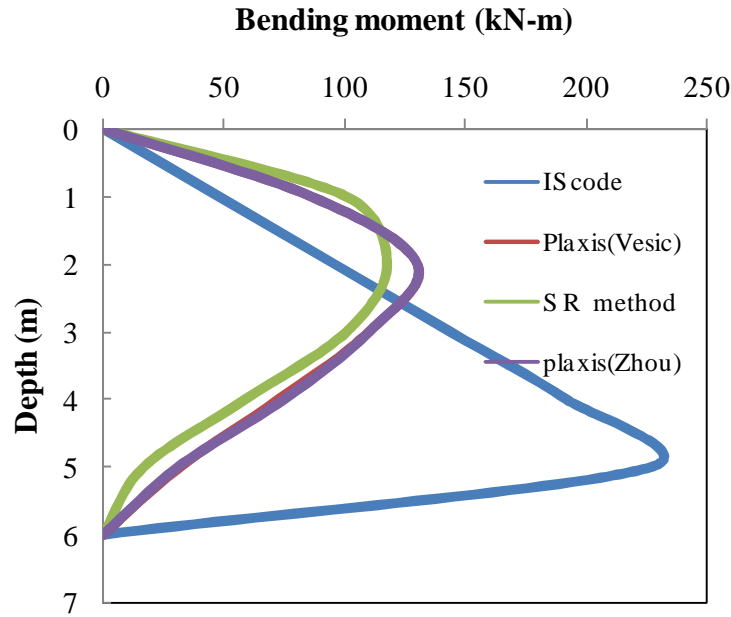


Figure 4.3: Bending moment distribution along the depth of the pile

Maximum bending moment obtained from IS code method is found to be 50% higher than that from numerical modeling and the maximum bending moment obtained from subgrade reaction method is comparable with that of numerical modeling and the deviation is within 10%.

#### 4.2 Normalised Charts for Sands

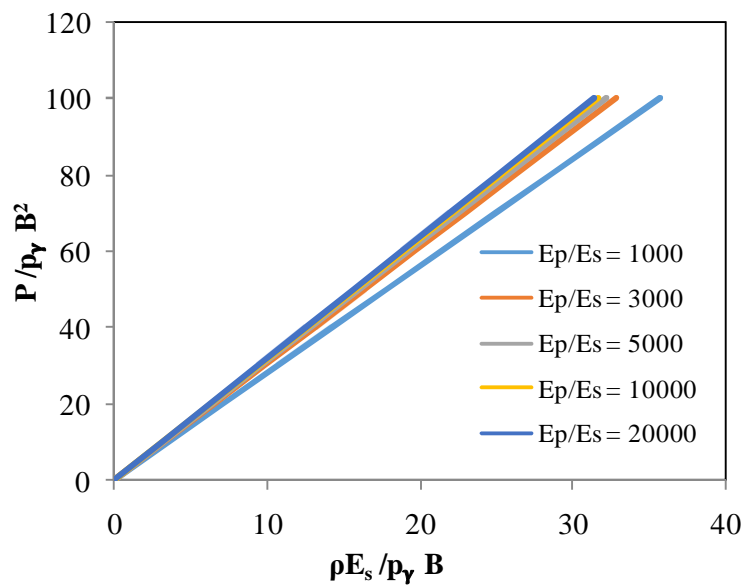
To overcome the above mentioned huge variations of deformations obtained from IS code method and subgrade reaction method, design charts of load against deformations are to be proposed using FE numerical modelling. If these charts are normalised then they could be used easily for other properties and geometries other than that used for modelling. Load is normalised by a reference stress  $p_y$  (say 100kPa) and square of diameter. Thus the normalized term for load is  $P / p_y B^2$ . Maximum lateral deformation for a particular load is normalised by stiffness of the soil  $E_s$ , reference stress as mentioned above and diameter of the pile  $B$ . The normalised term is  $\rho E_s / p_y B$ . The charts are proposed for various pile lengths, diameters, eccentricities, pile stiffness and soil stiffness.

### 4.2.1 Using LE Model

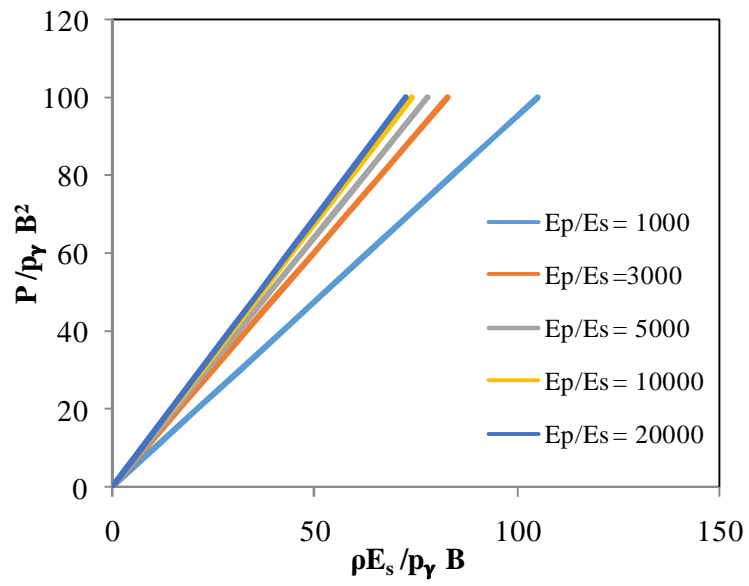
The stiffness values of piles ranges from  $20 \cdot 10^6$  kPa to  $200 \cdot 10^6$  kPa and the stiffness values of sands ranges from  $7 \cdot 10^3$  kPa to  $100 \cdot 10^3$  kPa. Considering the extreme combinations of  $E_p$  and  $E_s$  the charts are proposed for  $E_p/E_s$  ratios of 1000, 3000, 5000, 10000 and 20000. The unit weight of sand is considered as  $18 \text{ kN/m}^3$  and the poisons ratio of 0.3 is taken for modelling. The poisons ratio for pile is 0.15. For pile the drainage conditions are taken as non-porous. Drained behaviour of sands is considered. The boundary lengths and mesh size are implemented as mentioned above in 3<sup>rd</sup> chapter. The charts are proposed for L/B ratios 5, 10, 15 and 20. Further for each L/B ratio charts are proposed for different e/B ratios 0, 2, 4 and 6.

#### *Normalised charts for L/B = 5*

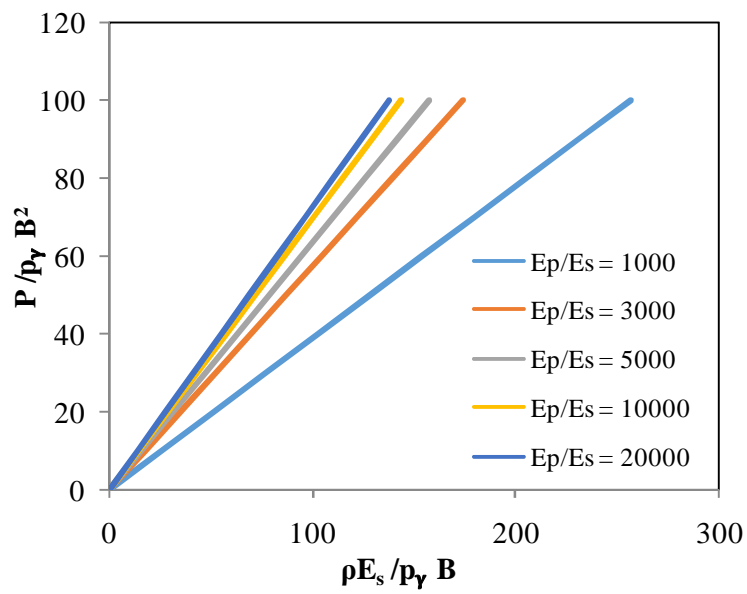
For a L/B ratio of 5 charts are proposed for e/B ratios of 0, 2, 4 and 6. The normalised charts for various e/B ratios and  $E_p/E_s$  ratios for L/B = 5 are shown in Fig 4.4



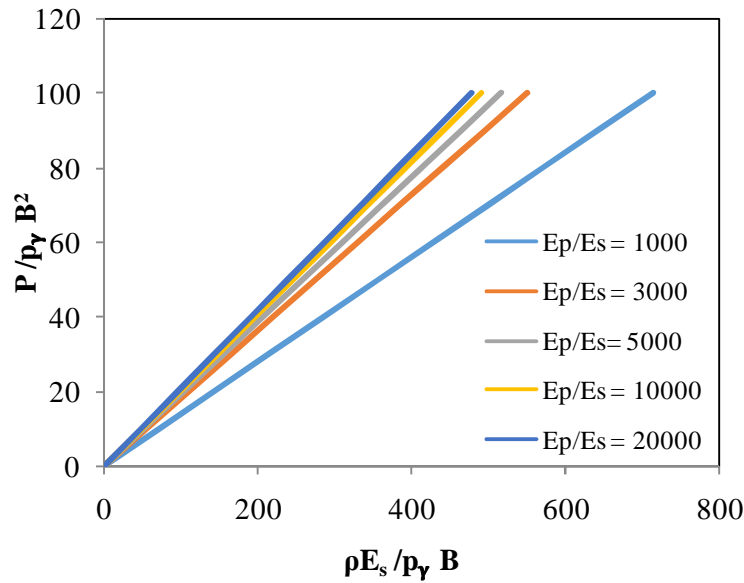
(a)  $e/B = 0$



(b)  $e/B = 2$



(c)  $e/B = 4$



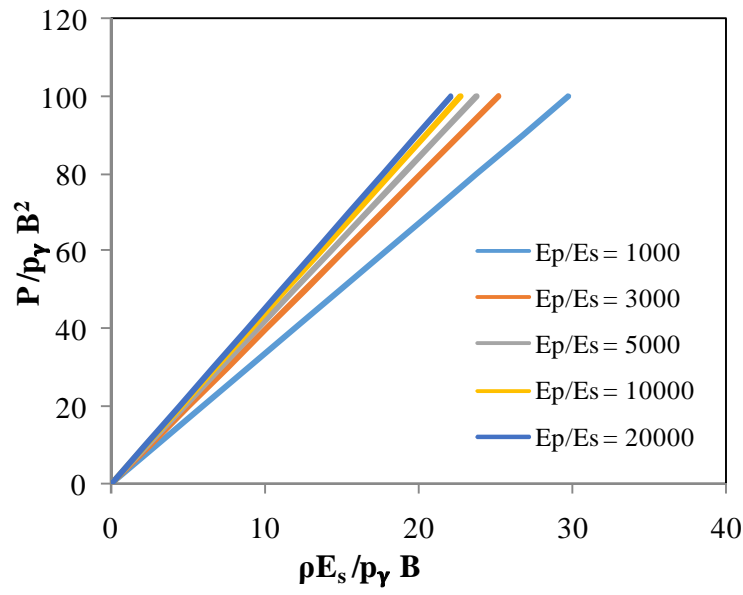
(d)  $e/B = 6$

**Figure 4.4: Normalised load- deformation charts for sands for  $L/B = 5$  and (a)  $e/B = 0$  (b)  $e/B = 2$  (c)  $e/B = 4$  and (d)  $e/B = 6$**

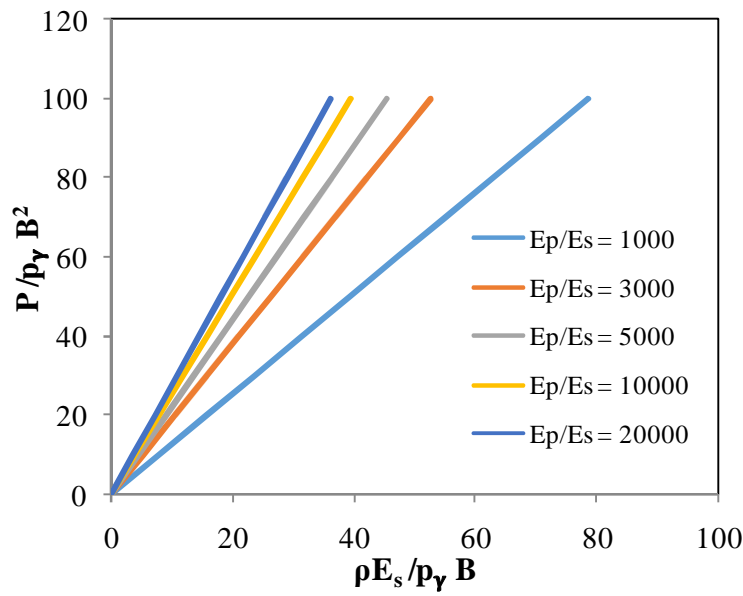
As linear elastic model is incorporated it can be observed that all the above charts are linear. The deformations are increasing with increasing eccentricities because that part of the pile above surface doesn't have any resistance offered by soil. For  $E_p/E_s$  ratios of 10000 and 20000 the graphs are almost coinciding for all the four cases because of same  $E_s$  value for both of them. Similarly for  $E_p/E_s$  ratios of 3000 and 5000 the graphs are almost coinciding for all the four cases because of same  $E_s$  value for both of them. That means though there is much difference in  $E_p$  value the deformations are not varying much due to same  $E_s$  value. Lesser the  $E_p/E_s$  ratio greater is the value of  $E_s$  and greater is the value of the term  $\rho E_s / p_y B$  and lower is the deformation. The graph of  $E_p/E_s = 1000$  is separating out from the rest in all the cases because of high  $E_s$  value.

#### ***Normalised charts for $L/B = 10$***

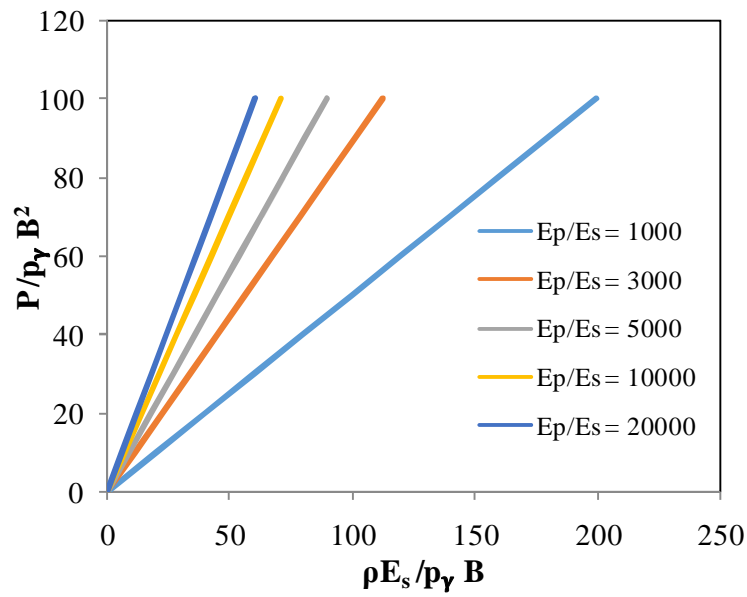
For a  $L/B$  ratio of 10 charts are proposed for  $e/B$  ratios of 0, 2, 4 and 6. The normalised charts for various  $e/B$  ratios and  $E_p/E_s$  ratios for  $L/B = 10$  are shown in Fig 4.5



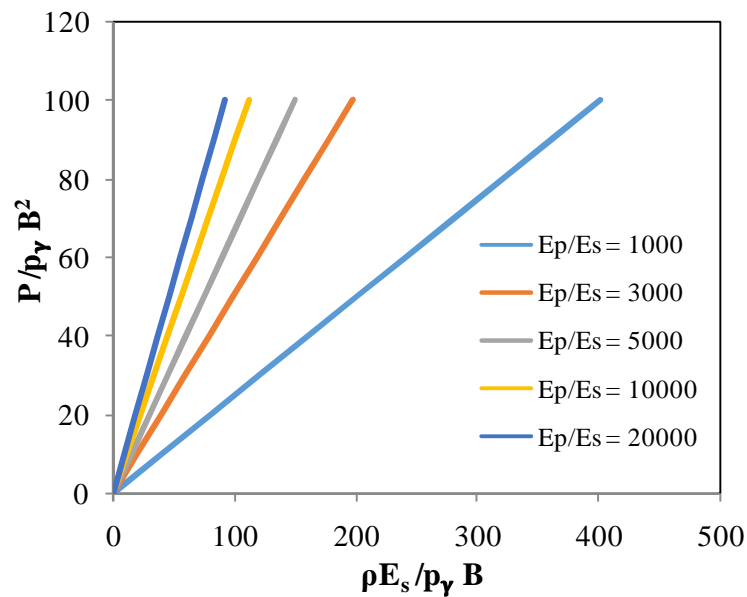
(a)  $e/B = 0$



(b)  $e/B = 2$



(c)  $e/B = 4$



(d)  $e/B = 6$

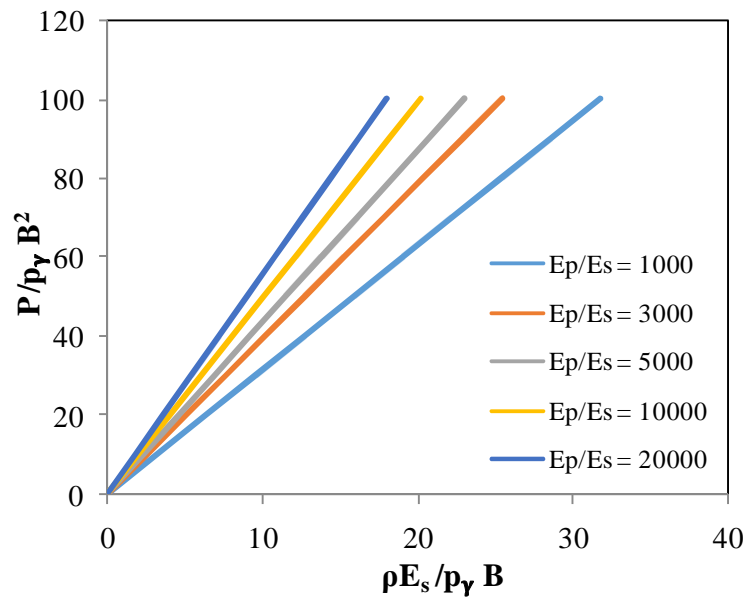
**Figure 4.5: Normalised load- deformation charts for sands for  $L/B = 10$  and (a)  $e/B = 0$  (b)  $e/B = 2$  (c)  $e/B = 4$  and (d)  $e/B = 6$**

The  $E_p$  and  $E_s$  values for various graphs under  $L/B = 10$  are same as that used for  $L/B = 5$ . So we can directly use the term deformation term instead of normalised term for comparison. It can be observed that the deformations are decreasing with increasing length. For a given length of pile the deformations are increasing with increasing eccentricity. Also for a given graph say  $e/B = 6$  (4.5 (d))

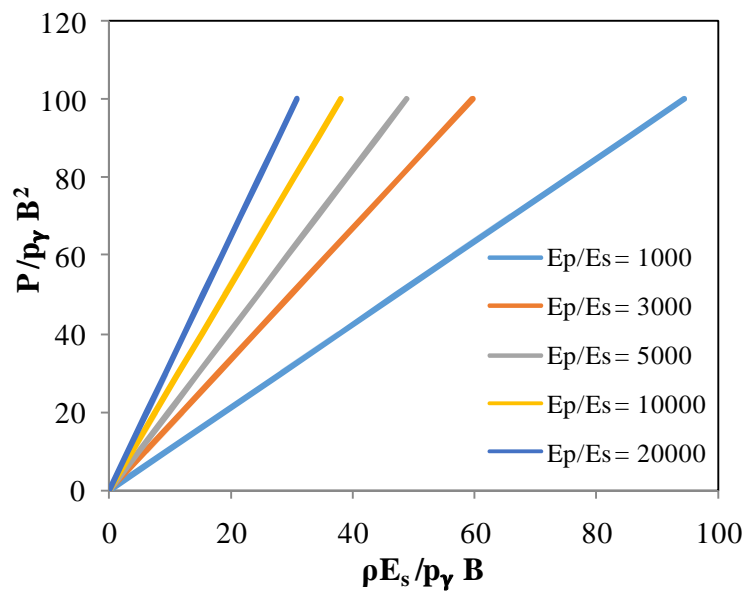
for a normalised load of 60 the maximum normalised deformation is for  $E_p/E_s = 1000$ , that means it have the lowest deformation of all the other graphs because  $\rho$  is inversely proportional to  $E_s$ .

**Normalised charts for  $L/B = 15$**

For a  $L/B$  ratio of 15 charts are proposed for  $e/B$  ratios of 0, 2, 4 and 6. The normalised charts for various  $e/B$  ratios and  $E_p/E_s$  ratios for  $L/B = 15$  are shown in Fig 4.6

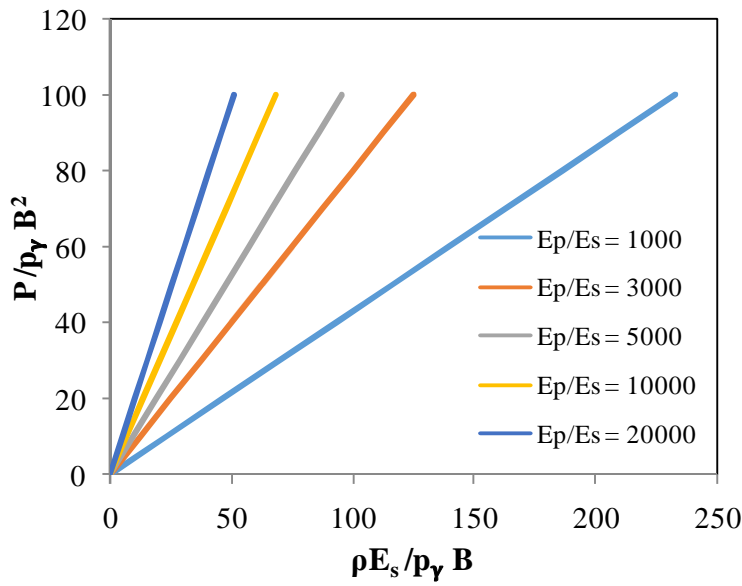


(a)  $e/B = 0$

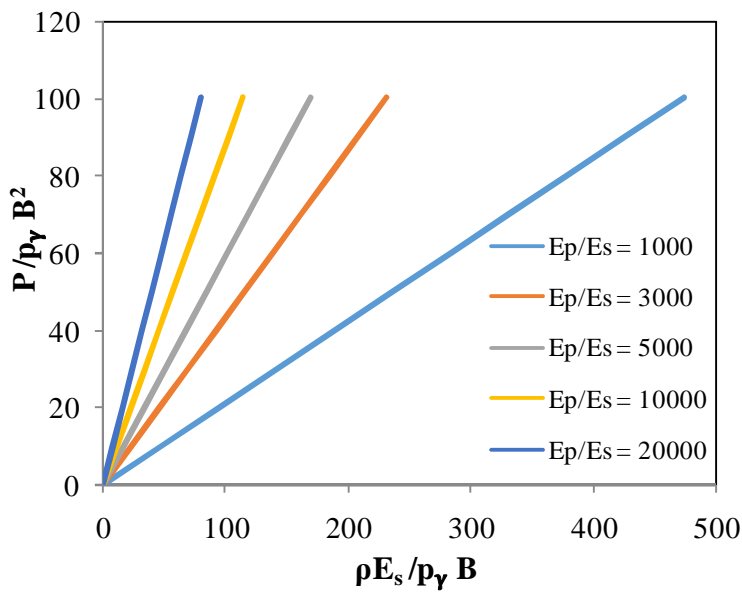


(b)  $e/B = 2$





(c)  $e/B = 4$



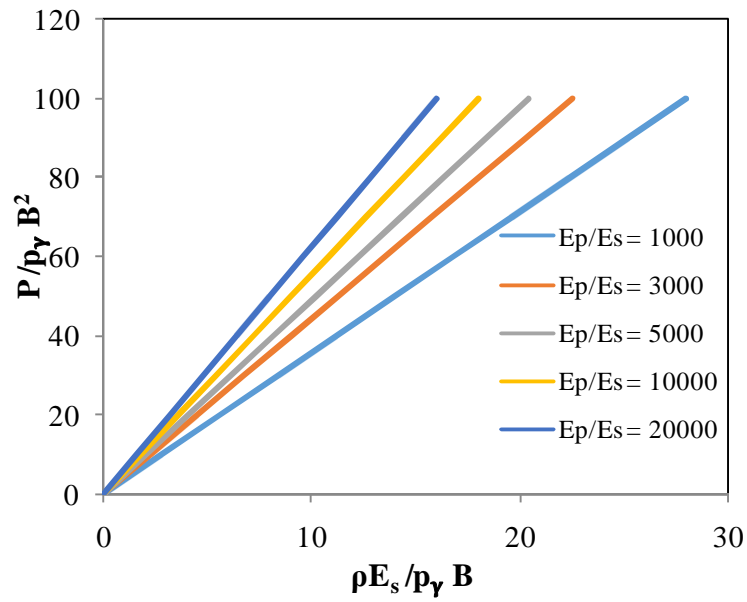
(d)  $e/B = 6$

**Figure 4.6: Normalised load- deformation charts for sands for  $L/B = 15$  and (a)  $e/B = 0$  (b)  $e/B = 2$  (c)  $e/B = 4$  and (d)  $e/B = 6$**

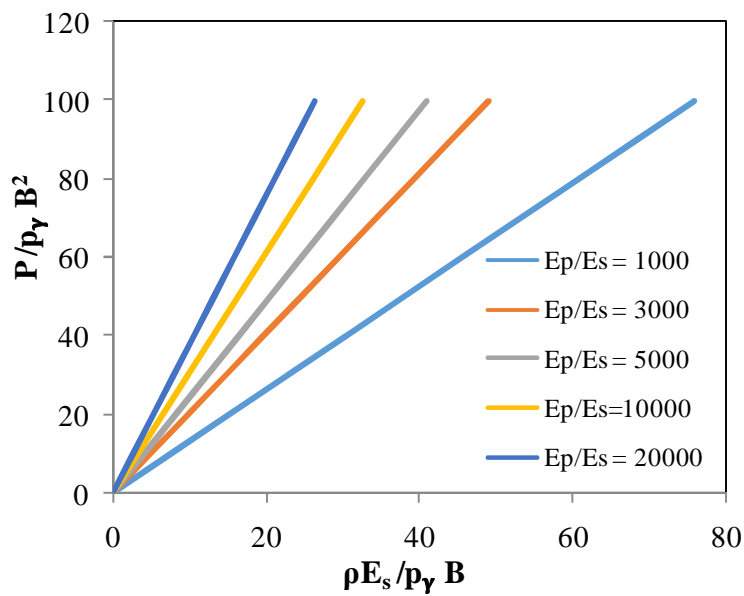
The charts under  $L/B = 15$  have lesser deformations compared to  $L/B = 10$  and  $L/B = 5$  and all the other observations are same as mentioned under  $L/B = 5$  and  $L/B = 10$ .

**Normalised charts for  $L/B = 20$**

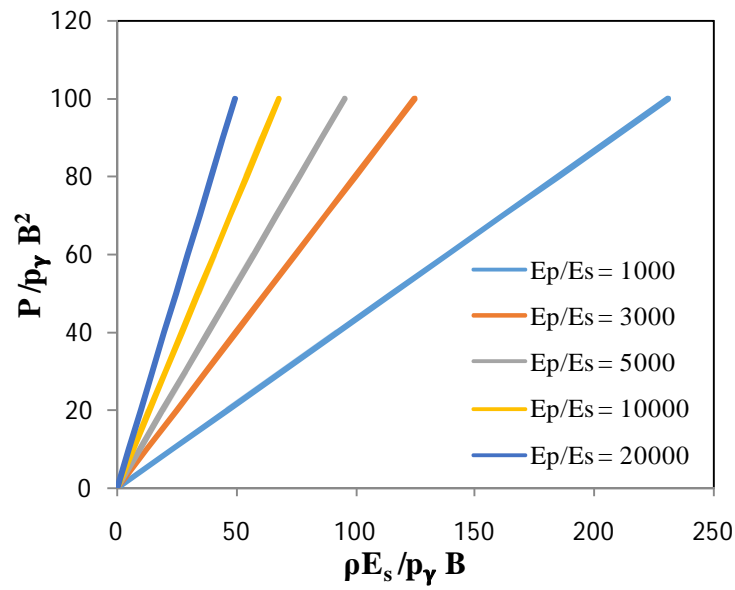
For a  $L/B$  ratio of 20 charts are proposed for  $e/B$  ratios of 0, 2, 4 and 6. The normalised charts for various  $e/B$  ratios and  $E_p/E_s$  ratios for  $L/B = 20$  are shown in Fig 4.7



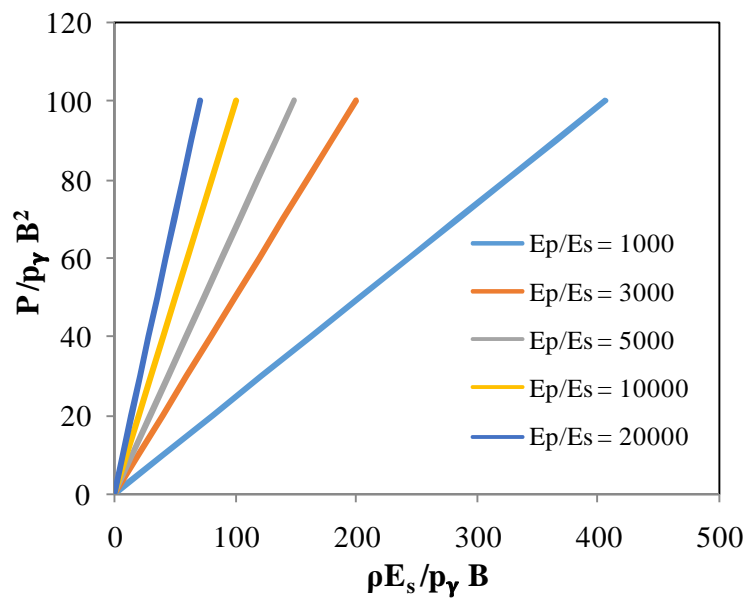
(a)  $e/B = 0$



(b)  $e/B = 2$



(c)  $e/B = 4$



(d)  $e/B = 6$

**Figure 4.7: Normalised load- deformation charts for sands for  $L/B = 20$  and (a)  $e/B = 0$  (b)  $e/B = 2$  (c)  $e/B = 4$  and (d)  $e/B = 6$**

Finally from all the above charts it can be concluded that the charts are all linear as soil is modelled using linear elastic model. For a given length of pile deformations increases with increase in eccentricities. Deformations are decreasing with increase in length because more resistance is offered

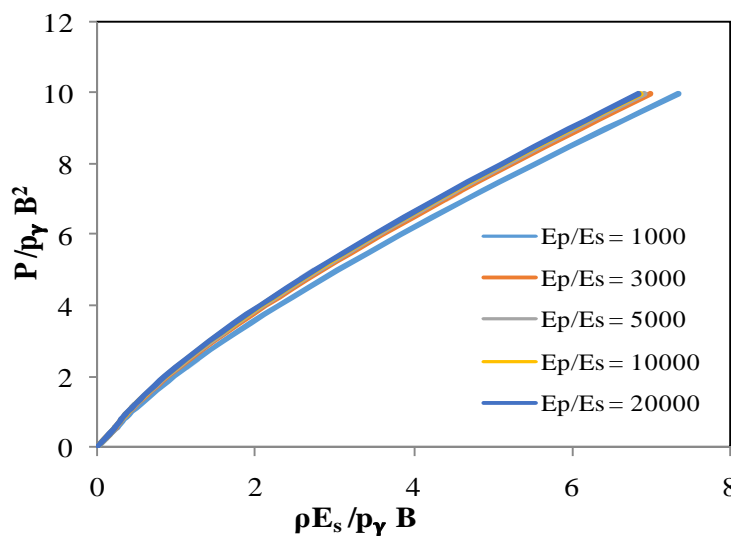
by soil along the length of the pile. It can be observed that the graphs are getting separated with increase in L/B ratio because with increasing L/B ratio  $E_p$  is coming into picture that means its influence is felt. Say for example if the chart 1-a is observed the graphs of  $E_p/E_s = 10000$  and  $E_p/E_s = 20000$  are coinciding whereas if we observe 4-a they are not coinciding and they are distinct. The graphs with lowest  $E_p/E_s$  ratio have the highest  $E_s$  value, highest  $\rho E_s / p_\gamma B$  value and lowest deformation. Similarly the one with highest  $E_p/E_s$  ratio have the lower  $E_s$  value, lower  $\rho E_s / p_\gamma B$  value and highest deformation. Also for a L/B ratio say 5, it is modeled for  $L = 5$  and  $B = 1$ , even if we change the L and B values for the same L/B ratio these charts can be used with error less than 1% between actual numerical modeling and charts. Similarly the charts are applicable for different values of  $E_p$  and  $E_s$  for the same  $E_p/E_s$  ratio. For the same ratio of  $e/B$  with different values of  $e$  and  $B$  other that used for modelling also these charts are applicable.

#### 4.2.2 Using MC Model

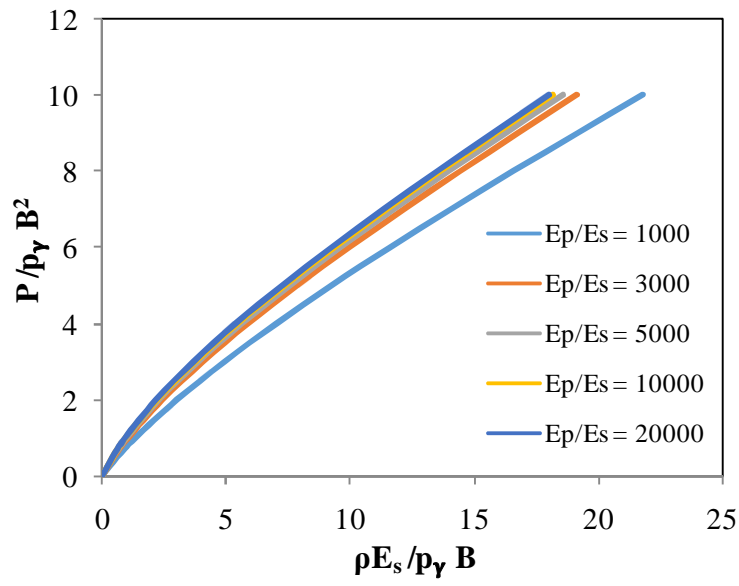
The normalised charts are proposed similar to that of linear elastic charts using Mohr Coulomb model for L/B ratios of 5, 10, 15 and 20,  $e/B$  ratios of 0, 2, 4 and 6,  $E_p/E_s$  ratios of 1000, 3000, 5000, 10000 and 20000. The unit weight of sand is taken as  $18\text{kN/m}^3$ ; a minimum value of cohesion of 2kPa is given for M-C modelling. The angle of internal friction was taken as  $32^\circ$  and dilatancy angle as  $12^\circ$ . The Poisson's ratio of sand is 0.3 and for pile it is 0.15. Modelling and dimensions of the model are similar to linear elastic model.

##### Normalised charts for $L/B = 5$

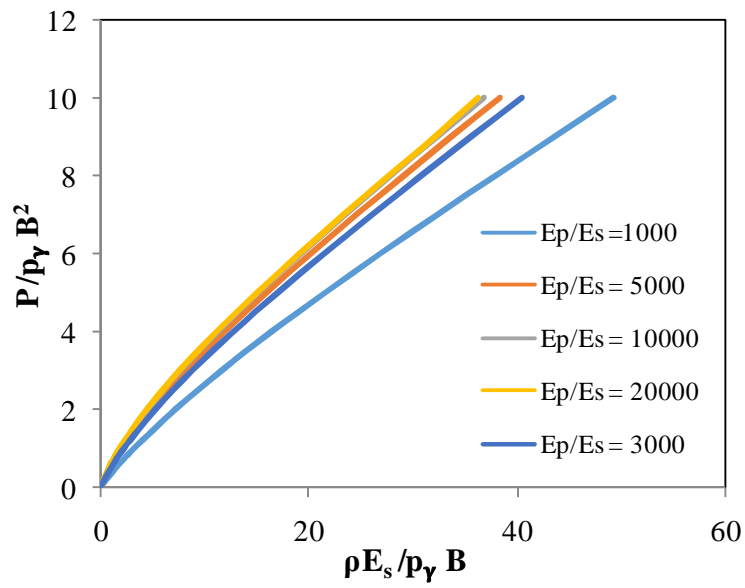
For a L/B ratio of 5 charts are proposed for  $e/B$  ratios of 0, 2, 4 and 6. The normalised charts for various  $e/B$  ratios and  $E_p/E_s$  ratios for  $L/B = 5$  are shown in Fig 4.8



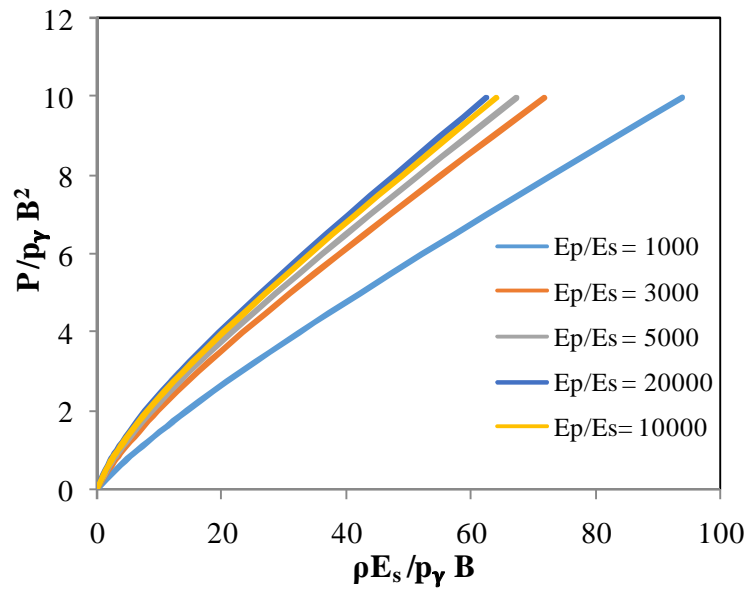
(a)  $e/B = 0$



(b)  $e/B = 2$



(c)  $e/B = 4$



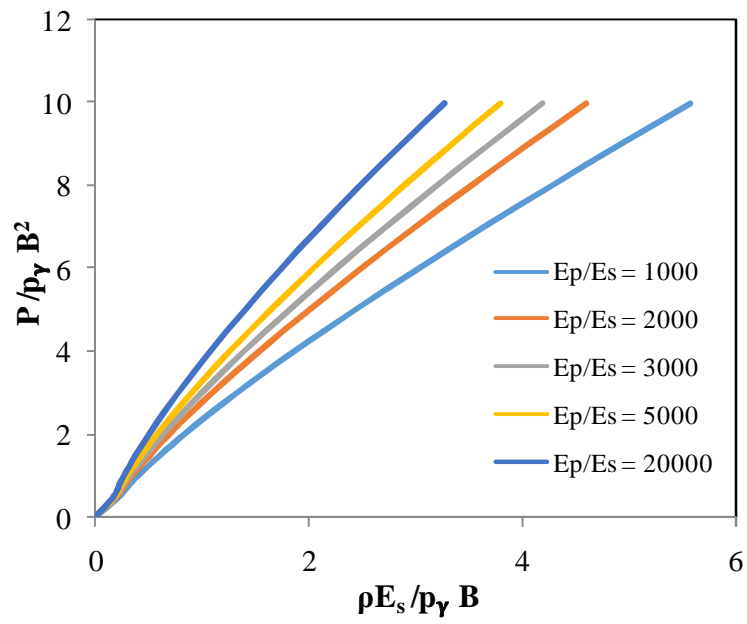
(d)  $e/B = 6$

**Figure 4.8: Normalised load- deformation charts for  $L/B = 5$  and (a)  $e/B = 0$  (b)  $e/B = 2$  (c)  $e/B = 4$  and (d)  $e/B = 6$**

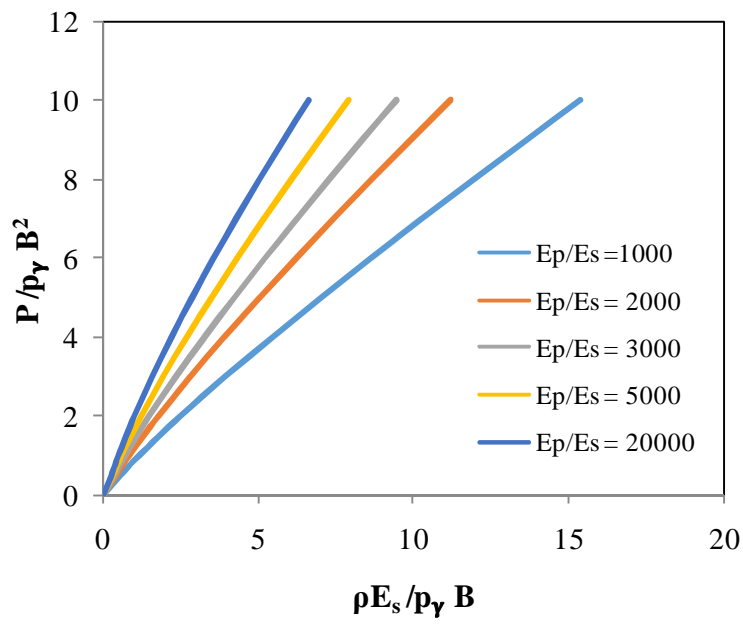
It can be observed that the graphs in all the charts are non-linear. That means for the given loading conditions the soil after overcoming elastic stage it has entered into non-linear plastic state. As the eccentricity is increasing the deformations are increasing.  $E_p/E_s = 1000$  graph is far beyond the other graphs because it has the highest value of  $E_s = 100 \times 10^3$  kPa and so it has the highest value of the term  $\rho E_s / p_\gamma B$  and lowest value of settlement. The graphs of  $E_p/E_s = 3000, 5000, 10000$  and  $20000$  are almost coinciding for  $e/B = 0$  and slowly they are separating out with increasing eccentricity but still they are behind  $E_p/E_s = 1000$  because of the difference in  $E_s$  value. If two cases have the same  $E_s$  value the one with higher  $E_p$  value remains stiff and transfer fewer loads to the soil. So higher  $E_p/E_s$  ratio will have less deformation.

#### **Normalised charts for $L/B = 10$**

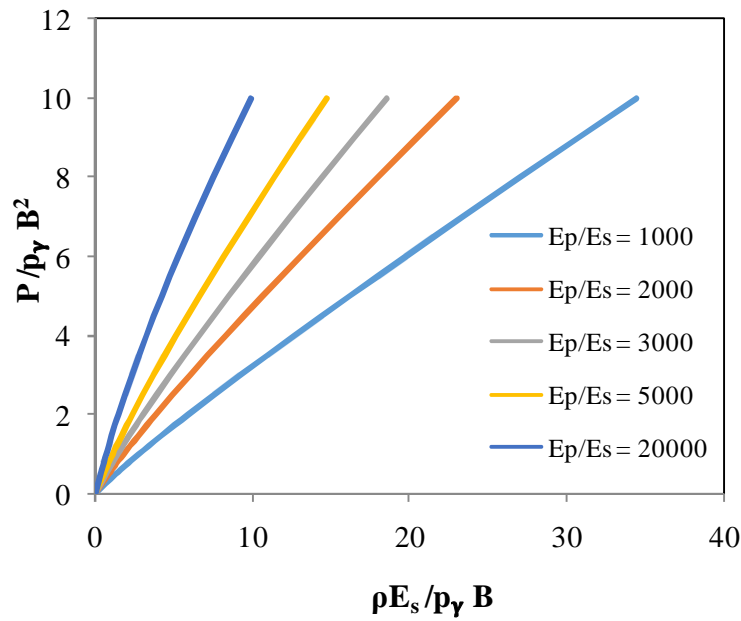
For a  $L/B$  ratio of 10 charts are proposed for  $e/B$  ratios of 0, 2, 4 and 6. The normalised charts for various  $e/B$  ratios and  $E_p/E_s$  ratios for  $L/B = 10$  are shown in Fig 4.9



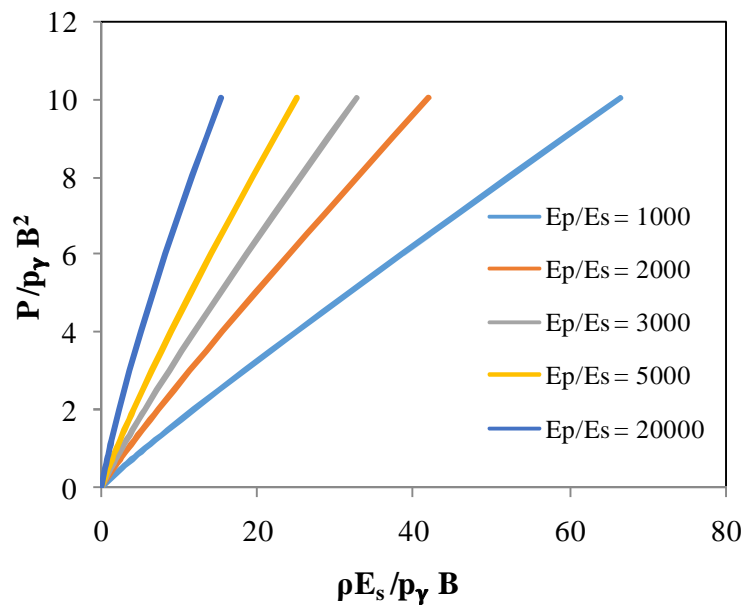
(a)  $e/B = 0$



(b)  $e/B = 2$



(c)  $e/B = 4$



(d)  $e/B = 6$

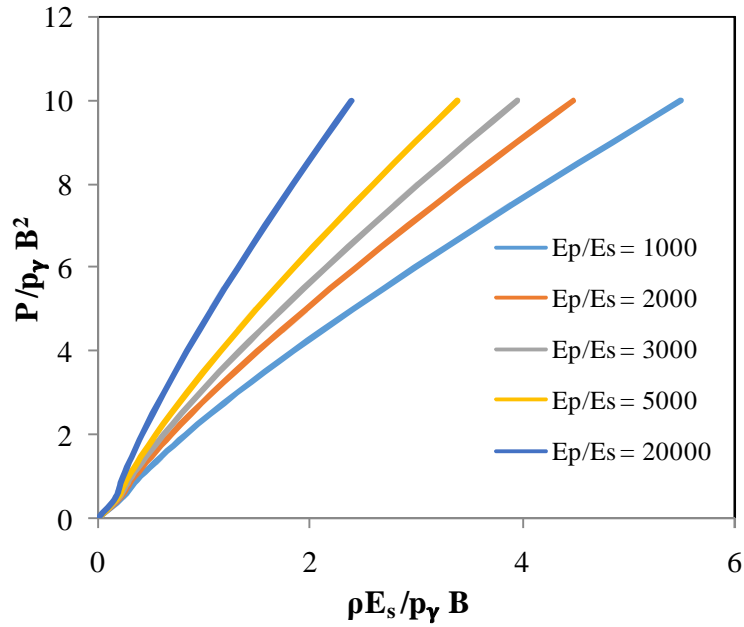
**Figure 4.9: Normalised load- deformation charts for  $L/B = 5$  and (a)  $e/B = 0$  (b)  $e/B = 2$  (c)  $e/B = 4$  and (d)  $e/B = 6$**

The deformations are increasing with increase in eccentricity. The deformations for  $L/B = 10$  are less compared to  $L/B = 5$ . The graphs are observed to be non-linear but not much compared to the graphs of  $L/B = 5$  because the deformations for this case are lesser. In each subcase of  $e/B$  ratio the graphs are moving farther with increasing  $e/B$  ratio.

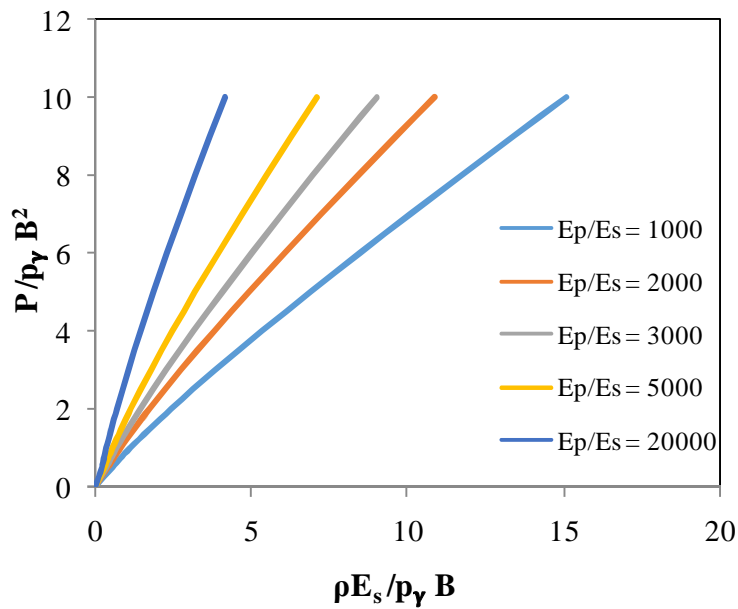


**Normalised charts for  $L/B = 15$**

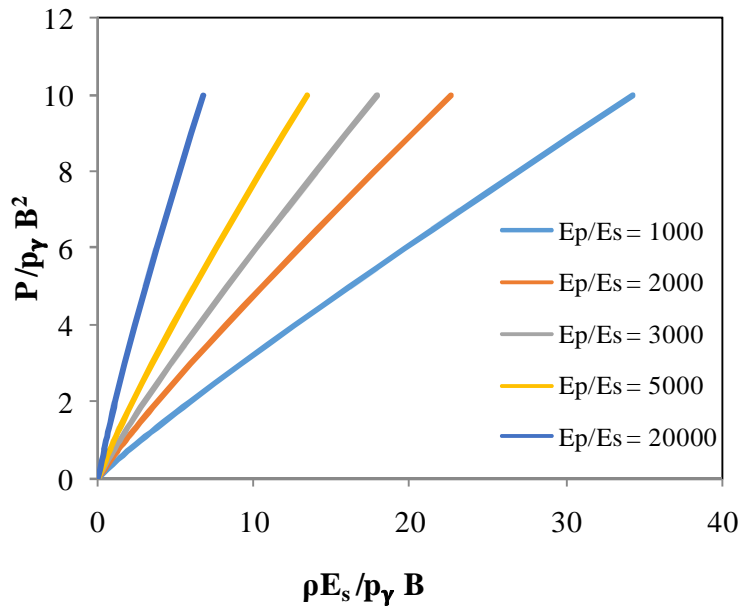
For a  $L/B$  ratio of 15 charts are proposed for  $e/B$  ratios of 0, 2, 4 and 6. The normalised charts for various  $e/B$  ratios and  $E_p/E_s$  ratios for  $L/B = 15$  are shown in Fig 4.10



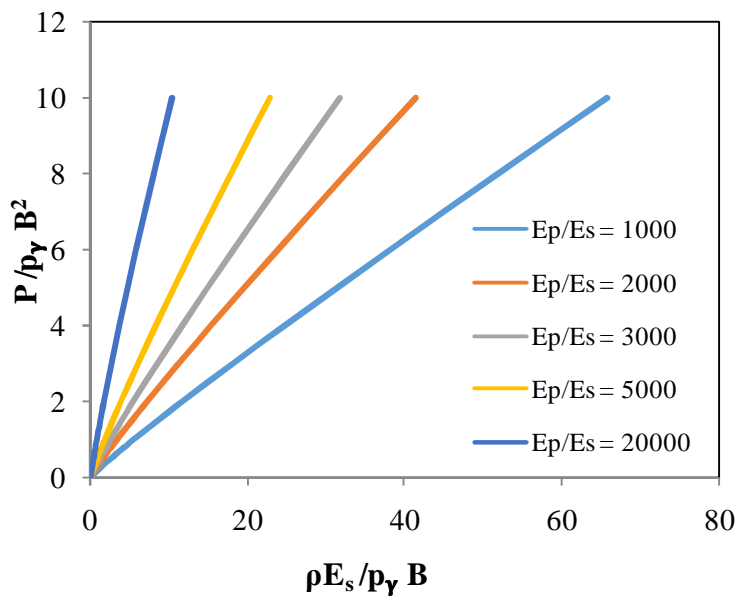
**(a)  $e/B = 0$**



**(b)  $e/B = 2$**



(c)  $e/B = 4$



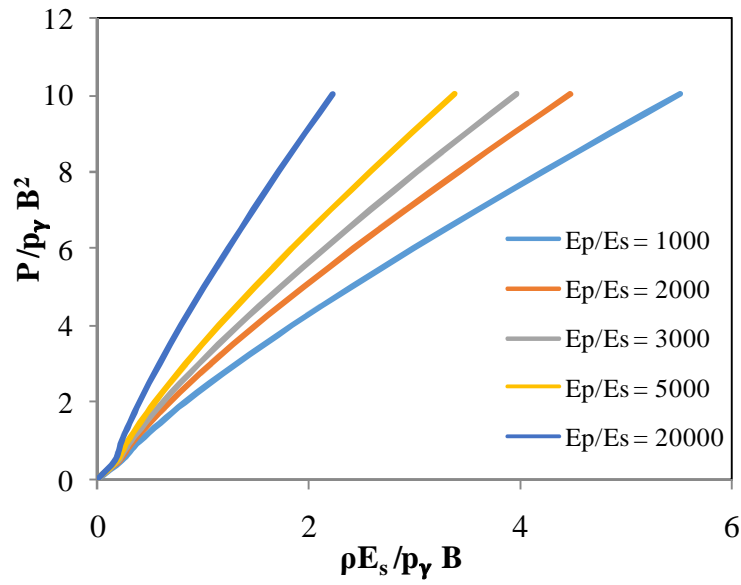
(d)  $e/B = 6$

**Figure 4.10: Normalised load- deformation charts for  $L/B = 5$  and (a)  $e/B = 0$  (b)  $e/B = 2$  (c)  $e/B = 4$  and (d)  $e/B = 6$**

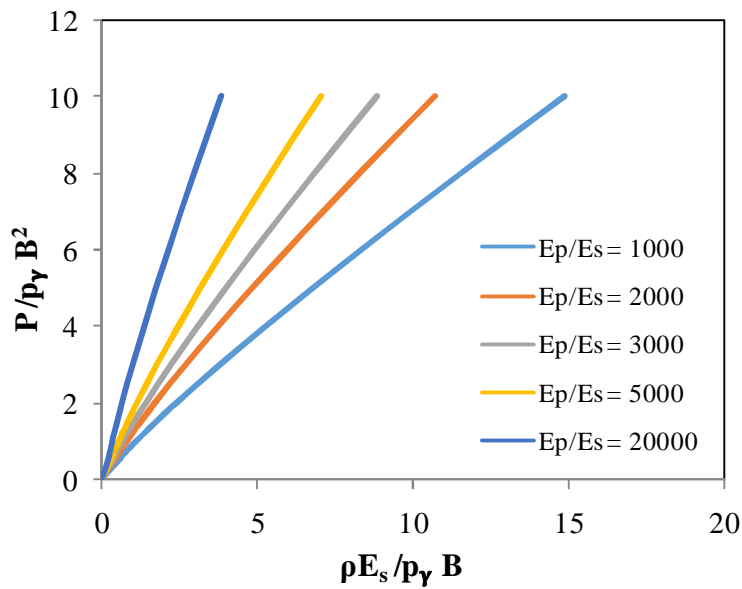
The deformations obtained for  $L/B = 15$  are lesser compared to  $L/B = 10$  and  $L/B = 5$ . The deformations in 4.10(a) are lesser compared to 4.10(d) because of increase in eccentricity. The graphs in each chart are getting farther with increasing eccentricity. Also the graphs appear to be little linear because the deformations are less and they haven't reached plastic state.

**Normalised charts for  $L/B = 20$**

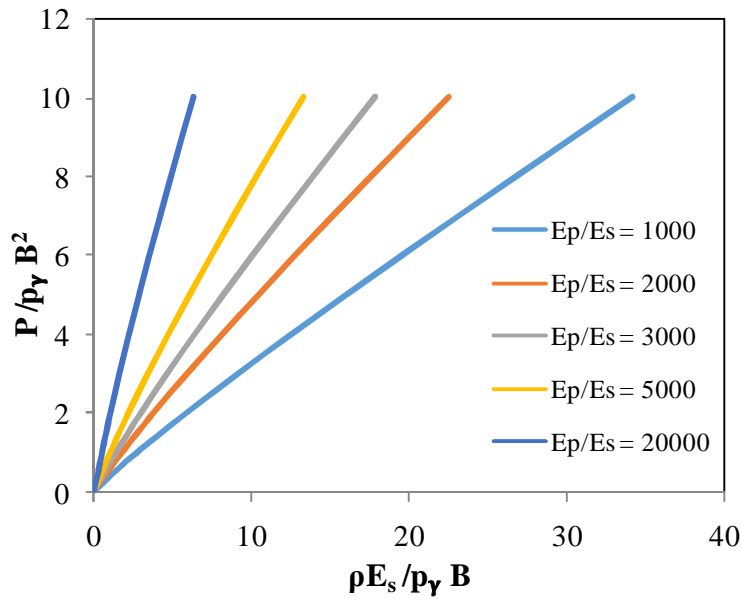
For a  $L/B$  ratio of 20 charts are proposed for  $e/B$  ratios of 0, 2, 4 and 6. The normalised charts for various  $e/B$  ratios and  $E_p/E_s$  ratios for  $L/B = 20$  are shown in Fig 4.11



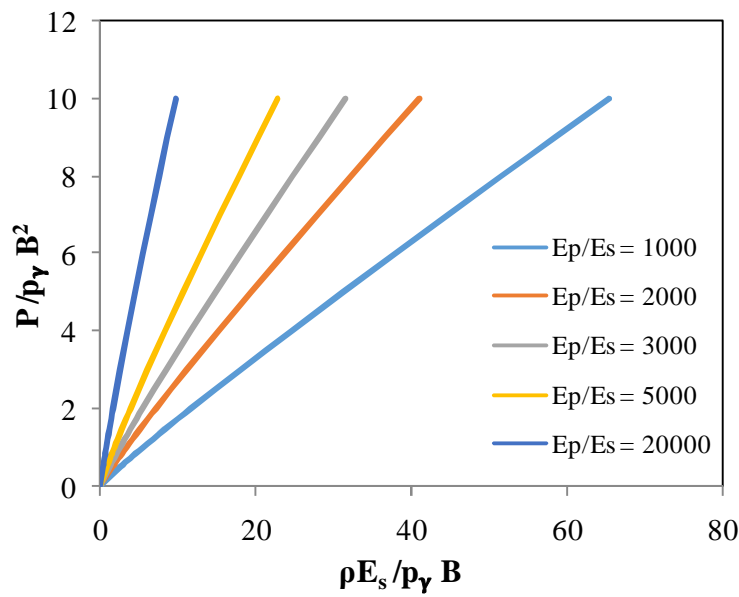
**(a)  $e/B = 0$**



**(b)  $e/B = 2$**



(c)  $e/B = 4$



(d)  $e/B = 6$

**Figure 4.11: Normalised load- deformation charts for  $L/B = 5$  and (a)  $e/B = 0$  (b)  $e/B = 2$  (c)  $e/B = 4$  and (d)  $e/B = 6$**

Finally it can be summarised that as Mohr Coulomb model is incorporated graphs are non-linear. Piles with lesser lengths are undergoing large deformations and so they are entering into the plastic stage. Perfect elastic-plastic graph is obtained. For piles with larger lengths they offer more resistance and so

the deformations obtained are not still completely plastic which can be observed from the graphs. For the same length of pile as the eccentricity is increasing pile deformations are increasing. For same eccentricity as the length of pile is increasing lateral deformations are decreasing. The graphs are becoming farther with increasing  $L/B$  and  $e/B$  ratios. The graphs are getting closer to each other with increasing  $E_p/E_s$  ratio.

When same lengths and diameters are implemented as above for given  $L/B$  and  $e/B$  ratio with change in  $E_p$  and  $E_s$  values other than those used for modelling for a given  $E_p/E_s$  ratio the error is around 5% when the results obtained from numerical modelling and design charts are compared. Similarly when same values of  $E_p$  and  $E_s$  are implemented as above for a given  $E_p/E_s$  ratio and  $L$ ,  $B$  and  $e$  values are changed for the same ratios the error is around 10%. Thus the above design charts can be implemented undoubtedly for various pile geometries and various soil and pile properties with an error less than 10%.

### **4.3 Comparison of Normalised Charts of LE and MC Model**

The design charts obtained for  $L/B = 5$  and  $e/B = 2$  from both LE model and MC model are compared as shown in Fig 4.12. It can be observed that the graphs are linear for LE model and they are non-linear for MC model. For  $E_p/E_s$  ratio of 1000 the actual values used for modelling are  $E_p = 100 \cdot 10^6$  kPa and  $E_s = 100 \cdot 10^3$  kPa. For  $E_p/E_s$  ratio of 3000 the value of  $E_p$  is  $60 \cdot 10^6$  kPa and  $E_s = 20 \cdot 10^3$  kPa. For  $E_p/E_s$  ratio of 5000 the value of  $E_p$  is  $100 \cdot 10^6$  kPa and  $E_s = 20 \cdot 10^3$  kPa. Since the value of  $E_s$  is same for both  $E_p/E_s = 3000$  and  $E_p/E_s = 5000$  the graphs are coinciding. Whereas for  $E_p/E_s = 1000$  the value of  $E_s$  is very high and so the graph is away from the other two.

Also it can be observed from Fig 4.12, that for lower load values the deformations obtained from LE model and MC model are coinciding. So LE design charts can be used for lower loads but for higher loads LE model is underestimating the deformations. Also for a given load MC model is giving higher deformations than LE model.

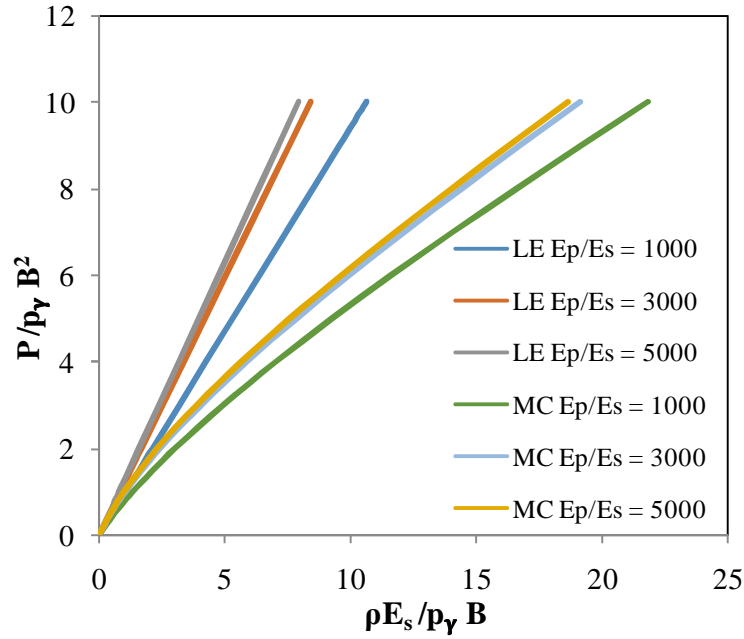


Figure 4.12 Comparison of LE model and MC model design charts for  $L/B = 5$  and  $e/B = 2$

#### 4.4 Study of Plastic Zone Formation for Sands

Zhaohui Yang and Boris Jeremic (2002) carried out studies on numerical analysis of pile behavior under lateral loads in layered elastic-plastic soils and stated that the formation of plastic zones is different for sands and clays. They carried out numerical modelling using LPILE Plus software. So here in this work the plastic zones formation is validated using PLAXIS-3D software.

The mode of plastic zones formation is studied for two cases when there is no eccentricity and when there is an eccentricity of 6m. A load of 5kN, 50kN and 500kN is applied separately for two cases and the development of plastic zones are observed. Plastic zones are actually presented by plastified gauss points.

When a load of 5kN is applied, the direction of application of load being left to right the plastic zone formations are shown in Fig 4.13.

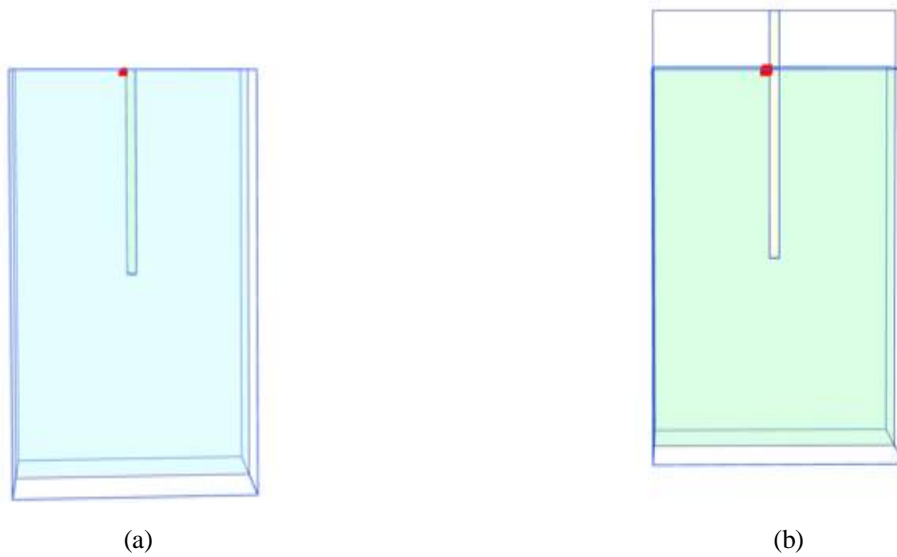


**Figure 4.13: Plastic zones formation for a load of 5kN for (a)  $e/B = 0$  and (b)  $e/B = 6$**

It can be observed from Fig 4.13 that the plastic zones first started on the left side of the pile that is on the tension side of the soil. The size of the plastic zone is more for  $e/B = 6$  when compared to  $e/B = 0$ .

When a load of 50kN is applied laterally on the pile then the plastic zone formation is shown in the Fig 4.14.

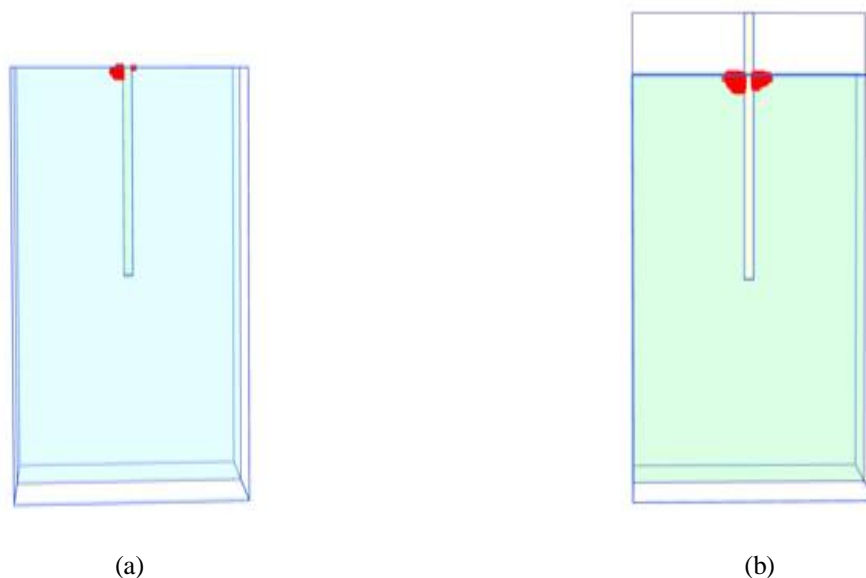


**Figure 4.14: Plastic zones formation for a load of 50kN for (a)  $e/B = 0$  and (b)  $e/B = 6$**

For a load of 50kN for  $e/B=0$  a clear plastic zone is seen on the left side of the pile whereas the plastic zones started forming on the right side of the pile. Whereas for  $e/B = 6$  the plastic zones are formed clearly both on the left and right sides of the pile. Also the plastic zones for  $e/B = 6$  are bigger than that for  $e/B = 0$ .

When a load of 500kN is applied on the pile then the plastic zones formed for  $e/B = 0$  and  $e/B = 6$  are as shown in the Fig 4.15

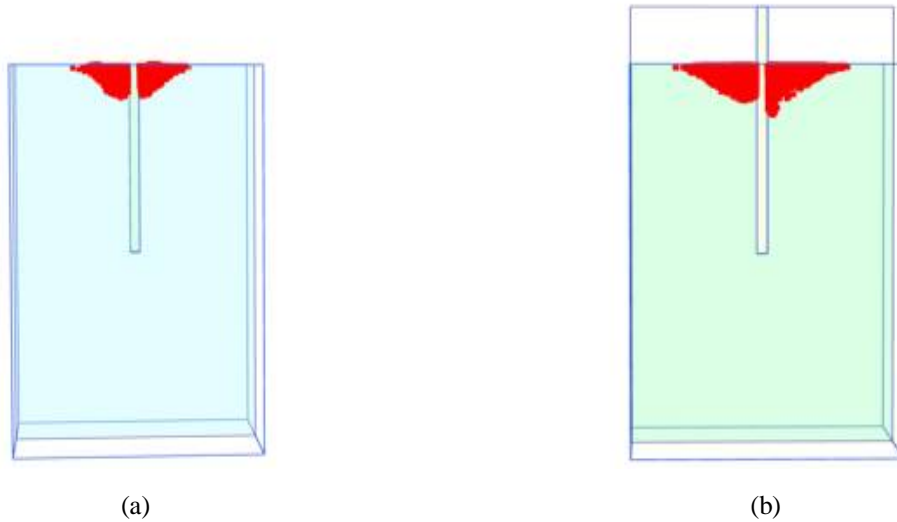


**Figure 4.15: Plastic zones formation for a load of 500kN for (a)  $e/B = 0$  and (b)  $e/B = 6$**

It is observed that for a load of 500kN a wedge shaped plastic zones are formed on either side of the pile both for  $e/B = 0$  and  $e/B = 6$ . These zones are bigger for  $e/B = 6$  in terms of both depth and length. It can be observed that the plastic zones extend to the boundary away from the pile with increasing load. Finally it can be concluded that for sands with increasing load the plastic zones extend away from the pile towards the boundary and then it starts growing slowly along the depth of the pile.



# Chapter 5

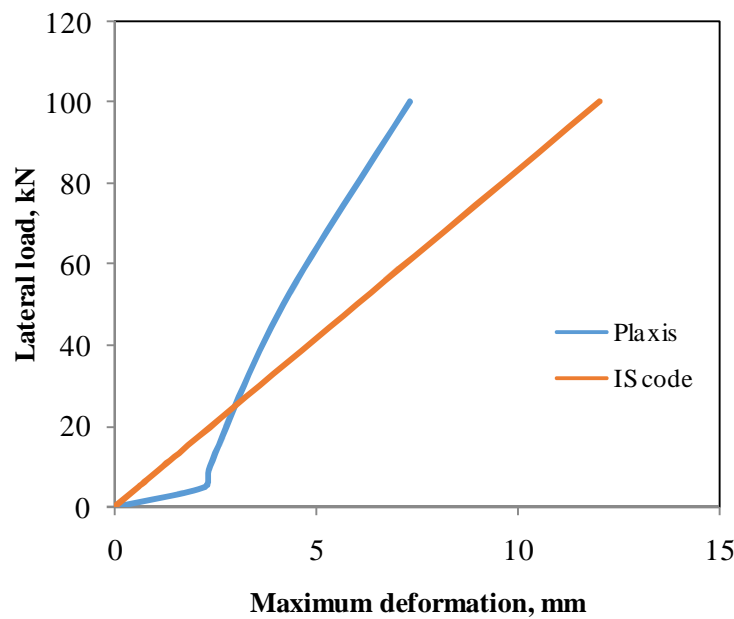
## Results and Discussion - Part 2 Clays

### 5.1 Comparison of Pile Responses of IS Code Method and Numerical Modelling for Clays

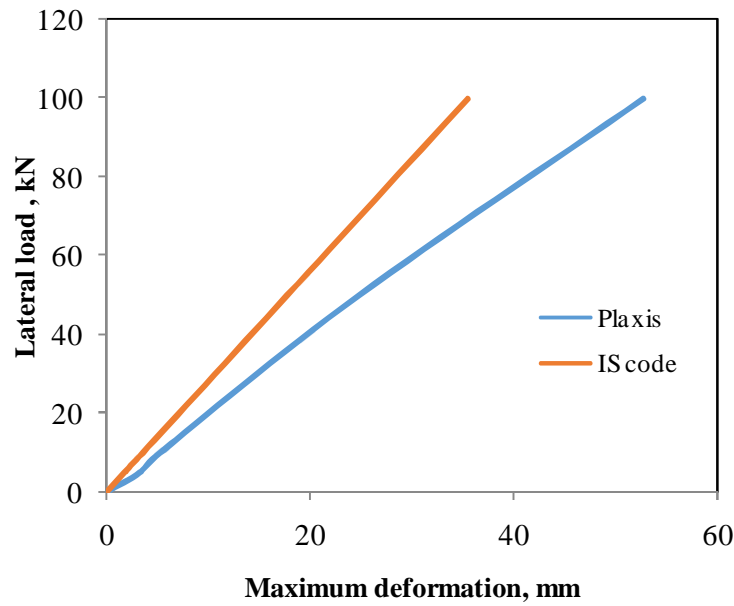
Before proposing the normalised charts for clays the IS code results and PLAXIS results of lateral deformations for a pile embedded in soft clay, medium stiff clay, stiff clay and very stiff clay are compared for two different  $e/B$  ratios of 0 and 6. A pile of length 5m and diameter of 1m is modelled.

#### *Comparison for soft clay*

For soft clay the range of unconfined compressive strength is 25-50 kPa. A value of 38kPa is used for numerical modelling. That means the cohesion value is around 19kPa. The comparison between numerical modelling and IS code is shown in the Fig 5.1



(a)  $e/B = 0$



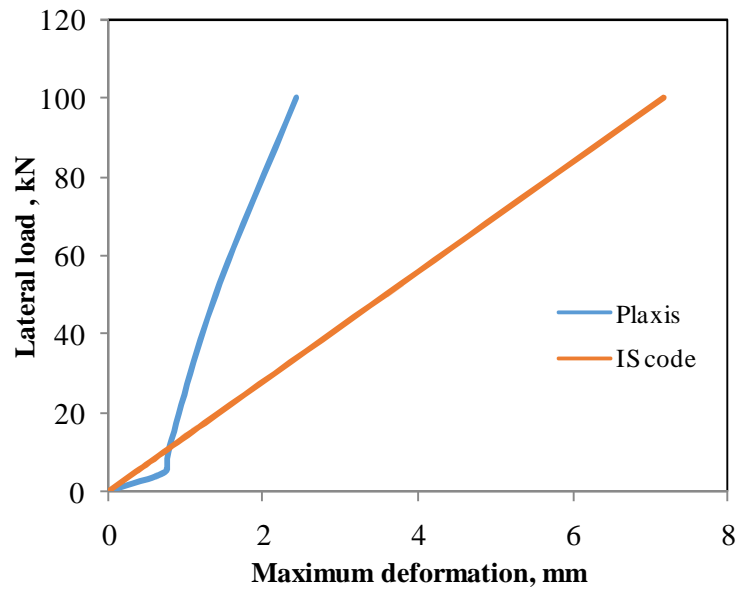
(b)  $e/B = 6$

**Figure 5.1 : Comparison of deformations of IS code and PLAXIS for (a)  $e = 0$  and (b)  $e = 6$**

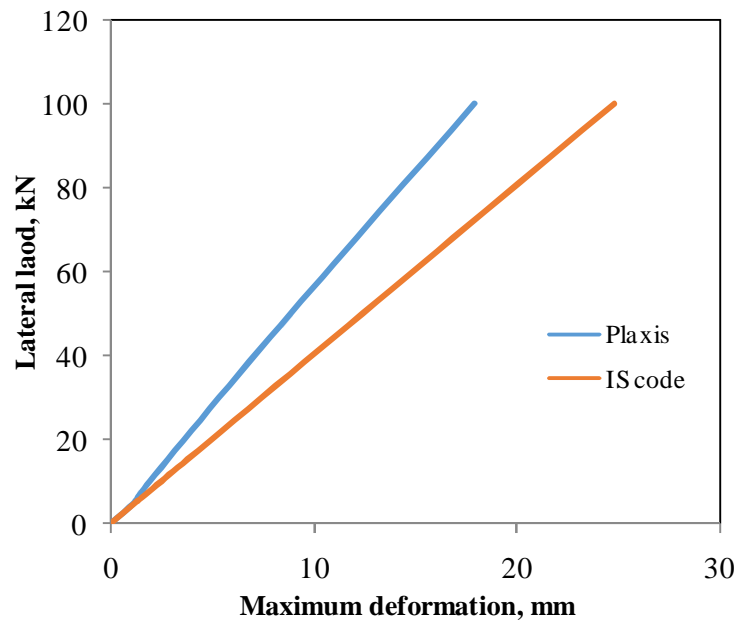
For soft clay when  $e/B = 0$  Fig. 5.1 (a) the graph of deformation against lateral load for IS code is linear. The IS code results are under estimating the deformations for loads below 20kN. For loads greater than 20kN IS code is over estimating the deformations. For  $e/B = 6$  as shown in Fig 5.1 (b) IS code is under estimating the deformations for all the loads.

***Comparison for medium stiff clay***

For medium stiff clay the range of unconfined compressive strength is 50-100kPa. A value of  $q_u = 75$ kPa is used for numerical modelling. That means cohesion  $c = 37.5$ kPa. The comparison of deformations are shown in Fig 5.2



(a)  $e/B = 0$



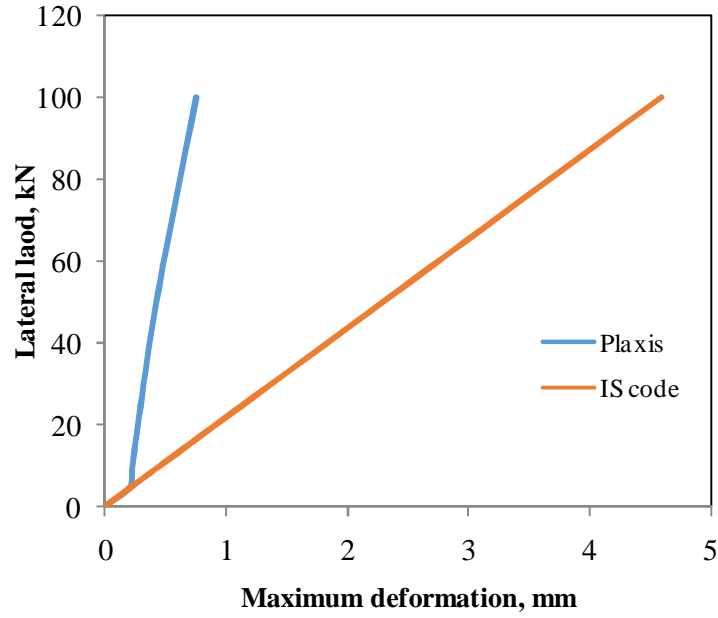
(b)  $e/B = 6$

Figure 5.2 : Comparison of deformations of IS code and PLAXIS for (a)  $e/B = 0$  and (b)  $e/B = 6$

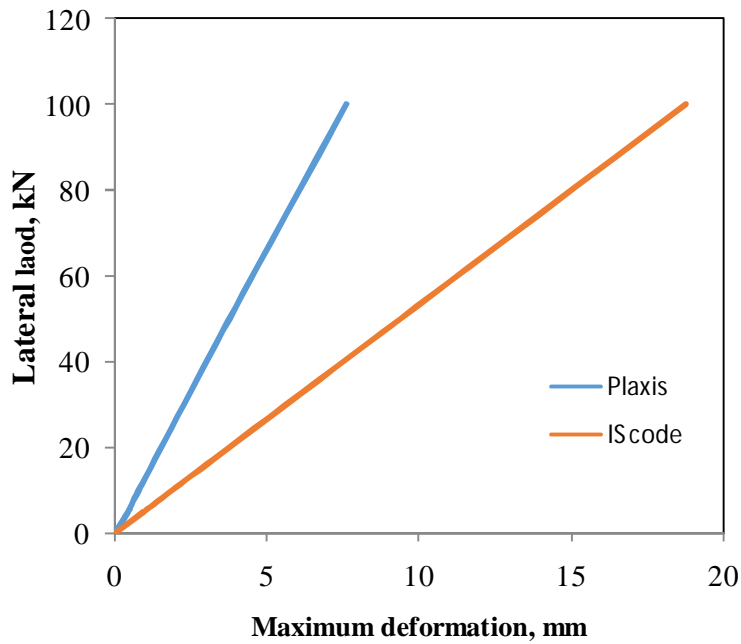
For medium stiff clay with no eccentricity the trend is similar to soft clay with  $e/B = 0$ . Here for very small loads of less than 10kN the deformations of IS code are lesser than that of PLAXIS results. Whereas for loads above 10kN the deformations of IS code are over estimating.

**Comparison for stiff clay**

For stiff clay  $q_u$  value ranges between 100-200 kPa. Cohesion value of 75kPa is used for numerical modelling. The comparison for stiff clay is shown in Fig 5.3



(a)  $e/B = 0$



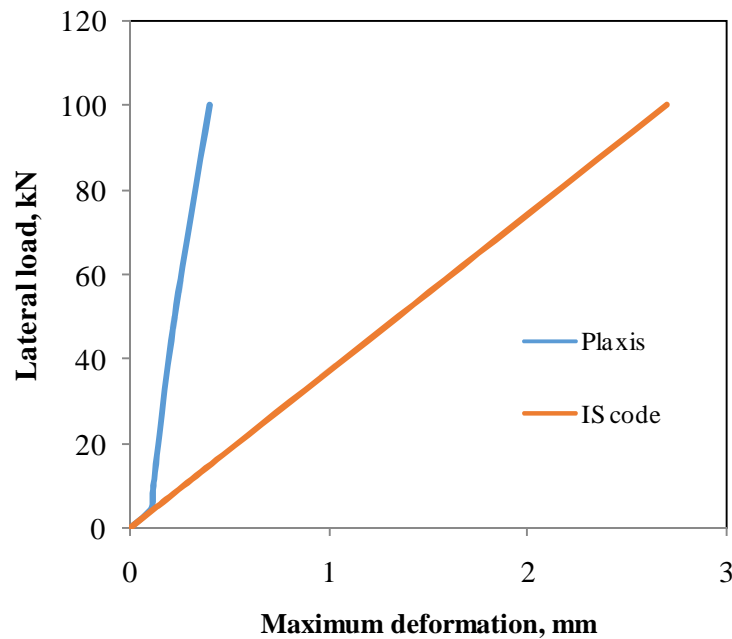
(b)  $e/B = 6$

Figure 5.3 : Comparison of deformations of IS code and PLAXIS for (a)  $e/B = 0$  and (b)  $e/B = 6$

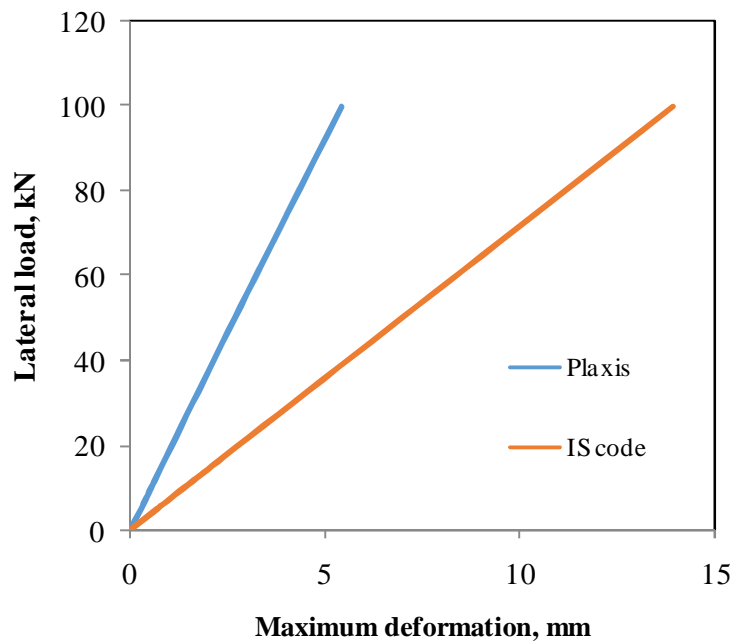
From Fig 5.3 (a) and (b) it is observed that IS code is over estimating the deformations in both the cases and this deviation is more for no eccentricity case.

**Comparison for very stiff clay**

For very stiff clay  $q_u$  ranges between 200-400kPa. Cohesion value of 150kPa is implemented in modelling.



(a)  $e/B = 0$



(b)  $e/B = 6$

**Figure 5.4 : Comparison of deformations of IS code and PLAXIS for (a)  $e/B = 0$  and (b)  $e/B = 6$**

The deformations of IS code are over estimating in both the cases Fig 5.4 (a) and (b) and the deviation is more for  $e/B = 0$ .

Finally it can be concluded that IS code over estimates the deformations in most of the cases and the deviation of the IS code results when compared to numerical modelling with increase in stiffness of the clay. Stiff clay has the maximum deviation of results. So in this work design charts which are accurate and which can be used easily are proposed using numerical modelling.

## **5.2 Normalised Load Deformation Charts for Clays**

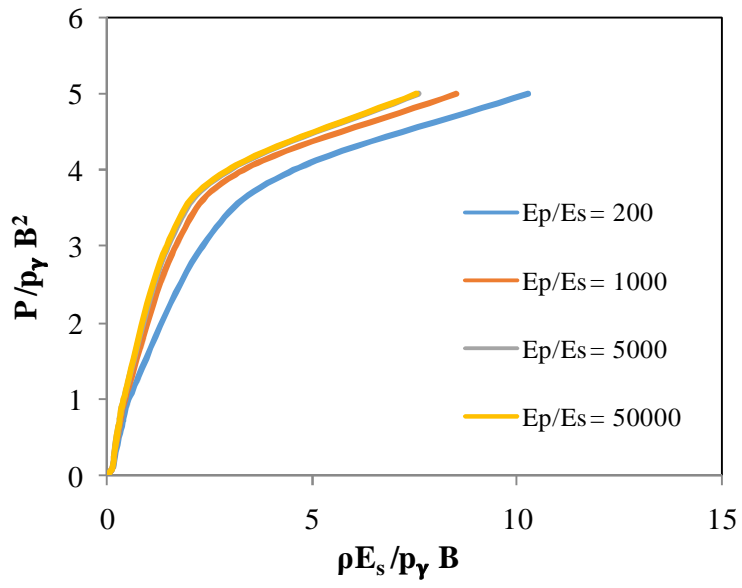
The normalised load and deflection terms are same as used for sands. Normalised charts are proposed separately for soft clay, medium stiff clay and stiff clay. This is because the undrained cohesion for clays varies from 12 – 250kPa. Due large range the charts are proposed separately for different consistencies. The soil stiffness for clays ranges between  $2-200 \times 10^3$  kPa and for pile material the stiffness ranges between  $20-200 \times 10^6$  kPa. Considering extreme combinations the charts are proposed for  $E_p/E_s$  ratios of 200, 1000, 5000 and 50000. Undrained conditions are implemented for clay so the value of poisson's ratio for undrained clay is 0.5. The poisson's ratio for pile material is 0.15.

### **5.2.1 Soft Clay**

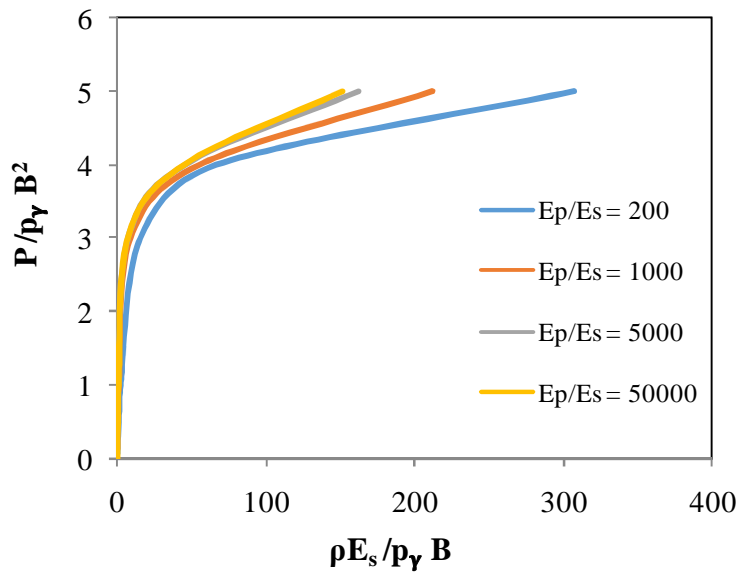
For soft clay  $S_u = 15$ kPa is used to propose charts. Charts are proposed for L/B ratios 5, 10, 15 and 20. For each L/B ratio charts are proposed for different e/B ratios of 0, 2 and 4.

#### ***Normalised charts for L/B = 5***

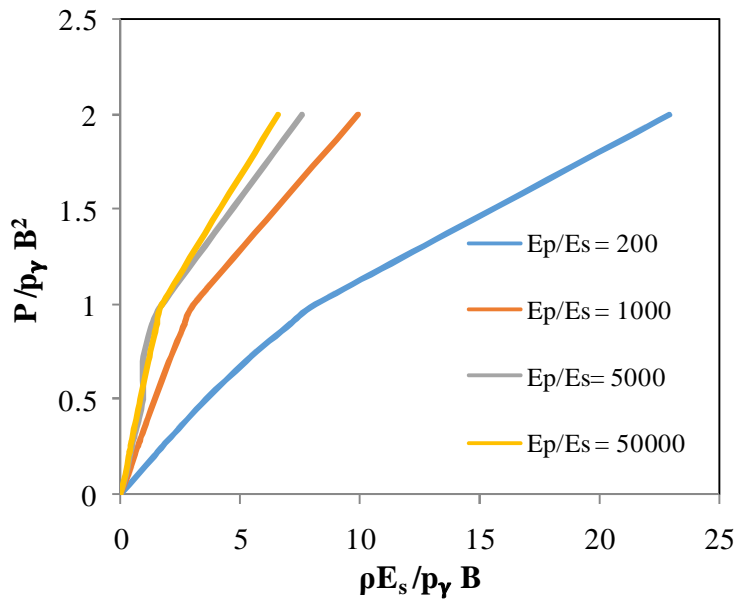
For a L/B ratio of 5 charts are proposed for e/B ratios of 0, 2, and 4. The normalised charts for various e/B ratios and  $E_p/E_s$  ratios for L/B = 5 are shown in Fig 5.5



(a)  $e/B = 0$



(b)  $e/B = 2$



(c)  $e/B = 4$

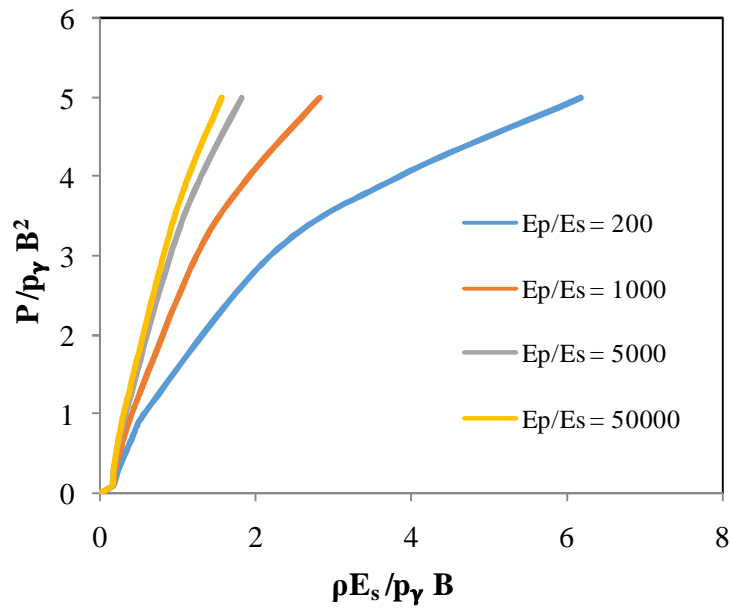
**Figure 5.5 : Normalised load- deformation charts for  $L/B = 5$  and (a)  $e/B = 0$  (b)  $e/B = 2$  and (c)  $e/B = 4$**

As M-C model is used it can be observed that the graphs are non-linear that means soil entered into plastic stage. Deformations are increasing with increase in eccentricity which can be observed from Fig 5.5 (a),(b) and (c). For  $E_p/E_s = 200$  the values of  $E_p$  and  $E_s$  used in modelling are  $E_p = 20 \cdot 10^6$  kPa and  $E_s = 100 \cdot 10^3$  kPa. For  $E_p/E_s = 1000$  the values of  $E_p$  and  $E_s$  used in modelling are  $E_p = 100 \cdot 10^6$  kPa and  $E_s = 100 \cdot 10^3$  kPa. It can be observed that for  $E_p/E_s = 200$  and 1000 same value of  $E_s$  is given. Though they have same  $E_s$  value the deformations are differing because of  $E_p$  value. The one with higher  $E_p$  value is undergoing lesser deformations because stiffer piles transfer less load to the soil. The graphs of  $E_p/E_s = 5000$  and 50000 are almost coinciding.

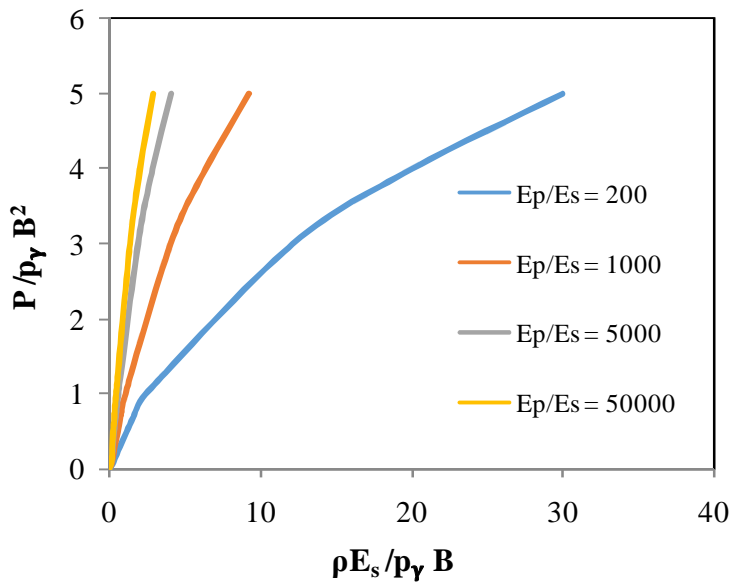
#### **Normalised charts for $L/B = 10$**

For a  $L/B$  ratio of 10 charts are proposed for  $e/B$  ratios of 0, 2 and 4. The normalised charts for various  $e/B$  ratios and  $E_p/E_s$  ratios for  $L/B = 10$  are shown in Fig 5.6

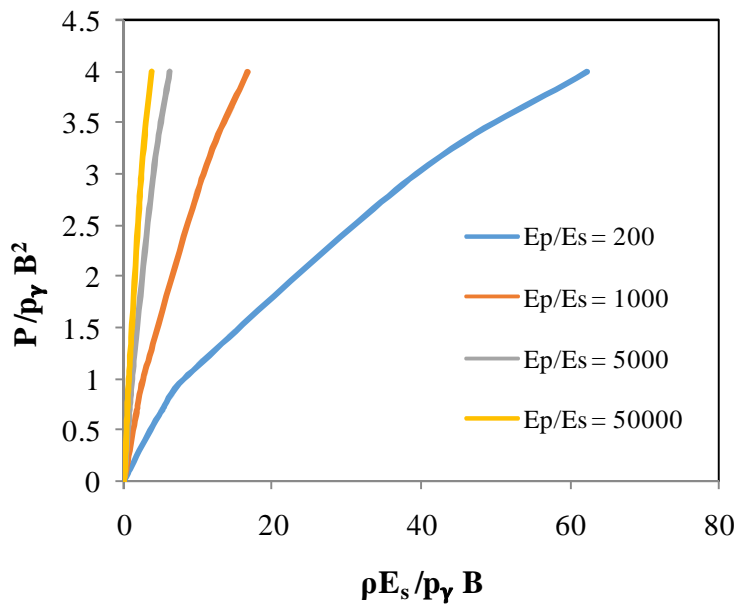




(a)  $e/B = 0$



(b)  $e/B = 2$



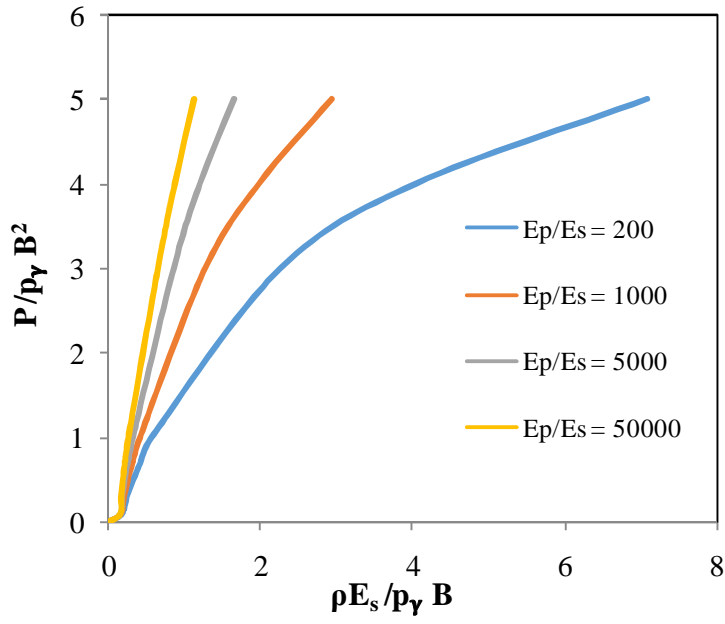
(c)  $e/B = 4$

**Figure 5.6 : Normalised load- deformation charts for  $L/B = 10$  and (a)  $e/B = 0$  (b)  $e/B = 2$  and (c)  $e/B = 4$**

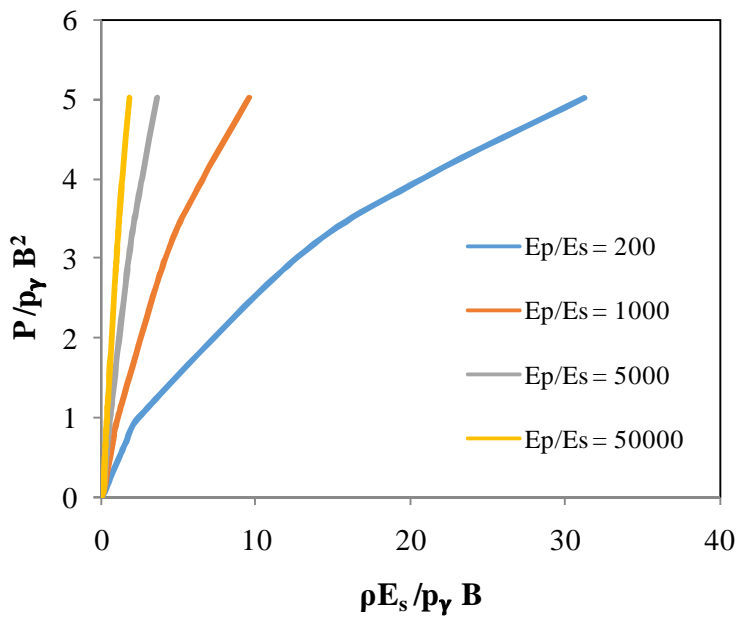
The graphs are not linear. From the Fig 5.6 it can be observed that the deformations of  $L/B = 10$  for all sub cases are less than the deformations of  $L/B = 5$ . Similar to the graphs of  $L/B = 5$  the deformations are increasing with increase in eccentricity. The deviation the graphs is increasing from each other with increasing  $e/B$  ratio.

#### ***Normalised charts for $L/B = 15$***

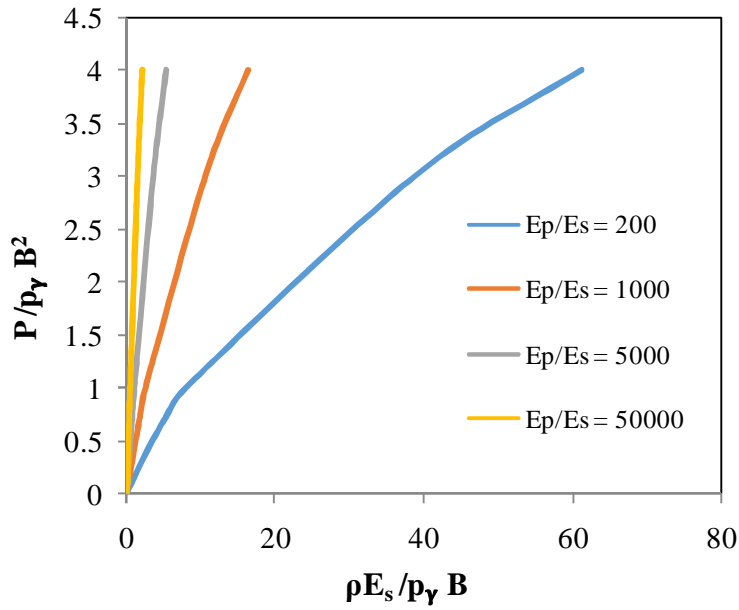
For a  $L/B$  ratio of 15 charts are proposed for  $e/B$  ratios of 0, 2 and 4. The normalised charts for various  $e/B$  ratios and  $E_p/E_s$  ratios for  $L/B = 15$  are shown in Fig 5.7



(a)  $e/B = 0$



(b)  $e/B = 2$



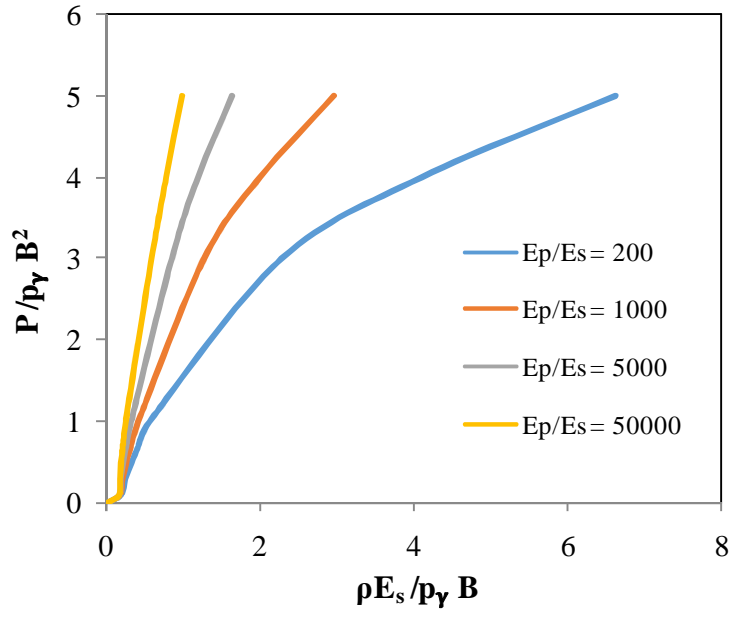
(c)  $e/B = 4$

Figure 5.7 : Normalised load- deformation charts for  $L/B = 15$  and (a)  $e/B = 0$  (b)  $e/B = 2$  and (c)  $e/B = 4$

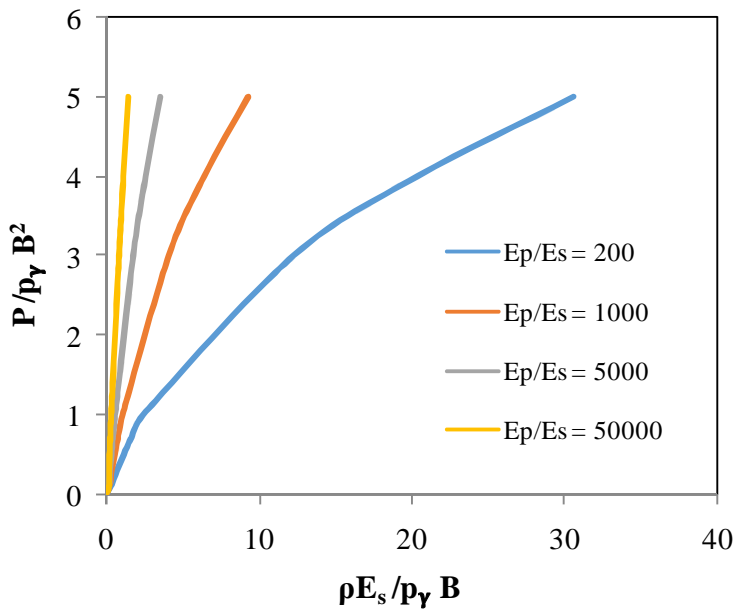
The graphs are in non-linear trend. The deformations of  $L/B = 15$  are lesser compared to  $L/B = 5$  and 10. Deformations are increasing with increase in eccentricity. Other trends are similar as explained under Fig 5.5 and Fig 5.6.

**Normalised charts for  $L/B = 20$**

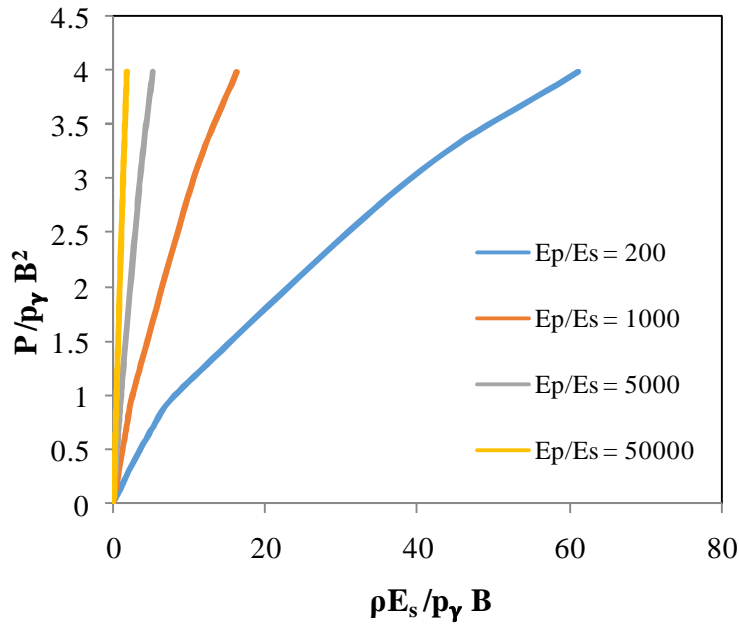
For a  $L/B$  ratio of 20 charts are proposed for  $e/B$  ratios of 0, 2 and 4. The normalised charts for various  $e/B$  ratios and  $E_p/E_s$  ratios for  $L/B = 20$  are shown in Fig 5.8



(a)  $e/B = 0$



(b)  $e/B = 2$



(c)  $e/B = 4$

Figure 5.8 : Normalised load- deformation charts for  $L/B = 20$  and (a)  $e/B = 0$  (b)  $e/B = 2$  and (c)  $e/B = 4$

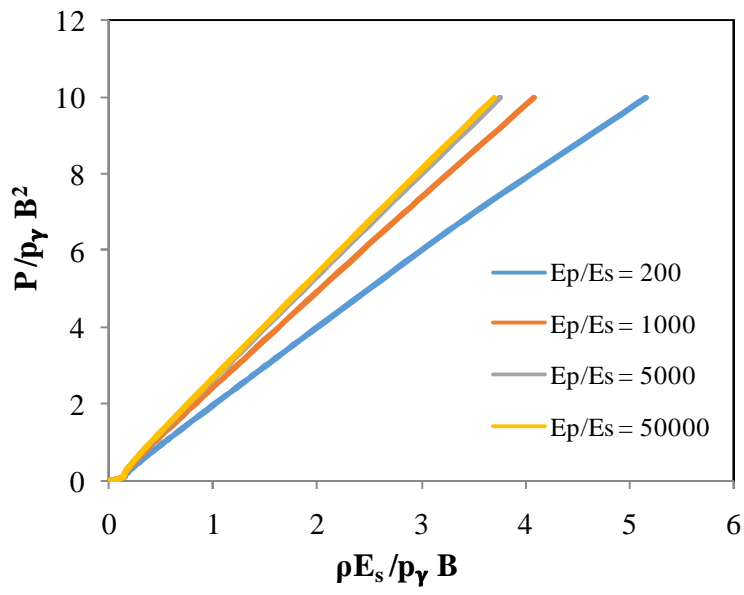
Finally it can be concluded that the  $E_p/E_s$  ratio with lowest  $E_s$  values gives highest deformations. If two soils have different  $E_p$  and  $E_s$  values the one with lowest  $E_s$  value undergo highest deformation though it has highest  $E_p$  value than the other. If two soils have the same  $E_s$  value then the pile with highest  $E_p$  value transfers less load to soil and so it results in less deformations.

### 5.2.2 Medium Stiff Clay

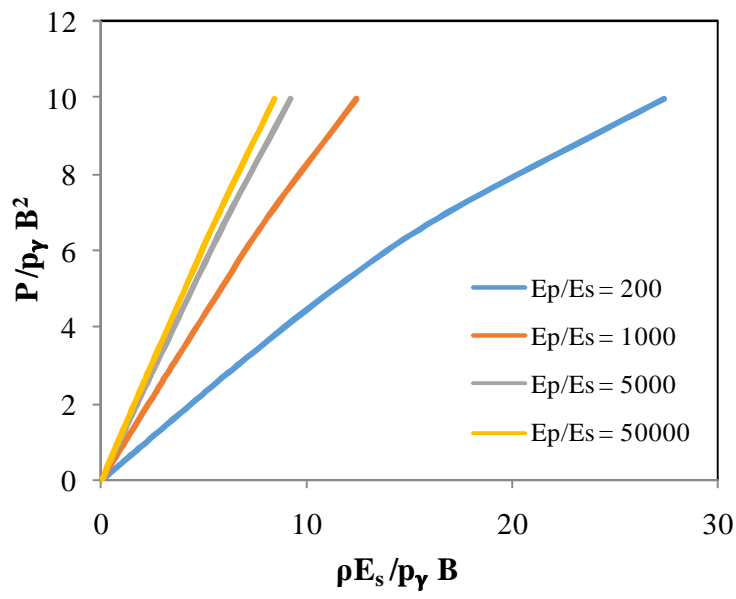
For medium stiff clay undrained shear strength of 100kPa is used in modelling. Other parameters required for modelling are implemented same as explained under 5.2.1 soft clay.

#### Normalised charts for $L/B = 5$

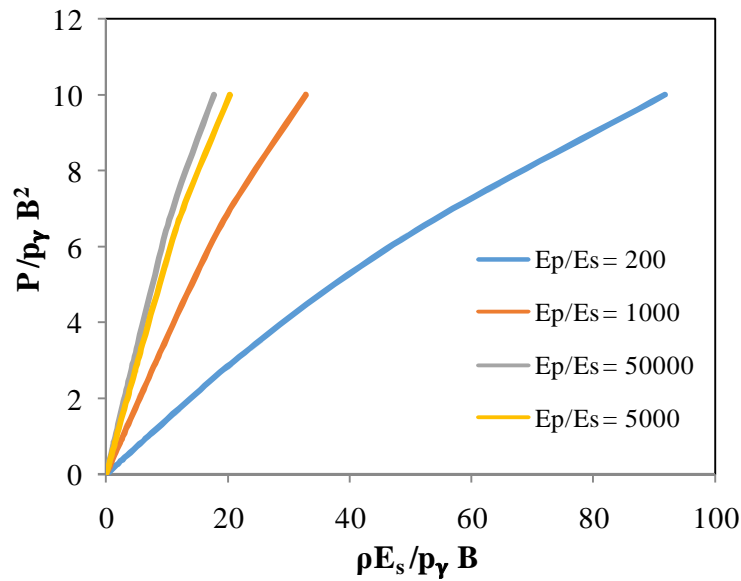
For a  $L/B$  ratio of 5 charts are proposed for  $e/B$  ratios of 0, 2 and 4. The normalised charts for various  $e/B$  ratios and  $E_p/E_s$  ratios for  $L/B = 5$  are shown in Fig 5.9



(a)  $e/B = 0$



(b)  $e/B = 2$



(c)  $e/B = 4$

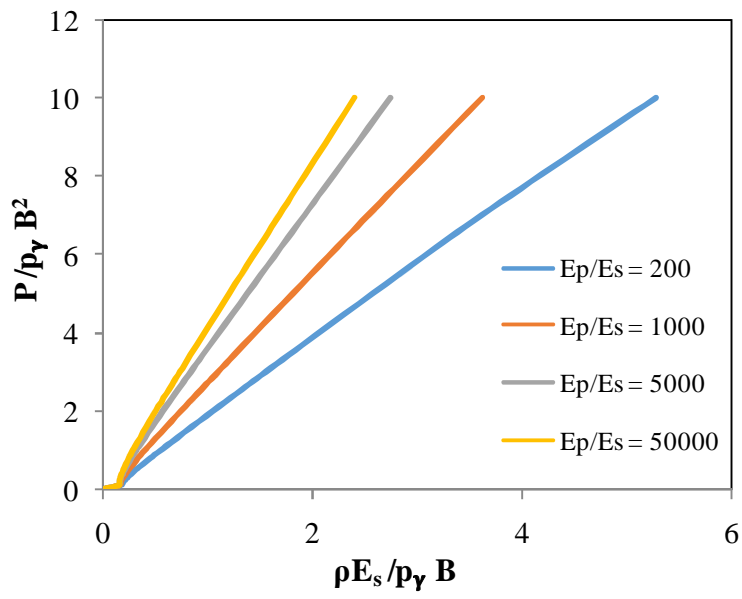
**Figure 5.9 : Normalised load- deformation charts for  $L/B = 5$  and (a)  $e/B = 0$  (b)  $e/B = 2$  and (c)  $e/B = 4$**

The normalised design charts for medium stiff clay for a pile of  $L/B$  ratio 5 are given in Fig 5.9. It can be observed that the deformations are more for pile with eccentricity 4m than the pile with no eccentricity. As the pile with  $e/B = 0$  undergoes less deformations the graphs seems to be linear. Whereas the graphs for  $e/B = 4$  seems to be non-linear. For uniformity the maximum load applied is 1000kN and the normalised load value is 10.

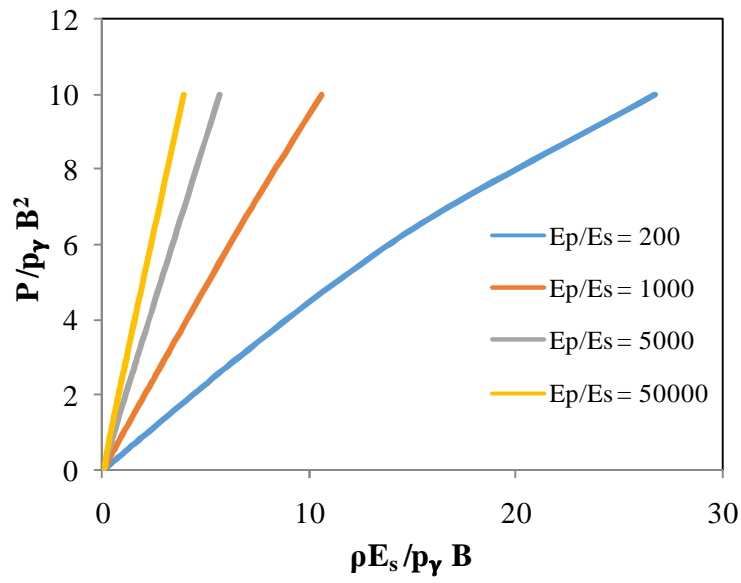
***Normalised charts for  $L/B = 10$***

For a  $L/B$  ratio of 10 charts are proposed for  $e/B$  ratios of 0, 2 and 4. The normalised charts for various  $e/B$  ratios and  $E_p/E_s$  ratios for  $L/B = 10$  are shown in Fig 5.10

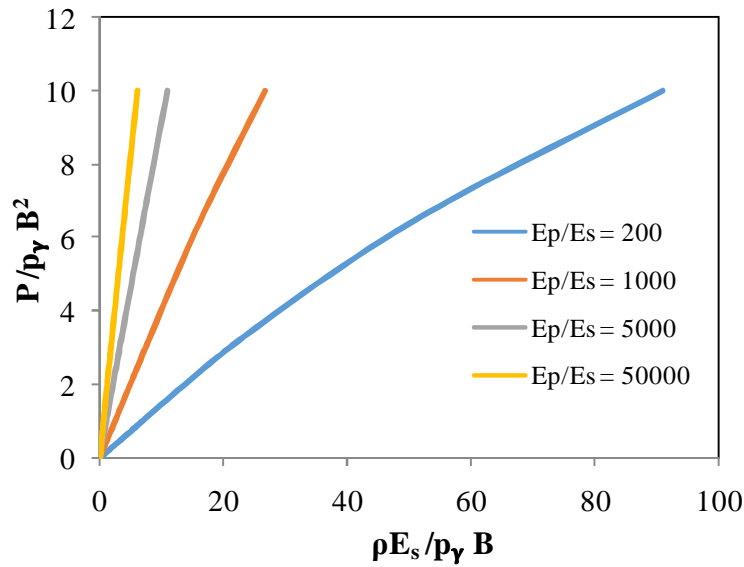




(a)  $e/B = 0$



(b)  $e/B = 2$



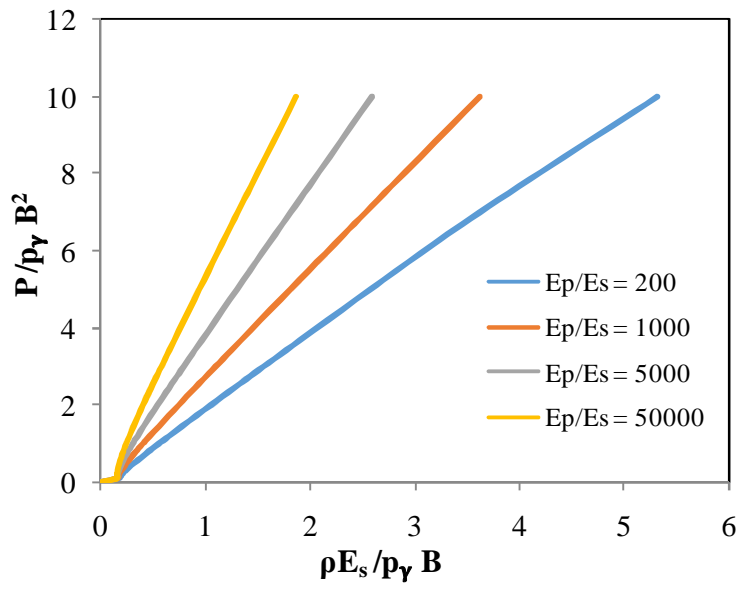
(c)  $e/B = 4$

**Figure 5.10 : Normalised load- deformation charts for  $L/B = 10$  and (a)  $e/B = 0$  (b)  $e/B = 2$  and (c)  $e/B = 4$**

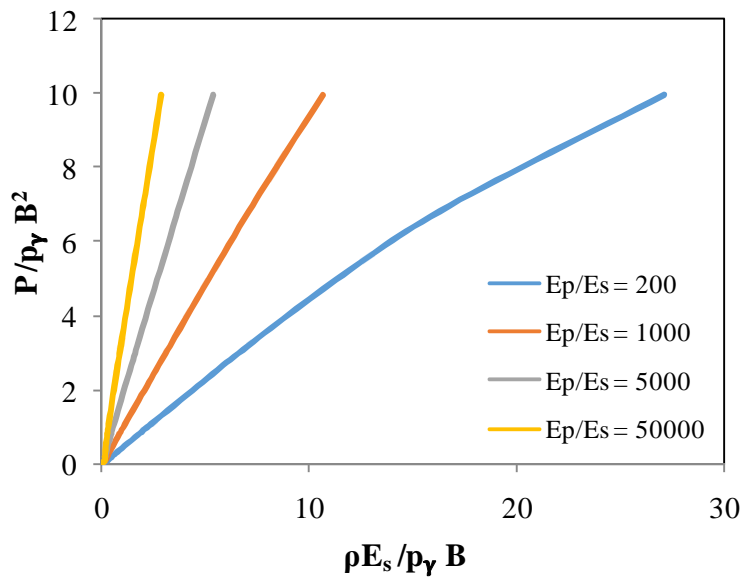
The normalised charts for a pile of  $L/B = 10$  in medium stiff clay are shown in Fig 5.10. The deformations for  $L/B = 10$  are lesser than that of  $L/B = 5$ . Also the deformations are increasing with increase in eccentricity. For the same 1000kN load the deformations of  $L/B = 10$  did not reach plastic state. The graphs in each chart are moving farther with increasing  $e/B$  ratio.

**Normalised charts for  $L/B = 15$**

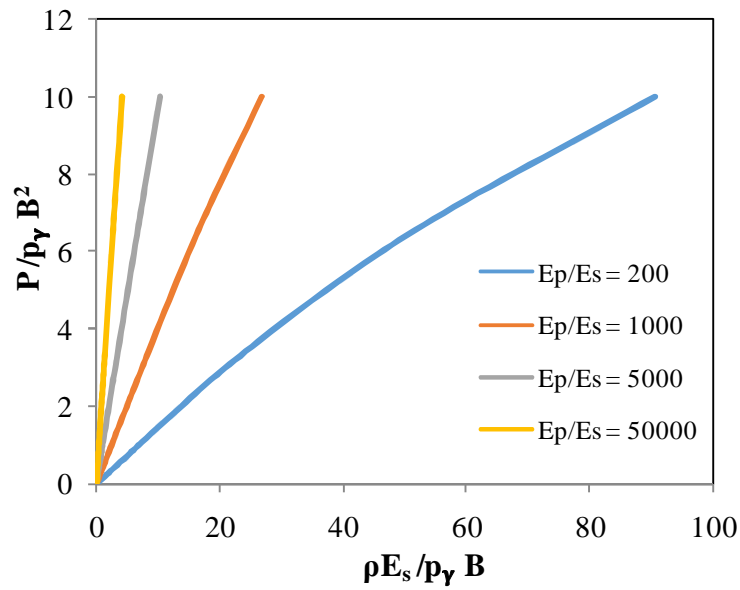
For a  $L/B$  ratio of 15 charts are proposed for  $e/B$  ratios of 0, 2 and 4. The normalised charts for various  $e/B$  ratios and  $E_p/E_s$  ratios for  $L/B = 15$  are shown in Fig 5.11



(a)  $e/B = 0$



(b)  $e/B = 2$



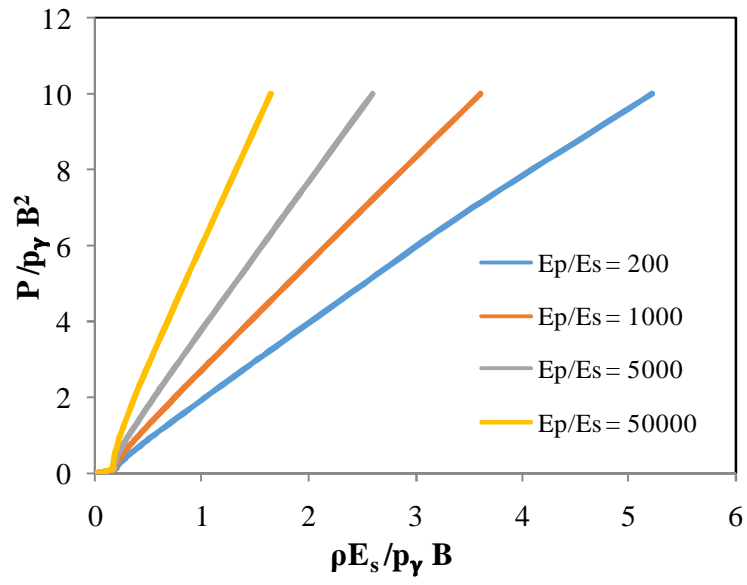
(c)  $e/B = 4$

**Figure 5.11 : Normalised load- deformation charts for  $L/B = 15$  and (a)  $e/B = 0$  (b)  $e/B = 2$  and (c)  $e/B = 4$**

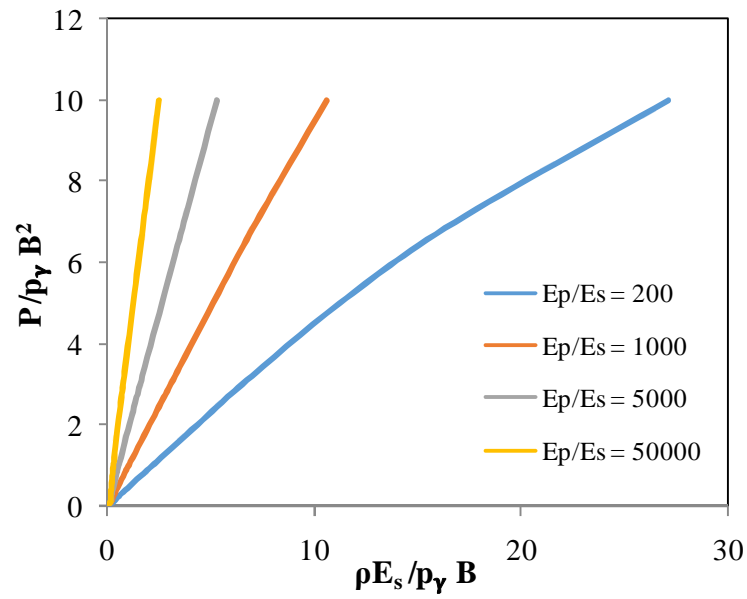
The normalised charts for a pile of  $L/B$  ratio 15 for various eccentricities are shown in Fig 5.11. The deformations are observed to be lesser than piles of  $L/B$  ratios 5 and 10. The graphs are linear and they are moving away from each other with increasing  $e/B$  ratio.

***Normalised charts for  $L/B = 20$***

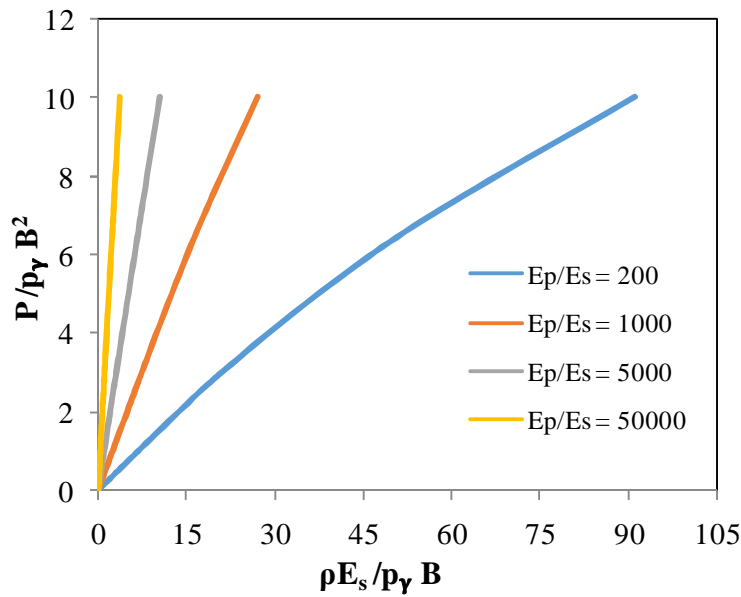
For a  $L/B$  ratio of 20 charts are proposed for  $e/B$  ratios of 0, 2 and 4. The normalised charts for various  $e/B$  ratios and  $E_p/E_s$  ratios for  $L/B = 20$  are shown in Fig 5.12



(a)  $e/B = 0$



(b)  $e/B = 2$



(c)  $e/B = 4$

Figure 5.12 : Normalised load- deformation charts for  $L/B = 20$  and (a)  $e/B = 0$  (b)  $e/B = 2$  and (c)  $e/B = 4$

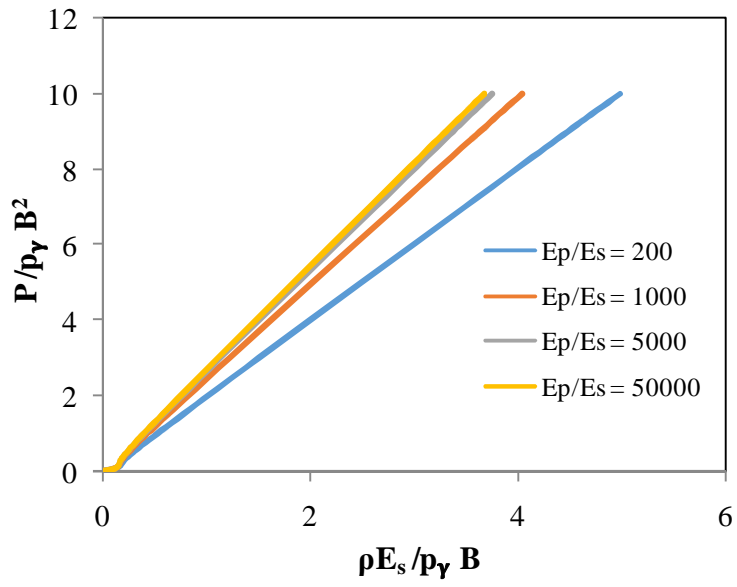
It can be concluded that the deformations are decreasing with increase in length. The deformations increases with increasing eccentricity. Among the  $E_p/E_s$  ratios the extreme ones like 200 and 50000 are undergoing large deformations compared to others. Among the  $E_p/E_s$  ratios 200 and 50000, for 50000  $E_s$  value is lower than the remaining so it is undergoing large deformations.

### 5.2.3 Stiff Clay

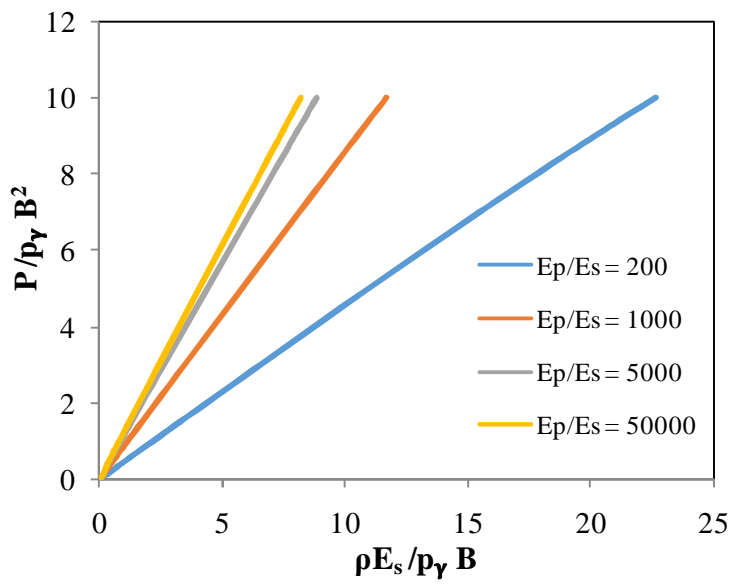
For stiff clay undrained shear strength of 200kPa is used in modelling. Other parameters required for modelling are implemented same as explained under 5.2.1 soft clay.

#### *Normalised charts for $L/B = 5$*

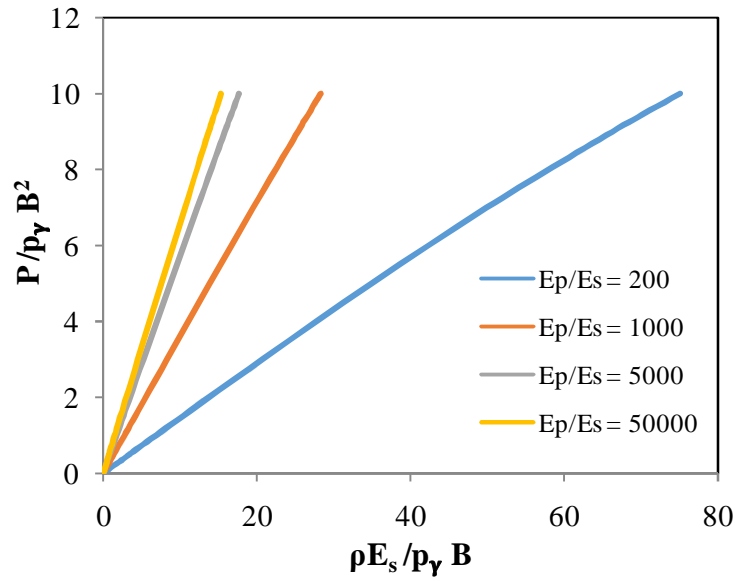
For a  $L/B$  ratio of 5 charts are proposed for  $e/B$  ratios of 0, 2 and 4. The normalised charts for various  $e/B$  ratios and  $E_p/E_s$  ratios for  $L/B = 5$  are shown in Fig 5.13



(a)  $e/B = 0$



(b)  $e/B = 2$



(c)  $e/B = 4$

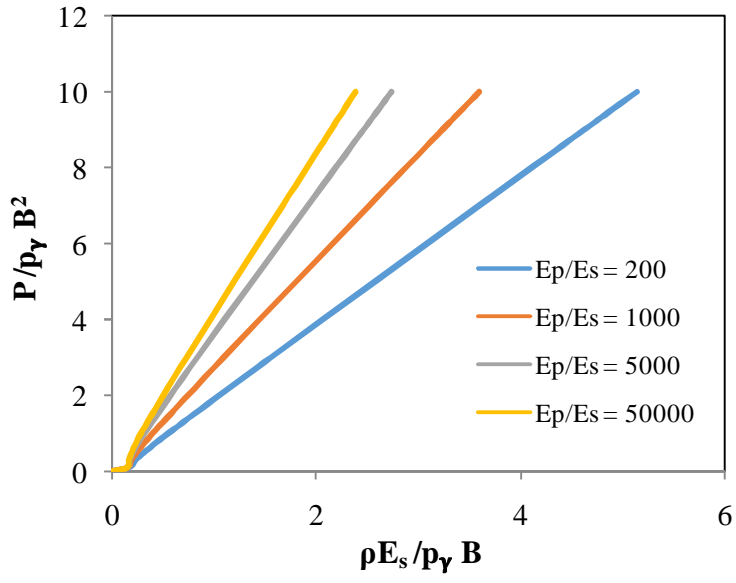
Figure 5.13 : Normalised load- deformation charts for  $L/B = 5$  and (a)  $e/B = 0$  (b)  $e/B = 2$  and (c)  $e/B = 4$

The normalised charts for stiff clay with  $L/B$  ratio 5 are shown in Fig 5.13. For the same maximum load of 1000kN the stiff clay did not enter into plastic stage as it has linear deformations as above because of its high undrained shear strength whereas for soft clay we observed that the graphs are non linear. The deformations are increasing with increase in eccentricity.

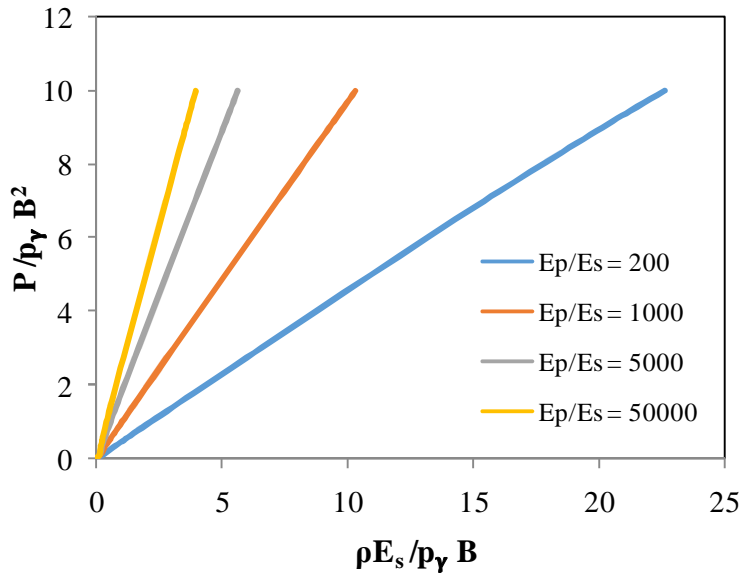
**Normalised charts for  $L/B = 10$**

For a  $L/B$  ratio of 10 charts are proposed for  $e/B$  ratios of 0, 2 and 4. The normalised charts for various  $e/B$  ratios and  $E_p/E_s$  ratios for  $L/B = 10$  are shown in Fig 5.14

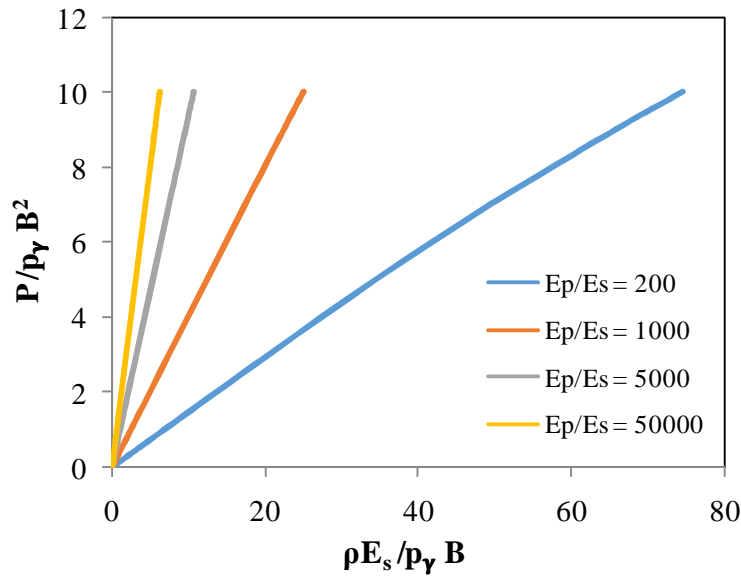




(a)  $e/B = 0$



(b)  $e/B = 2$



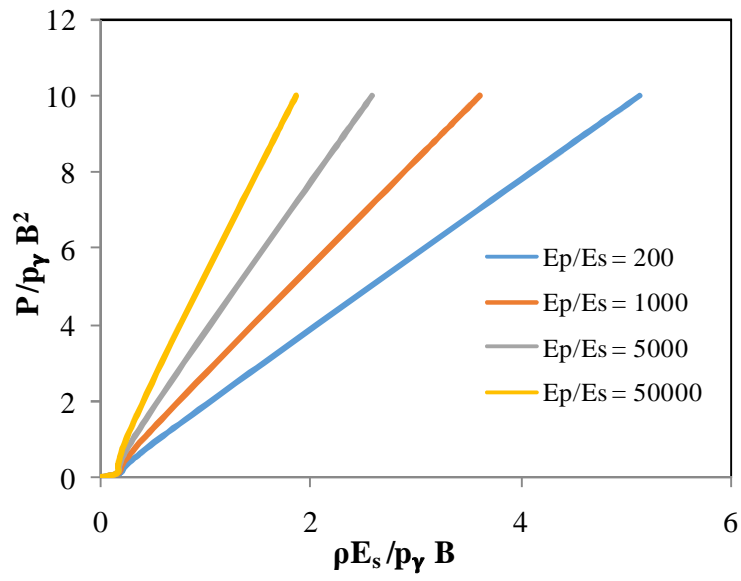
(c)  $e/B = 4$

**Figure 5.14 : Normalised load- deformation charts for  $L/B = 10$  and (a)  $e/B = 0$  (b)  $e/B = 2$  and (c)  $e/B = 4$**

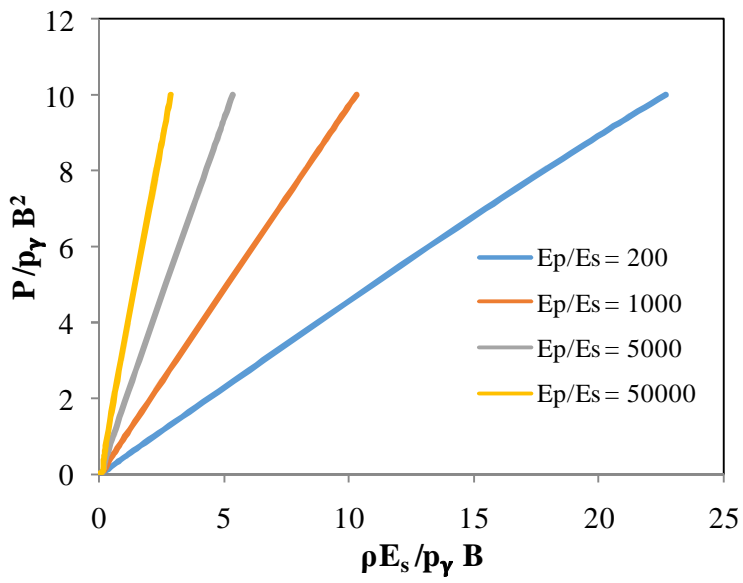
The graphs in Fig 5.14 are all linear though MC model is used because the deformations did not enter plastic stage. The graphs are all very close for  $e/B = 0$  and they are moving away from each other with increasing eccentricity. That means the deformations are increasing with increase in eccentricity. Also the deformations for  $L/B = 10$  are lesser when compared to  $L/B = 5$

***Normalised charts for  $L/B = 15$***

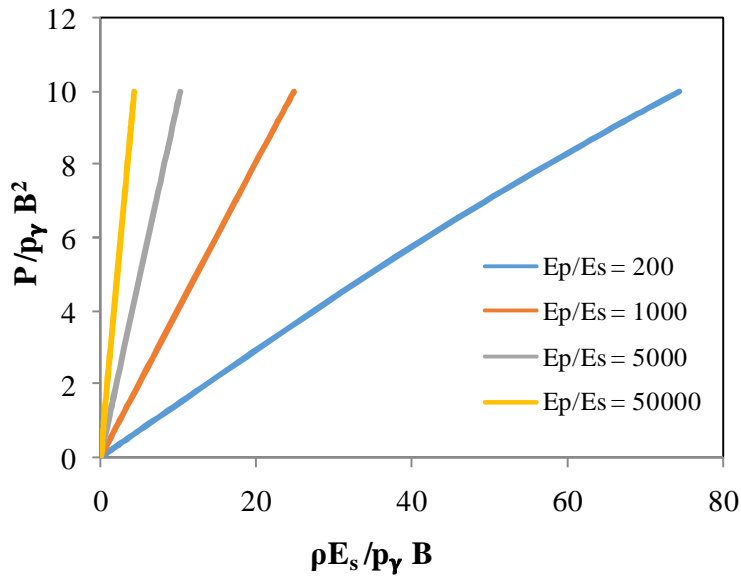
For a  $L/B$  ratio of 15 charts are proposed for  $e/B$  ratios of 0, 2 and 4. The normalised charts for various  $e/B$  ratios and  $E_p/E_s$  ratios for  $L/B = 15$  are shown in Fig 5.15



(a)  $e/B = 0$



(b)  $e/B = 2$



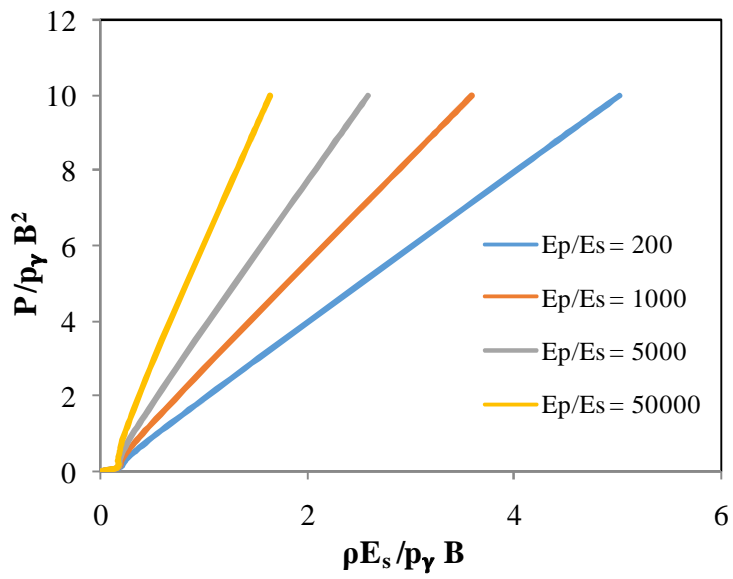
(c)  $e/B = 4$

**Figure 5.15 : Normalised load- deformation charts for  $L/B = 15$  and (a)  $e/B = 0$  (b)  $e/B = 2$  and (c)  $e/B = 4$**

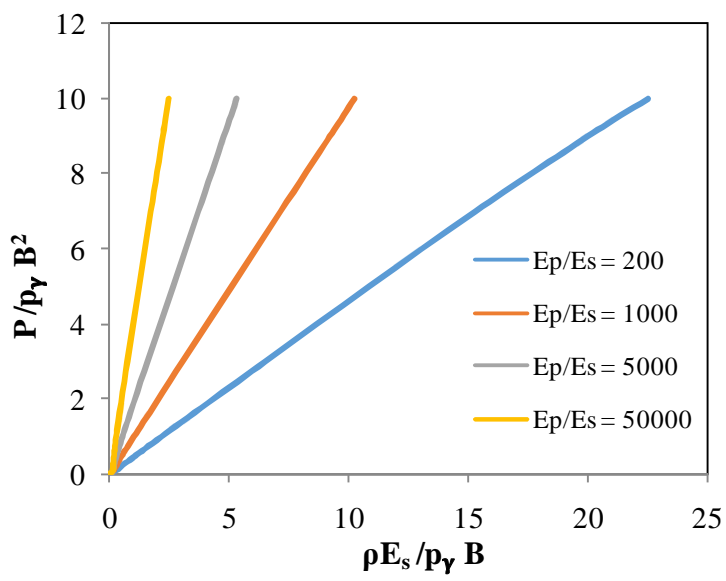
The deformations of stiff clay for  $L/B$  ratio 15 are shown in Fig 5.15. The deformations are increasing with eccentricity and decreasing with length.

***Normalised charts for  $L/B = 20$***

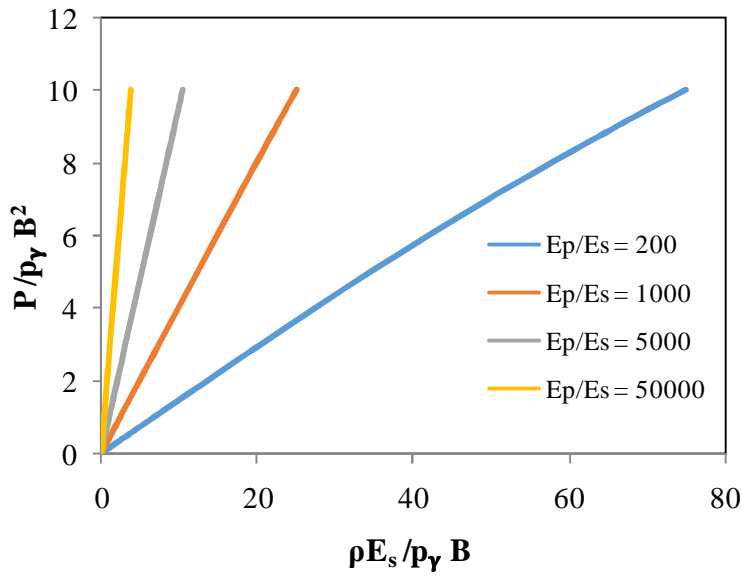
For a  $L/B$  ratio of 20 charts are proposed for  $e/B$  ratios of 0, 2 and 4. The normalised charts for various  $e/B$  ratios and  $E_p/E_s$  ratios for  $L/B = 20$  are shown in Fig 5.16



(a)  $e/B = 0$



(b)  $e/B = 2$



(c)  $e/B = 4$

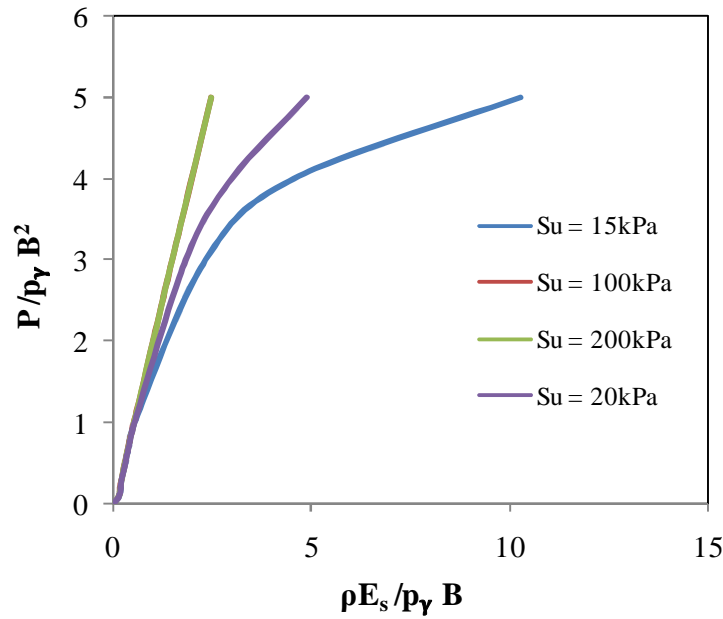
**Figure 5.16 : Normalised load- deformation charts for  $L/B = 20$  and (a)  $e/B = 0$  (b)  $e/B = 2$  and (c)  $e/B = 4$**

It can be concluded that the graphs in all the charts remain in linear state for a maximum applied load of 1000kN because of high undrained shear strength. Stiff clay has got the least deformations compared to soft and medium stiff clay.

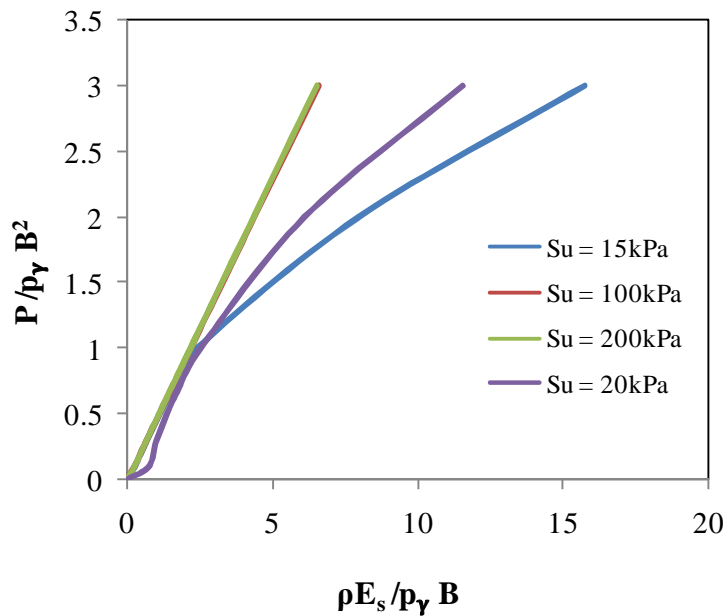
### 5.3 Comparison of Normalised charts of Soft Clay, Medium Stiff Clay and Stiff Clay

To study the state of deformations the normalised charts of clays of different consistencies are compared as shown in Fig 5.17 and Fig 5.18.

The comparison of charts for  $L/B$  ratio 5 and  $E_p/E_s = 200$  is shown in Fig 5.17



(a)  $e/B = 0$



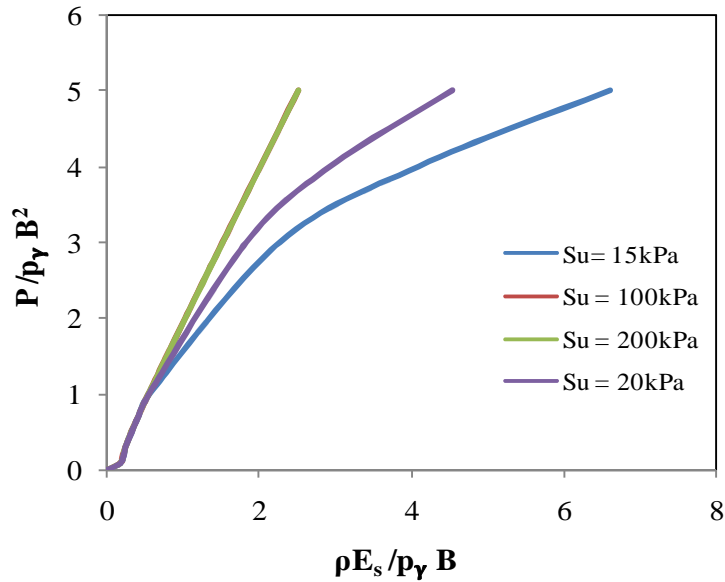
(b)  $e/B = 6$

**Figure 5.17: Comparison of normalised charts of different consistencies for a pile of  $L/B = 5$  and (a)  $e/B = 0$  (b)  $e/B = 6$**

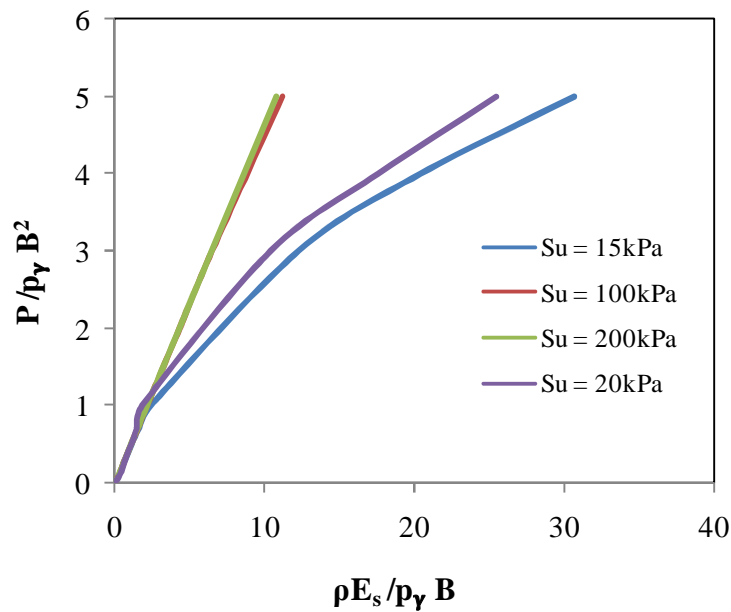
It is observed that the graph for  $S_u=15\text{kPa}$  and  $S_u=20\text{kPa}$  are non-linear in both the cases (a) and (b) that means soil entered into plastic stage. Whereas for  $S_u=100$  and  $200\text{kPa}$  the strength is so high that it is still remaining in elastic state for the same load. Also the deformations in case(b) are more

compared to case (a). The graphs of  $S_u=100$  and  $200\text{kPa}$  are coinciding because the load is so small for them and at lower loads the deformations coincide.

The comparison of charts for  $L/B$  ratio 5 and  $E_p/E_s = 200$  is shown in Fig 5.18



(a)  $e/B = 0$



(b)  $e/B = 6$

**Figure 5.18: Comparison of normalised charts of different consistencies for a pile of  $L/B = 20$  and (a)  $e/B = 0$  (b)  $e/B = 6$**



Similar to Fig 5.18 the trend is followed in 5.18. The graphs of  $S_u=15$  and  $20\text{kPa}$  are non linear both the cases  $e/B=0$  and  $6$ . The graphs of  $S_u=100$  and  $200\text{kPa}$  are linear , soil is in elastic state and they are overlapping each other.

#### 5.4 Study of Plastic Zone Formation for Clays

The study of formation of plastic zones is studied for clays for different loads. The loads applied are  $1000\text{kN}$ ,  $2000\text{kN}$ ,  $3000\text{kN}$  and  $5000\text{kN}$ . Though these loads are practically very high they are given because a high soil strength is given in modeling. This is only to study the evolution of plastic zones for clay. The load direction is left to right. The formation of plastic zones is studied for two cases one without eccentricity and the other one with eccentricity of  $6\text{m}$ .

When a load of  $1000\text{kN}$  is applied the plastic zones formed are shown in Fig 5.19

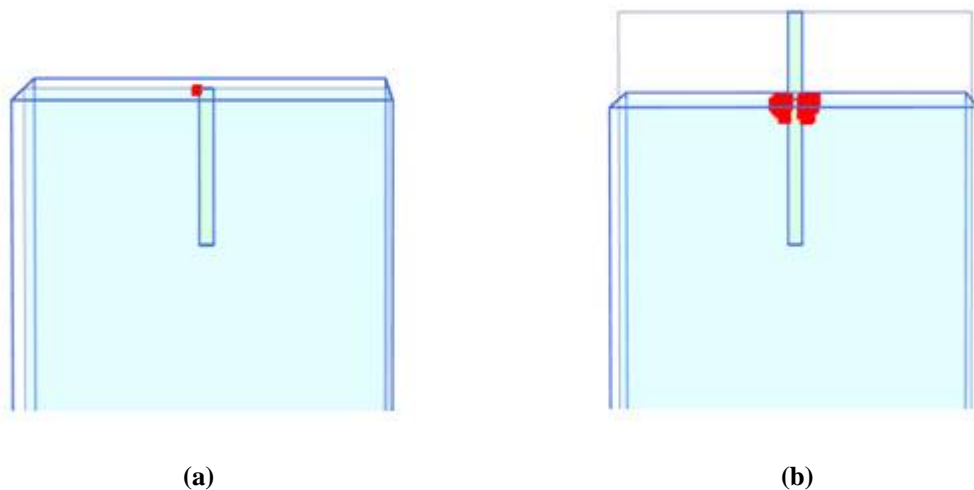


**Figure 5.19: Plastic zones for a load of  $1000\text{kN}$  when (a)  $e/B = 0$  and (b)  $e/B = 6$**

It can be observed that very small plastic zone at the top of the pile on the left side for no eccentricity case. For  $e/B = 6$  plastic zones are formed on both the sides of the pile at the surface. As the deformations are more for larger eccentricity, hence the plastic zones formed for  $e/B = 6$  are bigger.

When a load of  $2000\text{kN}$  is applied the plastic zones formed are shown in Fig 5.20

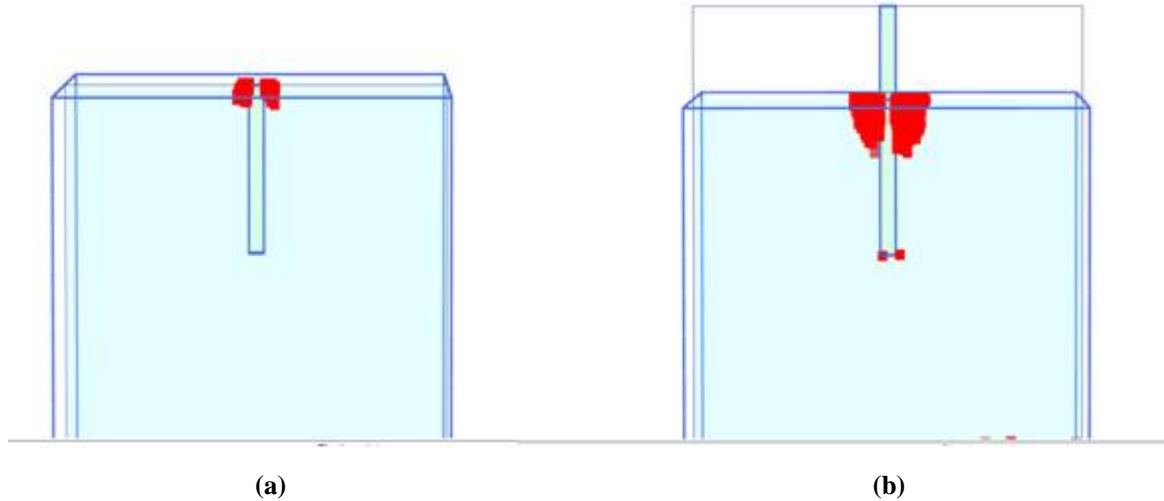


**Figure 5.20: Plastic zones for a load of 2000kN when (a)  $e/B = 0$  and (b)  $e/B = 6$**

It can be observed that for  $e/B = 0$  plastic zones started forming on both sides of the pile. For  $e/B = 6$  they grew deeper and at the bottom of the pile also few plastic points are observed.

When a load of 3000kN is applied the plastic zones formed are shown in Fig 5.21

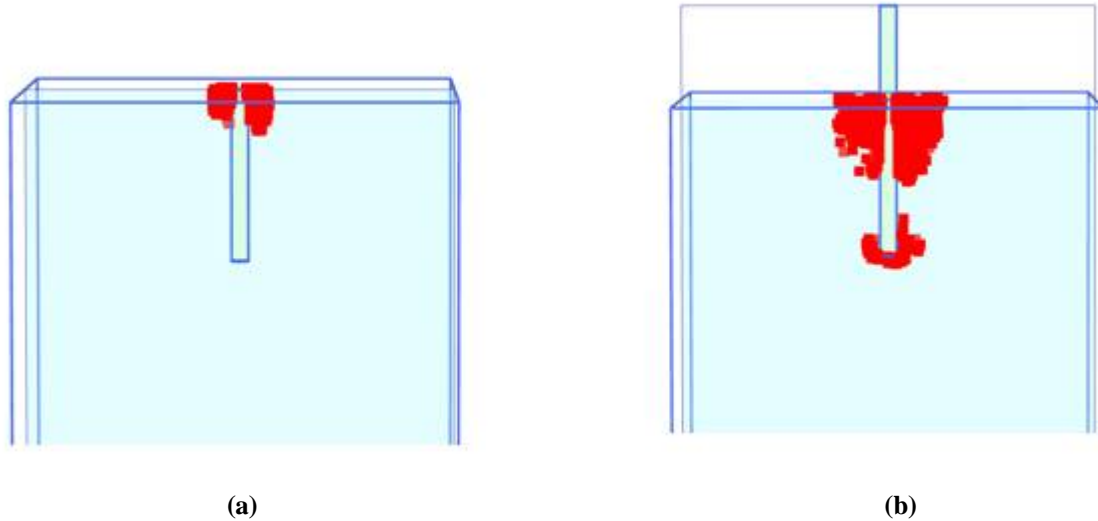


**Figure 5.21: Plastic zones for a load of 3000kN when (a)  $e/B = 0$  and (b)  $e/B = 6$**

It can be observed that the plastic zones are growing deeper for  $e/B = 0$  case and for  $e/B = 6$  plastic zones apart from growing deeper from top, they started forming from bottom of the pile also

When a load of 5000kN is applied the plastic zones formed are shown in Fig 5.22

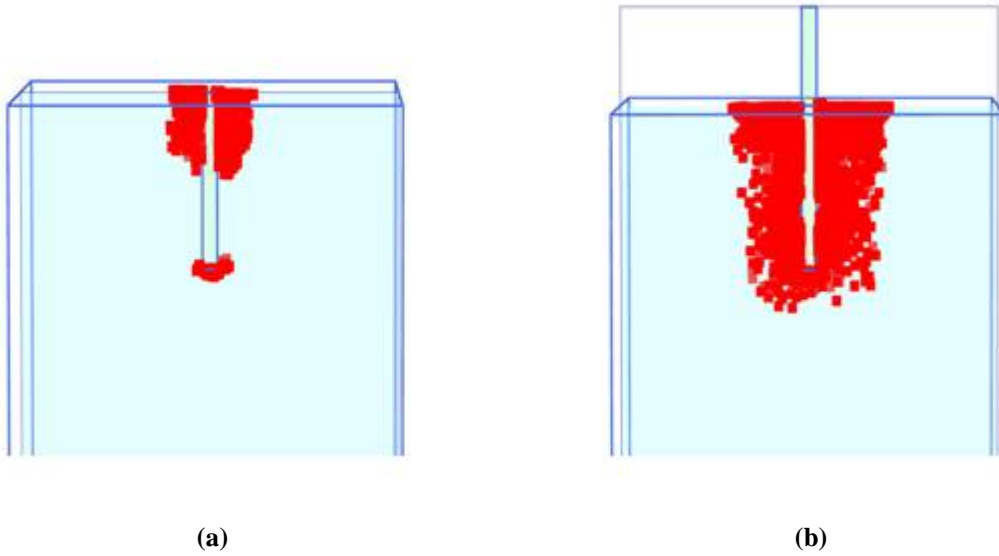


**Figure 5.22: Plastic zones for a load of 5000kN when (a)  $e/B = 0$  and (b)  $e/B = 6$**

For a load of 5000kN the plastic zones grew much deeper and they started forming from bottom of the pile also. For  $e/B = 6$  case the plastic zones from top and bottom grew towards each other and finally the plastic zone formed all around the depth of the pile.

Similarly when the load is further increased the complete plastic zone all around the pile will be formed for  $e/B = 0$  similar to the case of  $e/B = 6$ .

# Chapter 6

## Conclusions

IS code method is widely used by engineers around the country to determine maximum deformations of a laterally loaded pile. But the method is not rational as it is assuming the pile to behave as a cantilever fixed at certain depth. The comparison of deformations of a lateral pile embedded in sand and clay are compared for IS code method and numerical modeling. Normalised charts are proposed and evolution of plastic zones are studied for both sands and clays.

From this study the following conclusions are drawn out for sands:

- IS code is overestimating the deformations compared to numerical modeling about 30%-50% for lower modulus of subgrade reaction to higher values of subgrade reaction
- Normalised load-deflection charts are proposed for sands using LE model and MC model
- The charts of LE model can only be used for very low load values and the charts of MC model could be used for any loads as the soil is modelled more realistically using MC model
- Plastic zones formation for sands was evolved to increase laterally away from the pile, towards the boundaries along the surface with increasing load.

The following conclusions were drawn for a laterally loaded pile embedded in clay:

- IS code is overestimating the deformations compared to numerical modeling about 40%-70% for lower stiffness to higher stiffness with deviation increasing with consistency of the clay
- Normalised load-deflection charts are proposed for sands using MC model for soft clay, medium stiff clay and stiff clay
- Plastic zones formation for clays was evolved to increase along the depth of the pile with increasing load

# Reference

1. Bowles, J.E., 1968. "Foundation Analysis and Design," 2nd Edition, McGraw-Hill Book Company, New York.
2. Basu, D., Rodrigo, S., Prezzi, M., 2007. "Analysis of laterally loaded piles in Multilayered Soil Deposits," Final Report, FHWA/IN/JTRP-23, Purdue University.
3. Poulos, H.G., Davis, E.H., 1980. "Pile Foundation Analysis and Design," John Wiley and Sons, New York.
4. IS 2911 (Part1/Sec 1), 2010. "Analysis of Laterally Loaded Piles," Indian Standard Design and Construction of Pile Foundations - Code of practise, Annexure- C (Clause 6.5.2), Bureau of Standards, New Delhi, India.
5. Shukla, J.C., Shukla, P.J., Shah, D.L., 2013. "Comparison of lateral load capacity of pile using simplified linear spring approach and IS: 2911(2010)," Proceedings of Indian Geotechnical Conference, December, Roorkee, 22-24.
6. MATLAB, 2004. Programming Version 7, The Math Works, Inc.
7. Tomlinson, M.J., 1980. "Pile Design and Construction Practice," Fourth edition, E & FN Spon, London.
8. PLAXIS 3D Foundation. "PLAXIS 3D foundation user manual", Version 2.0.
9. Basack, S., Fatahi, B., Ryan, P., Khabbaz, H., 2013. "Behaviour of laterally loaded piles in layered soil," Proceedings of Indian Geotechnical Conference, December, Roorkee, 22-24.
10. Santra, S., Biswas, S.K., Moyukh, D., 2013. "Study of lateral deflection of short piles," Proceedings of Indian Geotechnical Conference, December, Roorkee, 22-24.
11. Dao, T. P. T., 2011. "Validation of PLAXIS Embedded Piles for Lateral Loading," MSc thesis, Delft University of Technology
12. Phanikanth, V.S., Choudhury, D., 2012. "Effects of lateral loads on a single pile," Journal of the Institution of Engineers (India), Ser. A, 93(3), 163-173
13. Phanikanth, V.S., Choudhury, D., Rami Reddy, G., 2010. "Response of single pile under lateral loads in cohesionless soils," Electronic Journal of Geotechnical Engineering, 15(10), 813-830.
14. Zhou, X., Yang, L., Li, M., Zhan, Y., 2013. "Numerical study for modulus of subgrade reaction of laterally-loaded piles in elastic soils," Electronic Journal of Geotechnical Engineering, 18, 3185-3194
15. Kim, Y., Jeong, S., 2011. "Analysis of soil resistance on laterally loaded piles based on 3D soil–pile interaction," Computers and Geotechnics, 38(2), 248-257

16. Khelifi, Z., Berga, A., Terfaya, N., 2011. "Modelling the behaviour of axially and laterally loaded pile with a contact model," *Electronic Journal of Geotechnical Engineering* 16(11), 1239-1258
17. Yang, Z., and Jeremic, B., 2002. "Numerical analysis of pile behaviour under lateral loads in layered elastic-plastic soils," *International Journal for Numerical and Analytical Methods in Geomechanics*, 26(10), 1385-1406